Aus der Radiologischen Universitätsklinik der Universität Heidelberg
Abteilung für Radioonkologie und Strahlentherapie
Ärztlicher Direktor: Prof. Dr. med. Dr. rer. nat. Jürgen Debus

Combined Photon - Carbon ion Radiotherapy Treatment Planning

**Inauguraldissertation zur Erlangung des
Doctor scientiarum humanarum (Dr. sc. hum.) an der Medizinischen
Fakultät Heidelberg der Ruprecht-Karls-Universität**

vorgelegt von
Amit Ben Antony Bennan
aus
Mumbai, India

June, 2021

Dekan: Herr Prof. Dr. Hans-Georg Kräusslich
Doktorvater: Herr Prof. Dr. Oliver Jäkel

For
Ivy ammamma
and
Philomena ammamma

Contents

List of Figures viii

List of Tables ix

I. Introduction 1

II. Background 5

II.1. Physics of Radiotherapy . . . 6
II.1.1. Photon Therapy Physics . . . 6
II.1.2. Particle Therapy Physics . . . 8
II.1.3. Techniques of modern radiotherapy . . . 12
II.1.3.1 Photon therapy treatment delivery techniques . . . 12
II.1.3.2 Particle therapy treatment delivery techniques . . . 12

II.2. Radiobiology . . . 13
II.2.1. Linear Quadratic model . . . 14
II.2.1.1 Translating *in vitro* to *in vivo* . . . 15
II.2.1.2 Clinical application of the Linear Quadratic (LQ) model . . . 17
II.2.1.3 Extensions of the LQ model . . . 17
II.2.2. Relative Biological Effectiveness (RBE) . . . 18
II.2.3. Modelling biological effects of Carbon ions . . . 20

II.3. Treatment Planning . . . 25
II.3.1. Imaging and volume definition . . . 25
II.3.2. Treatment Modelling . . . 26
II.3.3. Dose Calculation . . . 27
II.3.4. Treatment Plan Optimization . . . 28
II.3.4.1 Physical dose based optimization . . . 29
II.3.4.2 Effect Based Optimization . . . 30
II.3.4.3 Spatio-temporal Optimization . . . 31

II.4. Mixed Modality Treatments . . . 33
II.4.1. Clinical Practice . . . 33
II.4.2. Joint optimization of mixed modality treatments . . . 34

II.5. Motivation and Research questions . . . 37

III. Materials and Methods 38

III.1. Joint optimization framework for photon–carbon ion treatments . . . 38
III.1.1. Formulation of the joint optimization problem . . . 38
III.1.2. Fractionation in combined photon–carbon ion treatments . . . 41
III.1.3. Implementation . . . 44
III.1.3.1 Software framework . . . 44

III.1.3.2 Spatio-temporal optimization 44
III.1.3.3 Implementation of effect based joint optimization 45
III.1.4. Convergence 45
III.1.4.1 Convergence considerations 45
III.1.4.2 Preconditioning 46

III.2. Proof of concept 48
III.2.1. Spinal Metastasis 48
III.2.2. Treatment planning 49

III.3. Impact of treatment parameters 50
III.3.1. Impact of fraction allocation 50
III.3.2. Impact of Linear Quadratic model parameter selection 50
III.3.2.1 Base of skull chordoma 51
III.3.2.2 Treatment planning 51

III.4. Mixed modality treatments for Infiltrative disease 52
III.4.1. Glioblastoma 52
III.4.2. Fractionation in joint optimization 53
III.4.3. Glioblastoma patient cases 54
III.4.4. Treatment plan setup 54
III.4.5. Proton–carbon ion treatment 56

III.5. Impact of Local Effect Model version selection 57

IV. Results **58**

IV.1. Validation 58

IV.2. Spinal Metastasis 59
IV.2.1. Photon–carbon ion combined treatments 59
IV.2.1.1 Joint optimization with fixed fraction allocation 60
IV.2.1.2 Concurrent Irradiation 63
IV.2.1.3 Quantitative analysis 64

IV.3. Impact of fraction allocation 66

IV.4. Impact of LQ model parameter selection 68
IV.4.1. Spinal Metastasis 68
IV.4.2. Base of skull chordoma 70

IV.5. Glioblastoma 72
IV.5.1. Patient I 72
IV.5.2. Patient II 77
IV.5.3. Dose volume statistics 80

IV.6. Glioblastoma : Proton–carbon ion treatment 83

IV.7. Impact of Local Effect Model version selection 85

V. Discussion **87**

V.1. Validation of the joint optimization framework 88

V.2. Proof of concept: Spinal metastasis 89

V.3. Impact of fraction allocation 91

V.4. Impact of LQ model parameter selection 93

V.5. Mixed modality treatments for infiltrative disease: Glioblastoma 94

V.6. Fractionation objective for infiltrative diseases 96

V.7. Impact of Local Effect Model version selection 97

V.8. Physical uncertainty 98

V.9. Outlook 99

V.9.1. Biological models 99

V.9.2. Extension to other particle therapy modalities 101

V.9.3. Cost effectiveness of mixed modality treatments 101

VI. Conclusion **102**

VII. Summary **106**

VIII. Zusammenfassung **108**

Bibliography **110**

Disclosure **117**

Curriculum Vitae **118**

Acknowledgments **119**

Affidavit **120**

List of abbreviations

BED Biologically Effective Dose

CT Computed Tomography

CTV Clinical Target Volume

DNA Deoxyribonucleic Acid

EBRT External Beam Radiotherapy

EVH Biological Effect Volume Histogram

EQD Equivalent Dose

EVH Biological Effect Volume Histogram

GTV Gross Tumour Volume

HU Hounsfield Units

IMPT Intensity Modulated Particle Therapy

IMRT Intensity Modulated Radiotherapy

LEM Local Effect Model

LET Linear Energy Transfer

LQ Linear Quadratic

MKM Microdosimetric Kinetic Model

MLC Multi Leaf Collimator

MRI Magnetic Resonance Imaging

NTCP Normal Tissue Complication Probability

OARs Organs at Risk

OER Oxygen Enhancement Ratio

PET Positron Emission Tomography

PTV Planning Target Volume

RBE Relative Biological Effectiveness

rSP Stopping Power relative to Water

SBRT Stereotactic Body Radiotherapy

TCP Tumour Control Probability

TPS Treatment Planning System

VMAT Volumetric Arc Radiotherapy

WEPL Water Equivalent Path Length

VOIs Volumes of Interest

List of Figures

Figure I.1 Dose deposition characteristics of photons, protons and carbon ions . . . 2

Figure II.1 Mass attenuation as a function of photon energy . . . 7
Figure II.2 Mass Stopping power . . . 10
Figure II.3 Range and lateral scatter of protons and carbon ions . . . 11
Figure II.4 Basic cell survival curve . . . 14
Figure II.5 Radiation quality cell survival curve . . . 16
Figure II.6 Dependence of RBE on LET . . . 19
Figure II.7 LEM Concept . . . 20
Figure II.8 Carbon alphas and betas . . . 23
Figure II.9 Dependence of RBE on LET comparing Local Effect Model versions . . . 24
Figure II.10 Treatment planning workflow . . . 25
Figure II.11 Ray bixel concept . . . 26
Figure II.12 Point Spread Kernel . . . 27

Figure III.1 Iso-effective dose combinations in a one dimensional prototype . . . 43
Figure III.2 Evolution of the objective function and preconditioning . . . 46
Figure III.3 Spinal metastasis patient case . . . 48
Figure III.4 Base of skull chordoma patient case . . . 51
Figure III.5 Comparison of EQD2 in tumourous and healthy tissue from carbon ions and photons . . . 53
Figure III.6 Glioblastoma Patient Cases . . . 55

Figure IV.1 jointly optimized proton - photon plan: proof of concept . . . 59
Figure IV.2 jointly optimized photon–carbon ion plan: Spinal metastasis . . . 61
Figure IV.3 Dose difference maps for spinal metastasis plan comparison . . . 62
Figure IV.4 Dose distributions and supporting images of the concurrent irradiation strategy . . . 63
Figure IV.5 Spinal metastasis Effect Volume Histograms . . . 65
Figure IV.6 Treatment plan quality indicators for different fraction allocations: Spinal metstasis . . . 67
Figure IV.7 jointly optimized spinal metastasis treatment plan with and without fractionation gain . . . 69
Figure IV.8 jointly optimized treatment plans: Base of skull chordoma . . . 71
Figure IV.9 jointly optimized Dose maps: Glioblastoma Patient I . . . 74
Figure IV.10 jointly optimized treatment of Glioblastoma Patient I: Supporting images 75
Figure IV.11 LET maps of jointly optimized treatment of Glioblastoma Patient I . . . 76
Figure IV.12 jointly optimized Dose maps: Glioblastoma Patient II . . . 78
Figure IV.13 Jointly optimized treatment for Glioblastoma Patient II: Supporting images 79
Figure IV.14 Glioblastoma Effect Volume Histograms for 6 patient cases . . . 82
Figure IV.15 Proton - carbon ion jointly optimized plans: Glioblastoma Patient I . . . 84
Figure IV.16 jointly optimized photon–carbon ion considering different LEM models: Glioblastoma Patient I . . . 86

List of Tables

Table II.1 Dose based objectives 30
Table II.2 Effect based objectives 31

Table III.1 Effect based objectives for joint optimization 40
Table III.2 Spinal metastasis treatment planning objectives 49
Table III.3 Base of skull chordoma treatment planning objectives 52
Table III.4 Glioblastoma reference photon treatment planning objectives 55
Table III.5 Glioblastoma reference carbon ion treatment planning objectives 55
Table III.6 Glioblastoma photon–carbon ion jointly optimized treatment planning objectives 56

Table IV.1 Spinal Metastasis plan quality indicators 64
Table IV.2 Base of skull chordoma treatment plan quality indicators 70
Table IV.3 EQD2 based glioblastoma treatment plan quality indicators 81

"Growth for the sake of growth is the ideology of the cancer cell."

Edward Abbey, 1988

I Introduction

The etymological origin for the term cancer is attributed to Hippocrates, 400 BC; who, observing a tumour and its tendrils of irregular blood vessels stretching out, draws the vivid parallel to a crab: '*karkinos*'. Cancer is not a singular disease but many, and they all fundamentally share one feature: abnormal uncontrolled growth of cells with the ability to differentiate and spread to different locations and organs. The causes of cancer are largely unknown but genetic mutations and several environmental factors have been identified as contributing factors. Cancer is the cause for 1 in 6 deaths and is the second-leading cause of death worldwide after cardiovascular diseases. The number of cases is projected to grow from 14.1 million in 2012 to 24.6 million in 2030 (American Cancer Society, 2018).* The approach to cancer management for a patient is decided by a multidisciplinary cancer conference comprised of medical oncologists, surgical oncologists, radiation oncologists, radiologists and other specialists. There are three main branches of therapeutic oncology: surgical oncology focuses on excision and treatment by surgery, medical oncology focuses on systemic treatment with chemotherapy, targeted therapy, immunotherapy and hormonal therapy; and radiation oncology focuses on the use of ionizing radiation to induce cytotoxic effects in cancer cells. Radiotherapy is a fundamental tool for cancer therapy as it is applied in approximately 50% of cancer patients for local control and palliation (Atun et al., 2015).

The history of radiotherapy is as old as the story of radiation itself. Among the first experimental treatments, Victor Despeignes (Lyon) attempted to treat a gastric tumour with Roentgen rays in 1896, just a few months after their discovery by Wilhelm Roentgen in 1895. (Cosset, 2016). The biological effect of radiation stems from its ability to directly or indirectly cause damage to the Deoxyribonucleic Acid (DNA) of cells. Normal healthy cells can recognise and repair most of the damage to DNA, but cancer cells have a lower regenerative capacity and hence result in a higher kill rate. This differential regenerative capacity, known

*`https://www.cancer.org/research/cancer-facts-statistics/global.html` [accessed 29 December 2020]

as the therapeutic window, is exploited in radiotherapy with the use of fractionation, i.e., delivering therapeutic dose over multiple sessions. The ultimate goal in radiotherapy is to control the tumour with minimal damage to healthy tissue (Joiner and van der Kogel, 2009). The delivery of radiation to the tumour can, in present day, be realized in three ways: (1) with the aid of nuclear medicine, where radio-pharmaceuticals are used to systemically target the tumour, (2) Brachytherapy, a generally invasive procedure where radioactive sources are brought into close proximity of the tumour and (3) External Beam Radiotherapy (EBRT), a non-invasive method, where highly targeted beams of radiation are projected into the body to deliver dose. EBRT modalities include, most commonly, X-rays (MeV photons) and accelerated particles like electrons, neutrons, protons and heavier ions. Therapeutic X-rays are commonly generated with a Cobalt-60 source (1.25 MeV) or for higher energies, with a linear accelerator (LINAC) (starting from 6 MV) which is the current state of the art. As seen in figure I.1, dose deposited from photons (——) rises to an initial maximum as they enter matter, known as the build up region, after which dose deposition exponentially decreases along the length of its trajectory. This also implies that dose is delivered to the tumour at the cost of some dose delivered to healthy tissue in front of and behind the tumour. More recent technical developments in synchrotrons and cyclotrons have made it possible to use accelerated heavy charged particles to deliver the therapeutic dose. Unlike photons, heavy charged particles release increasing amounts of energy as they slow down, moving through matter, the loss of energy increases until a maximum point around which the particles come to a halt. This maximum is called a Bragg peak in honour of William Bragg who first studied this phenomenon. Compared to protons (——), carbon ions (——) exhibit a much sharper dose fall-off. Therefore carbon ions, compared to photons and protons, are theoretically capable of delivering dose distributions that are much more conformal to the tumour, hence sparing more healthy tissue from dose. Details regarding the physical interactions of photons and charged particles are given in section II.1.1 and II.1.2 respectively.

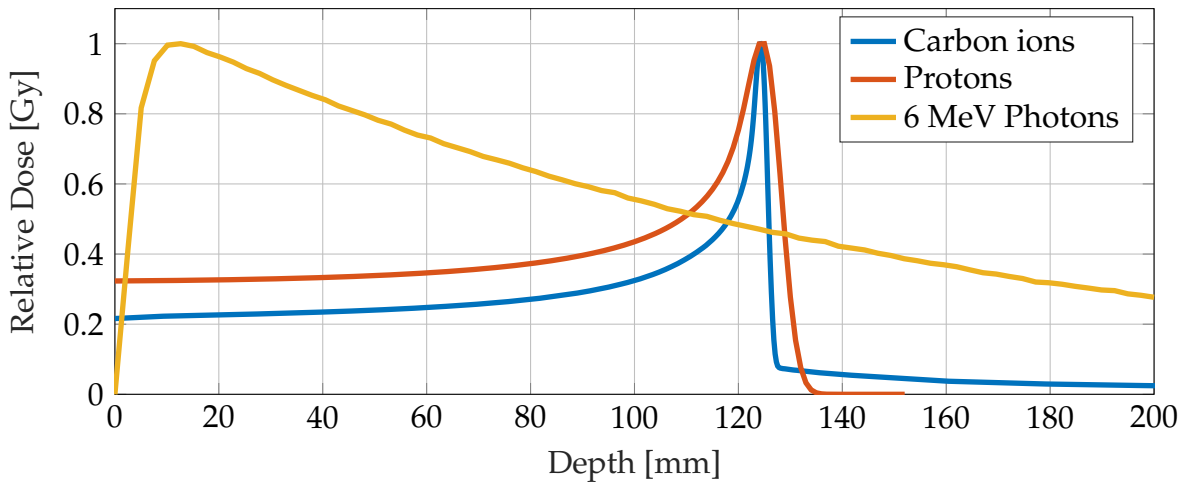

Figure I.1: Normalized depth dose profiles of 6 MV photons , 133 MeV u^{-1} protons and 250 MeV u^{-1} carbon ions in water.

The discovery of this interaction characteristics of particles resulted in an interest from the medical community, particularly by Robert Wilson, who attempted to treat patients with accelerated protons at nuclear research facilities, notably at the Berkley Radiation Laboratory in 1954. This led to a surge in investment into research and development of particle therapy centres. Currently, there are 89 active particle therapy centres around the world as of 2020 (PTCOG, 2020) [†]. The increased complexity of accelerator technology also demands an extremely high capital investment. Even with commercially available systems that are more economical and compact, a proton therapy facility costs 4 times as much as a photon therapy facility. On the patient side, proton therapy cost 3 times as much as photon treatments and therefore remains inaccessible to a large percentage of patients who would potentially benefit from it (Peeters et al., 2010). Carbon ion radiotherapy is a more experimental treatment approach that requires a larger and more complex accelerator in order to produce the therapeutic range of energies. Commercial carbon ion accelerators are still under development.
Apart from the technical improvements in contemporary radiation delivery systems, the knowledge of the negative side effects of radiation demanded innovation in the direction of accurate radiation delivery. Radiation oncology is a highly technical discipline, compared to other modalities of cancer treatment as improvements in radiotherapy have mainly resulted from improvements in technology of imaging, treatment planning and dose delivery. Radiotherapy treatment planning is a highly computerized process where it is possible to use imaging modalities such as Computed Tomography (CT) to generate precise three dimensional models of the patient and simulate treatment. This in conjunction with evidence based biological models can simulate the physical and biological effects of the treatment. Ideally, the entire tumour should receive the prescribed dose and the dose to the healthy tissues and surrounding Organs at Risk (OARs) is to be averted. In practice, however, this is not possible. Therefore, the treatment planner in coordination with the radiation oncologist is tasked with defining a trade-off between delivery of dose to the tumour and sparing OARs from dose. The infeasibility of this ideal situation arises from the anatomy of the patient and the physical characteristics of the radiation modality used. Details of the treatment planning process are presented in chapter II.3.
Another striking difference between charged particles and photons is in the effect they have on biological tissue. Charged particles exhibit an increased microscopic dose deposition density resulting in a greater number of DNA strand breaks, as compared to photons. Therefore, charged particles are particularly useful in the case of large, conventionally radio-resistant tumours. On the other hand, the increased localized DNA damaging dose deposition not only affects tumors but also transfers to healthy tissue. The biological effects of photon and proton radiation are well understood with established radiobiological models. Carbon ions, on the other hand, exhibit much more complex processes which are not as easily described. Details regarding radiobiology of radiation modalities is presented in section II.2.
All radiation modalities have their advantages and disadvantages which must be exploited

[†] `https://www.ptcog.ch/index.php/facilities-in-operation` [accessed December 2020]

and considered, respectively, in all its complexity and potential. In this body of work, the focus is placed on photon therapy and carbon ion therapy. Carbon ions possess superior biological dose deposition characteristics but have the drawback of the more detrimental biological effects in healthy tissue and a high cost of operations compounded by limited availability. Photons, on the other hand, are better at sparing healthy tissue through fractionated treatments and are accessible to more patients, the downside being, inferior depth dose characteristics. Therefore, a strategy of synergistic optimization of both modalities must be considered where photons and carbon ions cumulatively deliver a treatment that, hypothetically, conforms to the treatment objectives better than any individual radiation modality. Such combined treatments may benefit a much larger population of patients than unimodal carbon ion or photon treatments. Mixed modality treatments have been used in the past in boost treatments and re-irradiation treatments but the prevalent approach to combining modalities is based on the idea of a simple combination of two independent treatment plans. The combination of these individual plans is dependant on the experience of the treatment facility rather than a consistent mathematical and radiobiological framework. Such joint optimization strategies have been explored for combinations of photon - electron and proton - photon treatments within a relatively simple radiobiological model.
The aim of this thesis is to propose and explore a novel treatment planning strategy to combine photon therapy and carbon ion therapy within a consistent mathematical - radiobiological framework. One that takes into account the distinct physical and biological characteristics of the individual modalities and optimizes not just the physical spatial distribution of dose but also the temporal distribution of dose and in doing so, begin to describe the ideal combination of photons and carbon ions in terms of a biological effect.

"Mystery creates wonder and wonder is the basis of man's desire to understand"

Neil Armstrong, 1930-2012

II Background

Radiotherapy is a highly interdisciplinary treatment strategy that requires the joint expertise of many specialized fields. A team of radiation oncologists, radiation therapists and medical physicists design a personalized treatment plan which aims to deliver a set dose of radiation to the tumour. The choice of radiation modality is made based on the cancer indication and access to treatment modalities. The first course of action, pertinent to this work, is the process of treatment planning. The tumour is delineated on the CT with possible input from soft tissue imaging (Magnetic Resonance Imaging (MRI)) and functional imaging. The treatment plan optimization then performs a simulation of the treatment in this discretized patient geometry to deliver the prescribed dose. This involves modelling radiation physics of the modality/modalities and defining the most favourable dose distribution. A brief summary of the fundamentals of treatment planning are presented in section II.3. The plan quality is assessed based on therapeutic gains and disadvantages in balancing the tradeoff between dose to tumour and dose to healthy tissue using radiobiological models described in section II.2. The most favorable plan is then delivered to the patient.

Recent developments in the field of medical physics suggest a theoretical gain in plan quality from a synergistic optimization of mixed modality treatments. The thesis in hand investigates the implication of the combined optimization of photon–carbon ion treatments. section II.4 presents an overview of the development of the concept and status quo presented in literature that lays the foundation for the work presented in this thesis.

II.1 Physics of Radiotherapy

II.1.1 Photon Therapy Physics

Electromagnetic radiation is comprised of waves of electric and magnetic field vectors perpendicular to each other and to the direction of propagation and can be considered to be a stream of particles, i.e., photons, to aptly describe their interactions with matter. Photons are characterised by their frequency ν and energy $E = h\nu$, where h is the Planck constant.
In radiotherapy, photons in the therapeutic range are generated using Cobalt-60 teletherapy machines or, the more modern, LINAC machines. Cobalt therapy machines use the Cobalt-60 radioisotope which is a high activity gamma emitter of characteristic 1.17 MeV and 1.33 MeV gamma rays. LINACs produce photons in the MeV range by accelerating electrons against a high density (tungsten) target. The resulting photon spectrum covers energies up to the maximum energy of the accelerated electron impinging on the target. This section provides an overview of photon interaction with matter and dose deposition.
Photon interactions with matter are stochastic (random) processes. For a narrow beam of photons passing through matter, the attenuation of photons (change in number of primary photons) is proportional to the incident number of photons and the thickness of the absorber. For a thin slice of absorber material (z) this can be written as:

$$dN = \mu N(z)dz \tag{II.1}$$

Solving this differential describes an exponential reduction in the number of primary photons (N_o) at distance z in the absorber material and is referred to as Lambert-Beer law:

$$N(z) = N_o e^{-\mu z} \tag{II.2}$$

Here, μ is the linear attenuation coefficient [cm^{-1}] which is characterized by the anatomical make-up and the energy of the photons, $\mu = \rho_e.\sigma_e(E_\gamma, Z)$. ρ_e is the electron density in the tissue and σ_e is the electron cross section, which can be understood as the probability of interaction with electrons and depends on the energy of the photon (E_γ) and charge number of the absorber material (Z).

Photon interactions can be described by three fundamental pathways:

1. Photoelectric effect: when a photon is absorbed by an atom and as a result one of the orbital electrons is ejected (photoelectrons).
2. Compton Effect: a photon interacts with an atomic electron resulting in an ejected electron and a scattered photon with reduced energy.
3. Pair production: when a photon, of energy greater than 1.02 MeV, interacts with the nucleus of an atom resulting in an electron-positron pair.

The linear attenuation coefficient can be expressed as the sum of the contributing interactions mentioned above:

$$\mu(E_\gamma, Z) = \tau(E_\gamma, Z) + \sigma(E_\gamma, Z) + \kappa(E_\gamma, Z) \tag{II.3}$$

where τ, σ and κ are the attenuation coefficients from photoelectric effect, Compton scatter and pair production interactions respectively, dependant on the photon energy and material (Khan and Gibbons, 2019). Attenuation is usually reported as the mass absorption coefficient μ/ρ, where ρ is the mass density of the absorber material. As illustrated in figure II.1, for photon energies used in imaging (30 - 150 keV), the interactions are a combination of photoelectric effect (——) and Compton scatter (——). Compton scattering is the dominant type of interaction for the therapeutic range of photon energies (1 - 15 MeV). Pair production interactions (——) are probable for energies above 1.022 MeV, but their contribution is negligible at therapeutic energies.

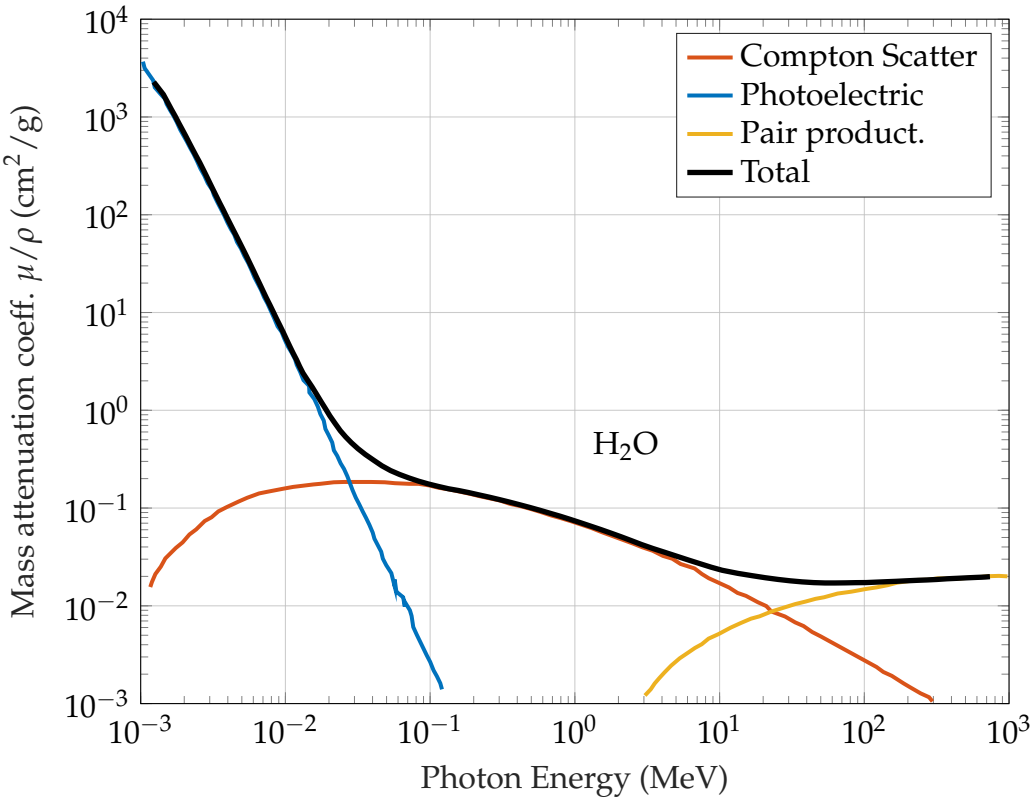

Figure II.1: Mass attenuation coefficients of water as a function of photon energy (——) and contributions from Compton scatter (——), photoelectric (——) and pair production (——) interactions. Adapted from Salvat and Fernández-Varea (2009)

When discussing radiation therapy, the primary quantity of interest is the absorbed dose,

$$D = d\vec{E}/dm \qquad [\text{Gy}] \tag{II.4}$$

As mentioned above, Compton scattering is the dominant interaction in the energy range used for radiotherapy. On generation, the Compton electron and photon travel away from the site of interaction and take with them most of the energy from the site of the interaction. Compton electrons have a range of a few mm, and most of the absorbed dose to the medium is delivered by these secondary electrons, therefore photons are also referred to as indirectly ionizing radiation. As photons cross the material interface into the medium, a cascade of secondary electrons is triggered and the number of secondary particles grows until a distance of approximately their maximum range which depends on the energy of the incident photons. This is seen as the rise in dose in figure I.1 and is referred to as the build up region. The dose rises to reach a maximum at which point the production and dissipation of secondary electrons reaches a state of equilibrium (Khan and Gibbons, 2019; Podgorsak, 2016). After this maximum, the deposited dose follows the Lambert-Beer law (II.2), given as

$$\psi(E,\vec{x}) = \phi(E,\vec{x})Ee^{-\mu(E,\vec{x})} \tag{II.5}$$

where at a point $\vec{x}$, $\psi(E,\vec{x})$ is the energy fluence of incident photons with energy E and particle fluence $\phi(\vec{x})$. In practice, the photons emitted by LINACs are not monoenergetic, hence, the Total Energy Released per unit Mass (TERMA) [Gray (Gy) = Jkg^{-1}] at location $\vec{x}$ by primary photons is given by

$$\text{TERMA}(\vec{x}) = \int_E \frac{\mu}{\rho}(E,\vec{x})\psi(E,\vec{x})dE \tag{II.6}$$

For the purposes of radiotherapy treatment planning, the mass attenuation coefficient can be estimated using imaging modalities (CT) and the energy fluence and distribution is defined by the treatment plan and treatment machine. The calculation of the total absorbed dose, i.e., from primary and secondary particles, is given in section II.3.3.

II.1.2 Particle Therapy Physics

Clinically used heavy charged particles are generally created using multiple pass particle acceleration techniques within cylcotrons and synchrotrons. Charged particles are incrementally accelerated by an electric field and held in motion, until they are delivered, in circular trajectory using a magnetic field. Cyclotrons and synchrotrons produce almost monoenergetic beams, the range of beams from a sychrotron can be controlled changing the energy of the beam from the accelerator itself. This is not possible with cyclotrons and therefore the change in energy of the particles is commonly done by focussing the beam onto a light material with adjustable thickness called a degrader.

Accelerated charged particles slow down as they pass through matter and deposit energy in the material as they slow down until they come to a halt. The range of charge particles is dictated by the initial kinetic energy and material characteristics. Unlike photons, charged particles are a directly ionizing form of radiation. This means that most of the energy is

deposited by the primary particle while traversing through matter. This absorbed dose d [Gy] at position $\vec{x}$ can be written as:

$$d(\vec{x}) = \int_E \frac{1}{\rho(\vec{x})} \frac{dE}{dx} \phi(E, \vec{x}) = \int_E \frac{S(E, \vec{x})\phi(E, \vec{x})}{\rho(\vec{x})} \tag{II.7}$$

where $\frac{dE}{dx}$ represents the linear stopping power ($S(E, \vec{x})$) [MeVcm^{-1}], $\phi(E, \vec{x})$ represents the particle fluence and $\rho(\vec{x})$ represents the mass density of the absorber. To express the energy loss rate independent of the mass density, the linear stopping power is often presented as the mass stopping power ($\frac{S}{\rho}$). The mass stopping power is the cumulative effect of the various interactions of charged particles (Newhauser and Zhang, 2015):

1. Inelastic Coulomb scattering: when the primary particle interacts with atomic electrons and lose kinetic energy while ionizing the medium.

2. Elastic Coulomb scattering: when the primary particle interacts with the static electric fields of nuclei in the medium resulting in a change of trajectory of the primary particle.

3. Inelastic nuclear reaction: when the primary particle interacts with the atomic nucleus resulting in secondary protons, heavier ions, neutrons and prompt gamma rays as the principal ejectiles.

4. Bremstrahlung: when the primary particle is deflected by the atomic nucleus resulting in a change of trajectory and loss of energy. This interaction emits energy as a Bremstrahlung photon.

The mass stopping power can be expressed as the cumulations of energy loss rates from the above interactions

$$\frac{S}{\rho} = \frac{S_{el}}{\rho} + \frac{S_{rad}}{\rho} + \frac{S_{nuc}}{\rho} \tag{II.8}$$

where $\frac{S_{nuc}}{\rho}$ is due to inelastic interactions with the nucleus of the medium and is relevant for low energies but has little contribution to the overall mass stopping power. $\frac{S_{rad}}{\rho}$ is attributed to the emission of Bremstrahlung photons and is negligible for therapeutic particle energies. $\frac{S_{el}}{\rho}$ is attributed to the Coulombic interactions with atomic electrons (Seltzer et al., 2011).

As seen in figure II.2, $\frac{S_{el}}{\rho}$ (protons ····· , carbon ions ·····) is the main contributor to the total mass stopping power and can be described for a beam of particles with the Bethe-Bloch formulation (Bethe, 1930; Bloch, 1933) given as:

$$\frac{S_{el}}{\rho} = 4\pi N_A r_e^2 m_e c^2 \frac{Z}{A} z^2 \frac{1}{\beta^2} \left[ln \frac{2m_e c^2 \gamma^2 \beta^2}{I} - \beta^2 - \frac{\delta}{2} - \frac{C}{Z} \right] \tag{II.9}$$

where N_A is the Avogadro's number, r_e and m_e are the radius and rest mass of an electron, Z and A the atomic number and the atomic weight of the absorbing material, z is the ion charge of incident particle and c the speed of light, $\beta = v/c$ where v is the velocity of the incident

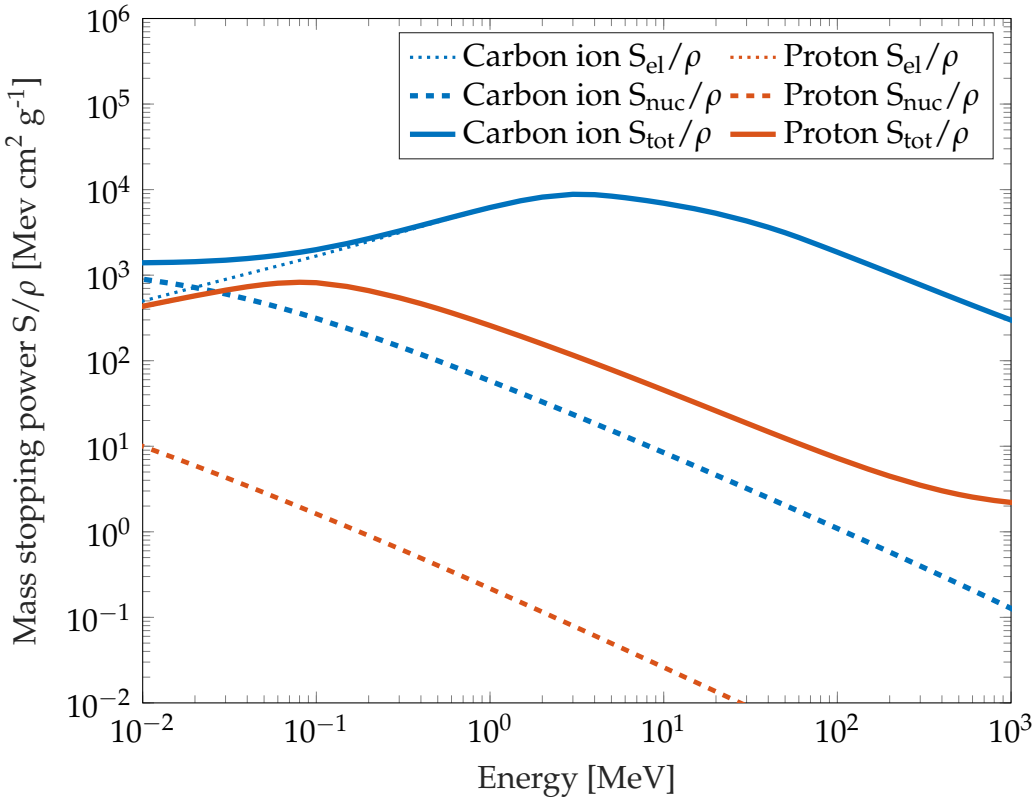

Figure II.2: Total mass stopping power (S/ρ) of water for protons (——) and carbon ions (——) along with the individual contributions of S_{el}/ρ (protons ·····, carbon ions ·····) and S_{nuc}/ρ (protons - - - -, carbon ions - - - -) with respect to their energy. For protons in therapeutic energy range S/ρ coincides with S_{el}/ρ. Based on data presented in ICRU 90 report (ICRU, 2014)

particle and $\gamma = (1-\beta^2)^{-1/2}$. I is the mean excitation potential. Correction factors δ and C are only applicable for very high or very low particle energies. In the equation above it is worth noting the projectile characteristics that affect the stopping power: the energy loss is independent of the projectile mass, inversely proportional to the square of the projectile velocity ($\frac{S_{el}}{\rho} \propto 1/v^2$) and directly proportional to the ion charge (z). Similarly from the point of view of the absorber material, the mass stopping power is proportional to the mass density (the electron density to be specific) and the mean excitation potential I (Newhauser and Zhang, 2015). The electronic mass stopping power (inelastic Coulomb interaction) also influences the range of the projectile into the medium. Carbon ions would require higher energy per nucleon to reach the same depth as protons due to the increased charge as seen in figure I.1.

Coulombic interactions with atomic electrons result in a psuedo-continuous loss of energy but as the difference in mass between primary particles and electrons is so high (protons by a factor of ∼1,800 and carbon ions by a factor of ∼22,000), these interactions do not cause great deviations in the trajectory of primary particles. However elastic interactions with the atomic nuclei of the absorber causing a deflection of primary particles resulting in a lateral penumbra. This scatter effect is more clearly observed in protons than carbon ions which are

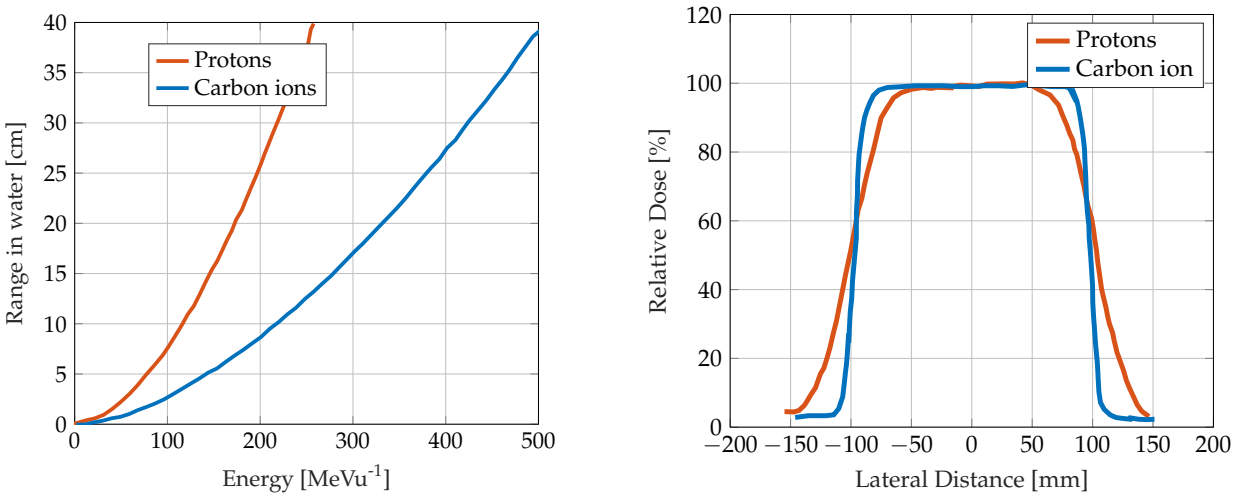

(a) Range of protons and carbon ions in water

(b) Lateral penumbra of protons and carbon ions in water

Figure II.3: (a) Increase in range in water for protons and carbon ions with respect to energy per nucleon [MeVu^{-1}], (b)lateral penumbra compared for equal beam widths. Adapted from Sánchez-Parcerisa et al. (2012)

heavier than protons by a factor of 12. Inelastic nuclear interactions on the other hand, occur when the the projectile breaks through the Coulomb barrier of the nucleus. These interactions are less probable but result in a reduction in the number of primary projectile. Depending on the target nucleus, this interaction may result in the generation of fragments of the primary particle (for carbon ions), fragments of target nuclei, neutrons and prompt gammas. In the case of ion projectiles heavier than protons, this interaction can result in lighter ions that can penetrate deeper into the absorber material. The dosimetric effect of this can be seen in figure I.1 for carbon ions (——), where a dose tail is seen after the Bragg peak, also known as the fragmentation tail.

An important physical quantity used often to describe the radiation quality or ionization density is Linear Energy Transfer (LET) [keV µm^{-1}]. LET is the amount of energy deposited by the ionizing particles per unit distance traversed through a medium. Therefore charged particles are considered as high LET radiation whereas photons, which are sparsely ionizing, are considered as low LET radiation. LET is also referred to as the restricted linear electronic stopping power given as

$$\mathrm{LET}_{\Delta} = \frac{dE_{\Delta}}{dx} = S_{el} - \frac{dE_{ke,\Delta}}{dl} \tag{II.10}$$

where dE_{Δ} is the mean energy lost by primary charged particles to electronic interactions while travelling a distance dx, discounting the energy carried away by secondary electrons $dE_{ke,\Delta}$ that have energies greater than the threshold energy Δ. It is referred to as the unrestricted LET (L_{∞}) if no energy cutoff is placed, and it is equal to the electronic stopping power S_{el} (Seltzer et al., 2011). The LET may be reported as track averaged LET (LET_t) which is the arithmetic mean of the fluence spectrum of LET or more commonly, dose averaged LET (LET_d). Biological outcomes depend on both dose and LET and the LET_d takes both into consideration as the deposited energy is weighted by the relative dose contribution of the

energy deposition event (Guan et al., 2015). LET_d at location $\vec{x}$ is given as

$$\mathrm{LET}_d(x) = \frac{\int_0^\infty S_{el}(E)d(E,\vec{x})dE}{\int_0^\infty d(E,\vec{x})dE} \tag{II.11}$$

II.1.3 Techniques of modern radiotherapy

The fundamental axiom of radiotherapy is to deliver dose to the tumour and to minimize the collateral damage to healthy cells. One of the methods to achieve this is to ensure the physical conformality of the dose to the tumour. Technologies developed to satisfy this need in photon therapy and particle therapy are summarized in the following sections.

II.1.3.1 Photon therapy treatment delivery techniques

The development of Multi Leaf Collimator (MLC) systems in photon therapy has enabled the efficient shaping of beams to closely match the shape of the tumour. This style of treatment delivery is known as Conformal Beam Radiotherapy (CBRT). Intensity Modulated Radiotherapy (IMRT), the next step in radiotherapy with MLC, is the current state of the art in photon therapy. In IMRT, the photon beam is sub-divided into beamlets where the intensity of each beamlet is regulated pseudo-independently using optimized MLC settings that model multiple beam window shapes. Each beam intentionally delivers a non-uniform intensity to the target. The superimposition of multiple intensity-modulated beams results in the desired dose distribution. Utilizing the additional degrees of freedom enables the generation of dose distributions that better conform to the target volume and/or better spare adjacent critical structures (Bortfeld, 2006; Khan and Gibbons, 2019).

II.1.3.2 Particle therapy treatment delivery techniques

There are two prevalent strategies to dose delivery with particle accelerators: (1) Passive scatter: which is the introduction of thin sheets of high-atomic-mass number materials to scatter and spread the beam. The shaping of the beam is done using custom built compensators that are created for each patient. (2) Pencil beam scanning: where magnets are used to scan the beam over a spatially discretized volume that is a close approximation of the target volume/tumour. Pencil beam scanning lends itself particularly well to the concept of Intensity Modulated Particle Therapy (IMPT). In addition to sharp physical dose characteristics of particles and pencil beam scanning in combination with depth control, the modulation of the beam intensity (controlled by the accelerator) results in a highly conformal dose that can model almost any tumour shape (Charlie Ma and Lomax, 2012; Lomax et al., 2001, 2004).

II.2 Radiobiology

Radiobiology facilitates the mechanistic understanding of radiation responses seen in the body which drives clinical decisions in radiotherapy. The fundamental biological responses result from damage to the DNA that programs the cell to initiate cell death which in turn triggers a retinue of other immunological responses to clear the dead cells. Although many models of radiation damage exist in literature, this thesis will employ the lethal-potentially lethal model to present a mechanistic description of radiation induced damage. The lethal-potentially lethal damage model broadly divides radiation induced damage into three categories (Bedford, 1991; Curtis, 1986; Hall and Giaccia, 2006):

1. Lethal damage: irreparable and irreversible cell damage that leads to cell death.
2. Sublethal damage: damage that can be repaired under normal circumstances within the time span of a couple of hours.
3. Potentially lethal damage: the component of radiation damage that can be modified by tumour micro-environment factors post irradiation.

The endpoint of tumour control, or lack of control, depends on a multitude of biological factors like the tumour micro-environment, tumour repopulation, immunological response, etc. (Joiner and van der Kogel, 2009).
The processes inducing biological damage occur at different time scales. The physical interactions initiate local effects where the incident particle interacts and ionizes atoms of the tissue occur in the range of 10^{-14} seconds. These interactions have been described in section II.1. The chemical reactions of the ionization products with molecules of the tissue occur in the chemical phase which is in the time scale of 10^{-12} to a few seconds. Physical interaction products chemically react to produce active free radicals that have the potential to produce damage by attaching themselves to DNA molecules. The biological phase corresponds to all effects seen following the chemical phase. These range from enzymatic response at the irradiation site within a few seconds to fibrosis which might present itself years after irradiation.
The primary cause of these biological effects is radiation induced cell death. The quantification of cell kill is done with the irradiation of clonogenic assays. Here colonies of cells grown in cell culture mediums are irradiated with varying doses and fractionation schemes to study the relation between cell kill, dose and fractionation. As shown in figure II.4, single fraction curves (- - - - , - - - -), on a log scale are quadratic in nature and are referred to as 'shouldered' dose response curves.

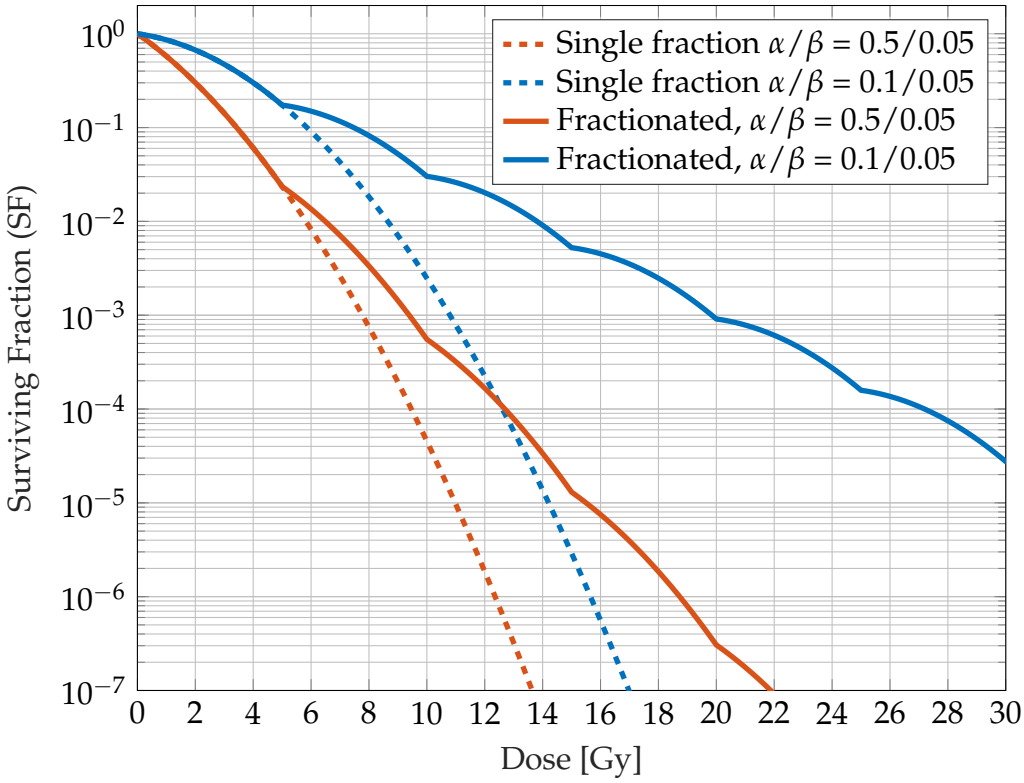

Figure II.4: Cell survival curves for two assays of cells different radiosensitivities ($\alpha/\beta = 0.5/0.05$ Gy and $\alpha/\beta = 0.1/0.05$ Gy) when (1) dose is given in a single fraction ($\alpha/\beta = 0.5/0.05$ Gy (- - - -) and $\alpha/\beta = 0.1/0.05$ Gy (- - - -)) and (2) dose is delivered in fractions of 5Gy ($\alpha/\beta = 0.5/0.05$ Gy (——) and $\alpha/\beta = 0.1/0.05$ Gy (——))

II.2.1 Linear Quadratic model

The LQ model is a fit of a simple mathematical function to cell survival curves. The surviving fraction (SF) of cells for an n fraction irradiation experiment is given as

$$SF = e^{-n(\alpha d + \beta d^2)} \tag{II.12}$$

where d is the dose delivered in each fraction, α [Gy^{-1}] and β [Gy^{-2}] are model fitting parameters, describing the radiosensitivity of the cell. After its formulation, many mechanistic models were suggested to ascribe meaning to the parameters of the LQ model. Sinclair described the process as *'to fit a mathematical expression to the shape of the curve and see if the result can be interpreted in terms of a model'* (Sinclair, 1966). In the context of the theory of lethal-potentially lethal damage, the initial region is dominated by the linear α term which is associated with lethal damage to the cell. As the dose is increased, the increasing curvature is related to the β term, which could be explained by an accumulation of potentially lethal and sublethal damages that turn in lethal damages. The general curvature of the survival curve is defined by the "α/β ratio" [Gy]. If cells are allowed to repair, the effect of the shouldered response curve is particularly significant as shown in figure II.4. Typically, healthy cells

(- - - -) have higher repair capacity, or lower overall radiosensitivity, compared to cancerous cells (- - - -). It is argued that prostate cancer is an example of an exception to this rule (van Leeuwen et al., 2018).
Fractionation of the dose is delivery of dose in sessions allowing the sublethal and potentially lethal damage to be repaired by the cell. Ignoring the effects of repair and repopulation, this accumulated fractional effects are seen as the bumpy curve shown in figure II.4. This results in a certain "linearization" of the cell survival curve that broadens the difference between the survival fraction of cells with low radiosensitivity or late responding tissues (——) and high radiosensitivity or early responding tissues (——). As cancer is the disease of uncontrolled proliferation of cells, it was assumed to have a high α/β ratio in the order of 10 Gy, comparable to early responding tissue. Therefore the fractionated doses would preferentially spare slowly dividing healthy cells. This allows for a safe escalation of doses to the tumour with acceptable normal tissues toxicity (Joiner and van der Kogel, 2009; McMahon, 2019).
Apart from the intrinsic radiosensitivity of different types of cells the LQ model parameters also depend on the radiation quality, as shown in figure II.5. The variation with radiation quality depends on the density of damage to the cell, i.e., the LET. Carbon ions and protons are considerably more effective than photons and this can be inferred from the steeper survival curves. It can also be observed that carbon ions, at the Bragg peak, show almost no gain from fractionation. Further details for the biological model for carbon ions are presented in sec II.2.3.

II.2.1.1 Translating *in vitro* to *in vivo*

There has been a persisent debate regarding the applicability of the LQ model derived from *in vitro* data to complex *in vivo* situations. The primary argument being the effect of difference in tumour microenvironments from the petri dish to the patient. This debate was colourfully described by the exchange between Dr. F.G. Spear and Dr. D. Gould in 1957 (Hall and Giaccia, 2006). Dr. Spear voices the skeptics with the statement: *'An isolated cell in vitro does not necessarily behave as it would have done, if left in vivo in normal association with cells of other types. Its reactions to various stimuli, including radiations, however interesting and important in themselves, may indeed be no more typical of its behaviour in the parent tissue than Robinson Crusoe on his desert island was representative of social life in York in the mid-seventeenth century'* .
The apt reply from Dr. Gould being: *'the in vitro culture technique measured the reproductive integrity of cells, and that there was no reason to suppose that Robinson Crusoe's reproductive integrity was any different on his desert island from what it would have been had he remained in York; all that Robinson Crusoe lacked was the opportunity! The opportunity to reproduce to the limit of their capability is afforded to cells cultured in vitro when they find themselves in the petri dish, with temperature and humidity controlled, and with an abundant supply of nutrients.'*
Therefore it can be argued that the LQ model presents an over estimation of the tumour cells' repopulation capacity but, the questions of the effect of tumour microenvironment on

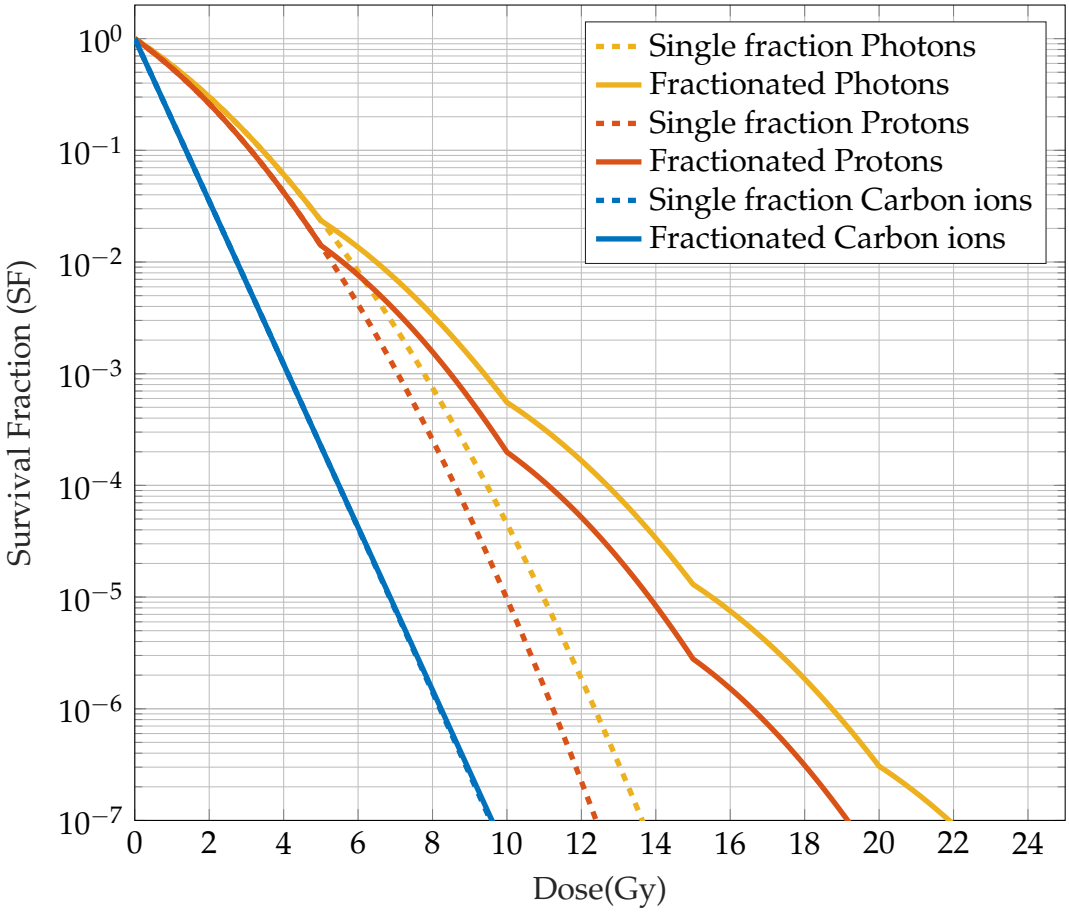

Figure II.5: Single fraction survival curves for photons (), protons () and carbon ions at the Bragg peak (); fractionated survival curves for photons (), protons () and a 255 MeVu^{-1} carbon ion beam at the Bragg peak () for tissue with constant intrinsic radiosensitivity ($\alpha/\beta = 0.5/0.05\,Gy$)

overall outcome of treatments remain a subject for research. The LQ model however, presents a simple model to explain the different responses from different tissues and the impact of fractionation. This model assumes that the clinical endpoints of tumour control or normal tissue response are driven by the death of a percentage of the cell population, which is related to surviving fraction of target cells (Douglas and Fowler, 1976).

There is evidence in literature that the LQ model does not describe all cellular responses. Some cells express a low-dose hyper sensitivity (< 0.5 Gy) after which the cell survival follows the LQ response (Joiner et al., 2001). It was also reported that the response at higher doses is linear, suggesting a linear-quadratic-linear response curve (Astrahan, 2008; Kirkpatrick et al., 2008).

II.2.1.2 Clinical application of the LQ model

The assumed clinical effect depends on the surviving fraction of cells, which is the ratio between the number of surviving cells and the initial number of cells. This can be described by a term known as the biological effect ε which is the negative logarithm of the surviving fraction SF. The biological effect to n fractions of dose d is given as

$$\varepsilon = -ln(SF) = n(\alpha d + \beta d^2) \tag{II.13}$$

where the total dose delivered is $D = nd$. Such a formulation also allows for the comparison of doses from different isoeffective fractionation schedules. As 2 Gy per fraction treatments are most prevalent in radiotherapy, treatments are commonly compared on the equivalence to dose in 2 Gy fractions, Equivalent Dose (EQD)2. For an arbitrary treatment schedule of dose d in n fractions the EQD2 is given as

$$\text{EQD2} = nd\left(\frac{d + \alpha/\beta}{2 + \alpha/\beta}\right) \tag{II.14}$$

Biologically Effective Dose (BED) is another concept used to compare treatment schedules without a specific reference treatment schedule. It can be interpreted as the isoeffective total dose needed as the fraction dose tends to zero (Barendsen, 1982; Fowler, 1989, 2010). It is closely related to the effect ε and is given as

$$\text{BED} = \frac{\varepsilon}{\alpha} = D\left(1 + \frac{d}{\alpha/\beta}\right) \tag{II.15}$$

It is particularly important to note that biological effect ε and its subsequent forms EQD2 and BED are additive. For treatments delivered in multiple fractions the individual biological effects can be summated to give the total biological effect (Jones et al., 2001).

II.2.1.3 Extensions of the LQ model

The issue of application of *in vitro* cell survival studies to patients is a very complex one riddled with several confounding factors apart from the expected cell kill. The success or failure of the treatment may be steered by an interplay of various intrinsic biological processes modulated by the tumour microenvironment commonly referred to as the 4 R's of radiobiology. Namely, repair of DNA damage, redistribution of cells in the cell cycle, repopulation and reoxygenation (Hall and Giaccia, 2006; Joiner and van der Kogel, 2009). Some of these factors can be accounted for with modifications and extensions to the LQ model, particularly in the context of repair and reoxygenation. However the clinical use of such models is quite uncommon due to the scarcity of data required to estimate clinically relevant model parameters. The effect of reoxygenation is one of the more clinically applied concepts.

The availability of oxygen plays a key role in the radiosensitivity of the tumour. Hypoxic cells exhibit a lower radiosensitivity than normoxic cells and this effective dose modifying factor is known as the Oxygen Enhancement Ratio (OER) given by

$$OER = \frac{d_{hypoxic}}{d_{normoxic}} \tag{II.16}$$

OER is the ratio between isoeffective dose to cells in hypoxic conditions $d_{hypoxic}$ to dose in reference oxic conditions $d_{normoxic}$. The mechanism behind this is described by the oxygen-fixation hypothesis which suggests that the presence of oxygen results in stable reaction products in the chemical interactions of free radicals with DNA, thereby "fixing" the damage (Joiner and van der Kogel, 2009). Therefore the influence of OER is minimal for particle therapy as compared to photons where free radical interactions are the main source of DNA lesions. The reoxygenation effect is primarily modulated by the vasculature around the tumour.

II.2.2 Relative Biological Effectiveness (RBE)

Higher LET radiation such as protons and carbon ions have a different microscopic dose distribution compared to photons and hence produce the same biological effect at lower doses. As most knowledge regarding protocols and dose prescription in radiotherapy comes from photon treatments there is a need to equate the two. The Relative Biological Effectiveness (RBE) enables the conversion of heavy ion dose into an isoeffective photon dose. The RBE is defined as the ratio between isoeffective dose from photons ($D_{photons}$) and high LET particles ($D_{particles}$) and is given as

$$RBE = \frac{D_{photons}}{D_{particles}} \tag{II.17}$$

RBE is an empirically derived quantity that depends on a multitude of factors such as choice of reference irradiation, which is usually Cobalt-60 gamma rays and on the biological aspects of the cell type being irradiated and the assumed end point for the irradiation experiment (Karger and Peschke, 2018; Kraft, 2000; Schlegel et al., 2008). It also depends on the physical aspects of the irradiation, such as dose and dose rate, type of particle, radiation quality and whether it is acute or fractionated exposure.

The isoeffective photon dose, i.e., RBE weighted dose ($RBE \times d$) for particles can be estimated by equating the biological effect (equation (II.13)) of particles $\varepsilon_{particles}$ to a photon effect, which gives

$$RBE \times d_{particles} = -\frac{\alpha_\gamma}{2\beta_\gamma} + \sqrt{\left(\frac{\alpha_\gamma}{2\beta_\gamma}\right)^2 + \frac{\varepsilon_{particles}}{\beta_\gamma}} \tag{II.18}$$

where α_γ, β_γ represent the intrinsic LQ model parameters for photons. The RBE increases with LET up to about 100 keVμm^{-1} after which the RBE decreases due to the overkill effect, as shown in figure II.6. The overkill effect is reduction of cell kill efficiency as single particle

interactions deposit much more energy than what is required to kill a cell. In the case of protons there is an expected increase in RBE at the end of range of the beam estimated to be between 1.2 - 1.4. However, as this increase is seen for a very small fraction of range of protons (McNamara et al., 2020), the clinically used RBE for protons is often assumed to be a constant 1.1 (Paganetti et al., 2002). On the other hand, RBE for carbon ions varies substantially over its entire trajectory. The modelling of RBE for carbon ions is described in the following section.

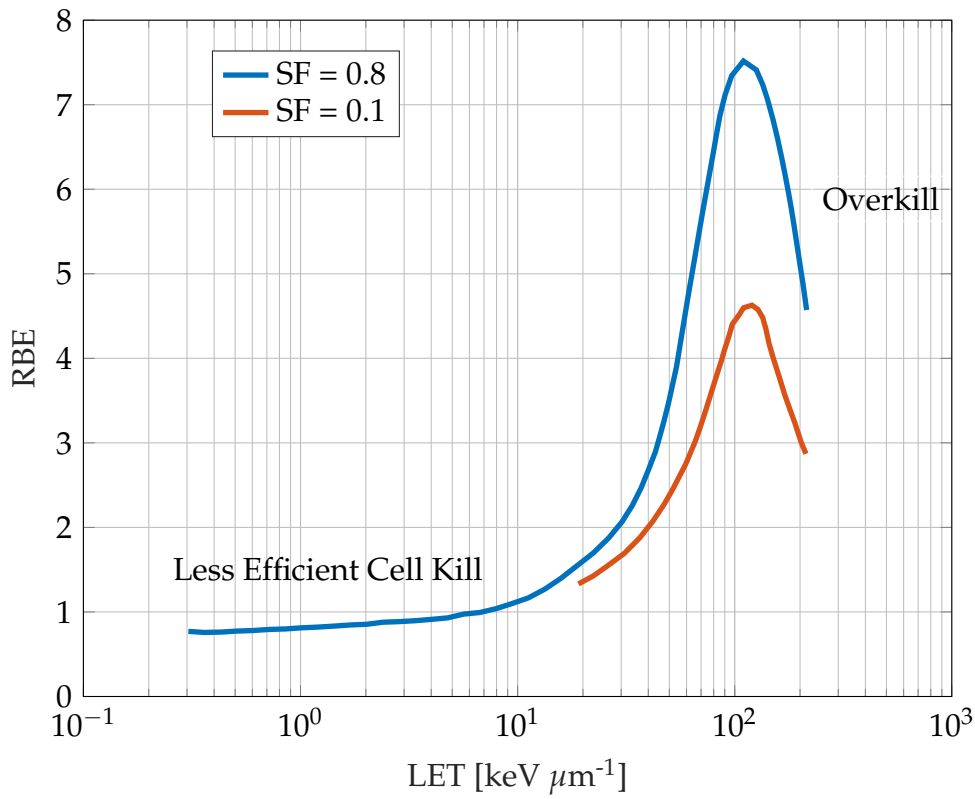

Figure II.6: RBE-LET relationship and the overkill effect for kidney cells at SF level of 0.8 and 0.1. Adapted from Barendsen (1968); Joiner and van der Kogel (2009)

II.2.3 Modelling biological effects of Carbon ions

When talking of modelling the biological effect of clinical carbon ion therapy, there are two main schools of thought:

1. Microdosimetric Kinetic Model (MKM) : It is the Japanese microdosimetric approach to modelling the biological effects of carbon ions in tissue. The surviving fraction of cells is predicted from the "specific energy" deposited in critical subcellular structures called domains. For further details the reader is referred to (Inaniwa et al., 2010; Karger and Peschke, 2018).

2. Local Effect Model (LEM): It is the approach used by the European carbon ion therapy centres. In this model, the biological target (cell nucleus) is divided into smaller subvolumes, where energy deposition from an incident particle is assumed to incite a local biological response comparable to that of a photon dose of the same magnitude (Karger and Peschke, 2018; Kraft, 2000; Scholz and Kraft, 1996).

This section will provide a brief overview of the fundamentals of LEM.

LEM was developed at Gesellschaft für Schwerionenforschung mbH (GSI) to calculate cell survival after heavy ion irradiation based on the understanding of cell survival effects for photon irradiations. The microscopic dose distribution of carbon ions is very different from that of photons as the energy deposition of heavy charged particles is peaked around the particle trajectory. To account for this, LEM uses the concept of local dose, i.e., the expectation value of the energy deposition at a spatial location for a given set of particle trajectories, as illustrated in figure II.7.

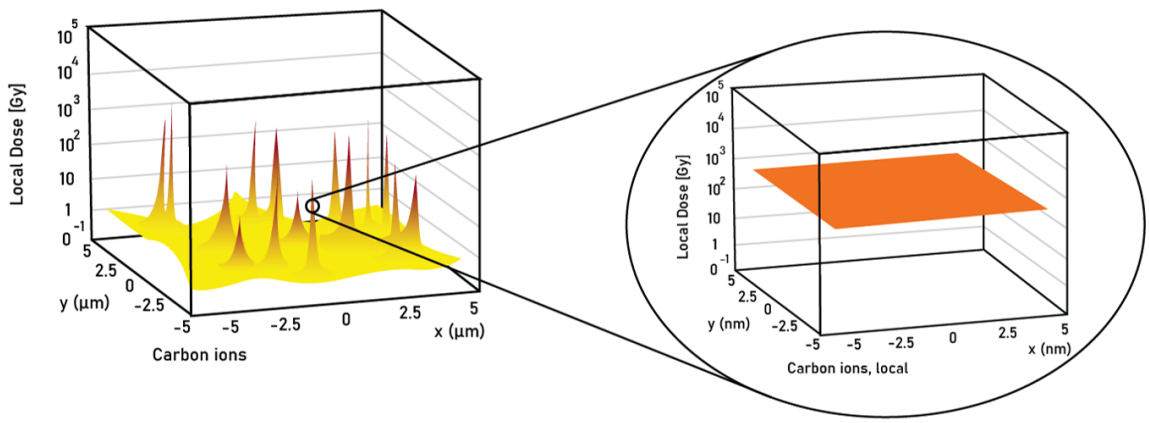

Figure II.7: Conceptual representation of microscopic dose deposition in cell nucleus and the concept of local dose. Adapted from Friedrich et al. (2011)

To calculate the local effect, LEM makes two fundamental assumptions: firstly, it assumes that the cell nucleus is the sensitive target that, when hit, results in cell kill and secondly, equal local doses should lead to equal local biological effects. This is extended to global effect

by first averaging local effects over the cell nucleus and secondly averaging over multiple cells. The functional modules required for LEM are (Karger and Peschke, 2018; Scholz and Kraft, 1996) :

1. Cell survival data for photons: As the local dose close to ion trajectories may be in order of 1000 Gy, the cell survival curve is described by an extended form of the LQ model where the shouldered curve is assumed to be purely exponential for doses greater than a threshold dose, d_t. The curve is described by the photon α_γ, β_γ parameters which are tissue specific, and the biological effect is given as

$$-ln(SF) = \begin{cases} \alpha_\gamma d + \beta_\gamma d^2 & d \leq d_t \\ \alpha_\gamma d_t + \beta_\gamma d_t^2 + s_{max}(d - d_t) & d > d_t \\ where: \quad s_{max} = \alpha_\gamma + 2\beta_\gamma d_t & \end{cases} \tag{II.19}$$

2. The radial dose distribution around the particle track is assumed based on the range of the most energetic δ- electrons produced by the primary charged particle.

3. The size of the target structure, i.e., cell nucleus, is specified.

4. The particle track distribution over the target structure is estimated using a Monte Carlo simulation. The dose distribution from fragments of incident carbon ion interactions is also modelled and adds on to the local dose.

5. The linking of photon effects to carbon ion effects. For photons, the probability of the target structure survival depends on the distribution and number of lethal events N_γ which is modelled using Poisson statistics

$$SF_\gamma(d) = e^{-N_\gamma(d)} \tag{II.20}$$

$$N_\gamma(d) = -ln\, SF_\gamma(d) = \alpha_\gamma d + \beta_\gamma d^2 \tag{II.21}$$

As the target substructures are uniformly distributed over the cell nucleus V, the overall photons lethal event density $v_\gamma(d)$ can be given as

$$v_\gamma(d) = \frac{N_\gamma}{V} = \frac{-ln\, SF_\gamma(d)}{V} \tag{II.22}$$

Similarly the local lethal event density resulting from ion dose at an arbitrary point $v_{ion}(d(x, y, z))$ is integrated over the entire target structure to obtain the average number of lethal events N_{ion}

$$N_{ion} = \int_x \int_y \int_z v_{ion}(d(x, y, z))\, dx\, dy\, dz \tag{II.23}$$

As mentioned above, LEM assumes that equal local doses result in equal biological effects, therefore equating v_γ and v_{ion} gives

$$N_{ion} = -ln\, SF_{ion}(d) = \int_x \int_y \int_z \frac{-ln\, SF_\gamma(d(x,y,z))}{V}\, dx\, dy\, dz \tag{II.24}$$

The α_{ion} parameter is estimated using the initial slope of the charged particle survival curve, a 'low-dose' approximation. The β_{ion} parameter is calculated by a proportional scaling of the intrinsic LEM β_z obtained from s_{max} in equation (II.19). Detailed description of estimation of α_{ion} and β_{ion} can be found in Krämer and Scholz (2006); Scholz et al. (1997); Wieser (2020). Over the years, LEM has gone through a few iterations of updates. As mentioned above the LEM I (first version) assumed equal local doses produce equal local effects. This version of the model reported deviations in the order of 10 % to 20 % for therapy relevant conditions (Grün et al., 2012). The LEM II improved on the estimation of yield of double strand breaks from the induction of single strand breaks in close proximity to the particle trajectory. It also considered indirect effects from free radical diffusion (Elsässer and Scholz, 2007). LEM III boasted of a more detailed track structure (Elsässer et al., 2008). The current most updated version, LEM IV makes a fundamental change, stating that: the biological response is directly linked to the initial spatial distribution of DNA damage rather than the dose distribution itself, i.e., similar patterns of double strand breaks lead to similar biological effects. It introduces an intermediate step of estimating double strand breaks and clusters of lesions in DNA, that are homogeneously distributed over the cell nucleus, using Monte Carlo simulations.
Compared to LEM I (——, - - - -), LEM IV (——, - - - -) predicts a lower magnitude of the effective carbon α_C and a higher effective β_C value, as shown in figure II.8.

This results in a lower RBE prediction, calculated by equation (II.18), in the intermediate LET region (Friedrich et al., 2012). Figure II.9 shows a comparison of predicted RBE dependence on LET between LEM I, LEM IV and cell survival data (Furusawa et al., 2000) for heavy ions (Friedrich et al., 2012). LEM IV, compared to LEM I, is able to better predict the *in vitro* RBE for carbon ions.

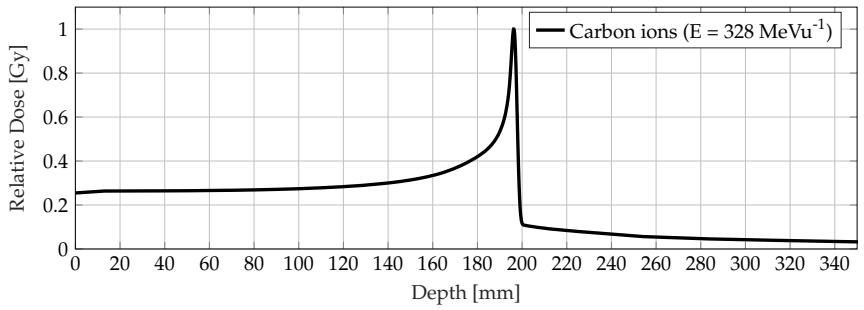

(a) Relative depth dose profile

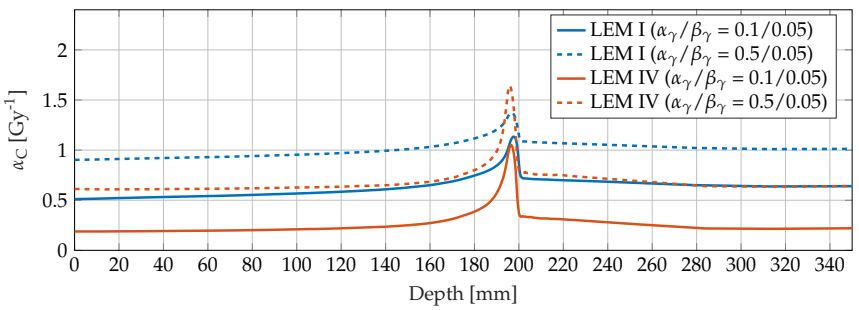

(b) Carbon α^C

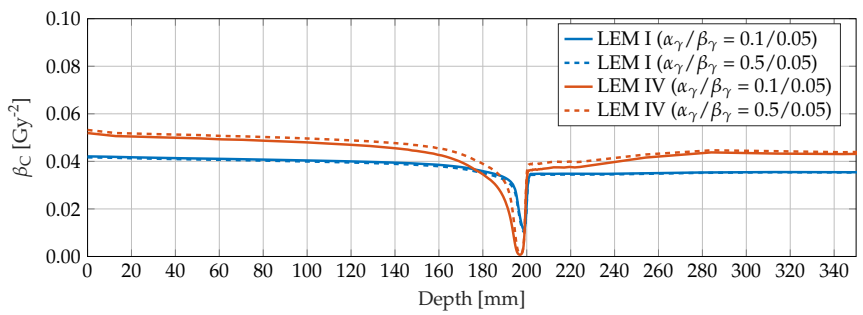

(c) Carbon β^C

Figure II.8: Carbon α and β prediction by LEM I and LEM IV for photon α/β of $0.1/0.05$ Gy and $0.5/0.05$ Gy for a carbon ion beam of 328 MeVu^{-1}

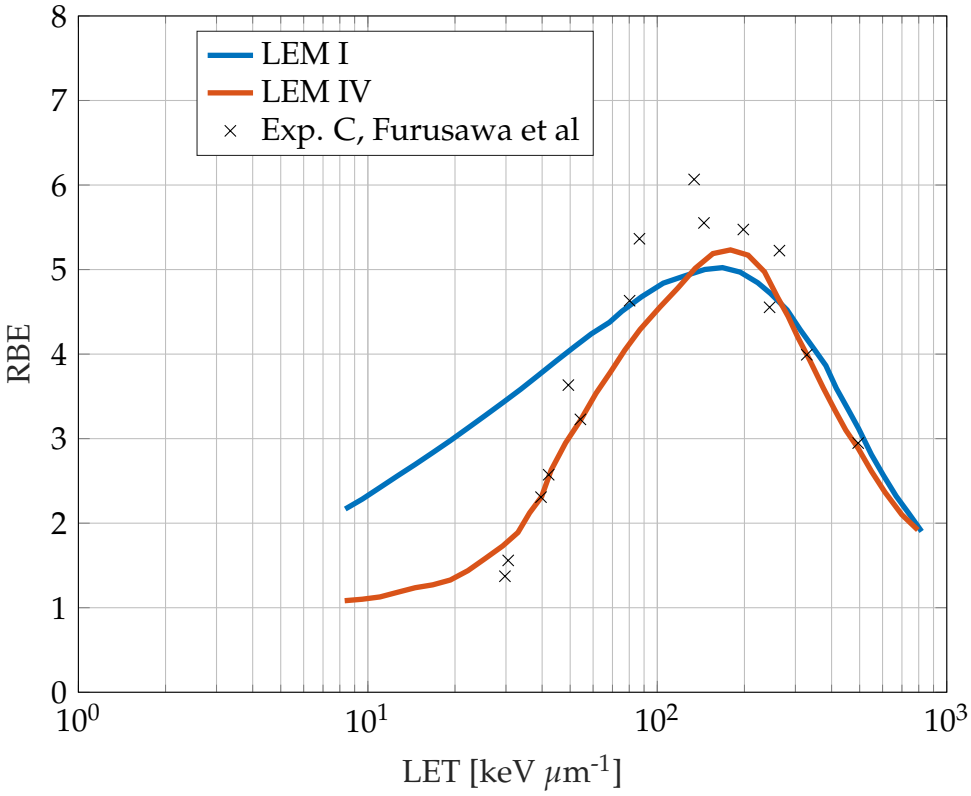

Figure II.9: Comparison of predicted RBE from LEM I and LEM IV models against experimental data for carbon ion irradiation from (Furusawa et al., 2000). Figure adapted from (Friedrich et al., 2011)

II.3 Treatment Planning

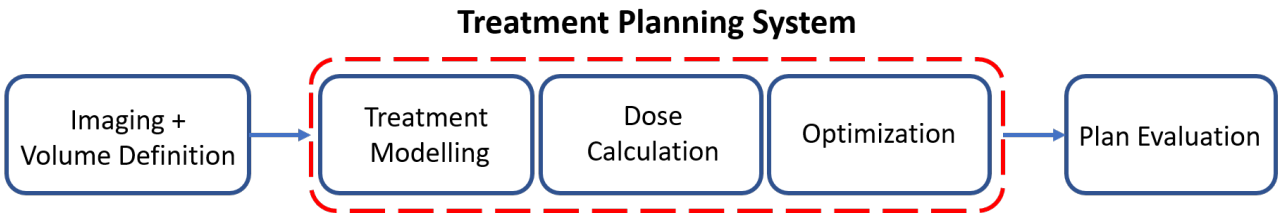

Figure II.10: Treatment planning workflow with particular emphasis one the tasks carried out within the treatment planning system (▬).

Figure II.10 describes elements of a treatment planning workflow emphasizing the treatment planning system and its components. A summary of each component of the workflow is presented in the following sections.

II.3.1 Imaging and volume definition

The first step in any treatment planning workflow is to obtain imaging data used for planning. CT is the primary imaging modality used and it serves two purposes. First, the planning CT in combination with diagnostic imaging (diagnostic CT, MRI and Positron Emission Tomography (PET)) is used by the oncologist to identify anatomical regions of interest in the patient (Burnet et al., 2004; ICRU, 2010):

1. The extent and position of the palpable or imaged tumour is known as the Gross Tumour Volume (GTV).

2. The Clinical Target Volume (CTV) contains the GTV plus a margin to account for sub-clinical disease spread that cannot be visualized in imaging. This is primary volume to be irradiated to achieve a cure.

3. The Planning Target Volume (PTV) is a margin around the CTV that accounts for uncertainties in treatment planning and delivery.

4. OARs are the critical structures in and around the target volumes that must be spared of dose.

These delineations serve as a map of the tumour to be irradiated, of adjacent OARs to be spared of dose and a map of the uncertainty associated with the treatment. A series of such images taken over the course of the treatment and to monitor and adapt the treatment to physical and physiological changes in the patient. Secondly, the CT also provides material characteristics of the tissue which is described in the next section II.3.2.

II.3.2 Treatment Modelling

In order to simulate a treatment within the Treatment Planning System (TPS), a physical model of the patient and the treatment must be created. Physical characteristics of the tissue are modelled using a CT where the attenuation of photons is measured with a dimensionless quantity known as Hounsfield Units (HU). The HU act as a surrogate for the linear attenuation coefficient. However it must be noted that the linear attenuation coefficient for photons in the keV range is not equal to that of photons in the MeV range. The HU also provides an estimate of the electron density of the tissue. In the context of photon therapy, the electron density is an essential part of dose calculation as most of the dose deposited by photons in the tissue is deposited by secondary electrons which in turn depends on the electron density. However HU itself does not directly describe the electron density, the conversion to electron density is achieved using an experimentally derived calibration curve known as the Hounsfield lookup table (HLUT). In the context of particle therapy, the HU is used to estimate the Stopping Power relative to Water (rSP) using a experimentally derived machine-specific look up table (Moyers et al., 2010; Newhauser and Zhang, 2015). The integral of the rSP is a quantity know as the Water Equivalent Path Length (WEPL). For a particle travelling through tissue, it is a measure of the equivalent distance travelled by the particle in water (Ma and Wang, 2013). WEPL is essential in dose calculation for particle therapy to estimate the residual energy of the particle and hence deduce the spot position.

The electron density / rSP information is stored as a discretized three-dimensional cube, where each sub unit, a voxel, defines a point in space. The center of mass of the tumour is usually defined as the isocenter. In the treatment machine, the patient, particularly for deeper tumours, is positioned such that the axis of rotation of the treatment head passes through the isocenter.

The treatment delivery planning process itself begins with the identification of ideal beam

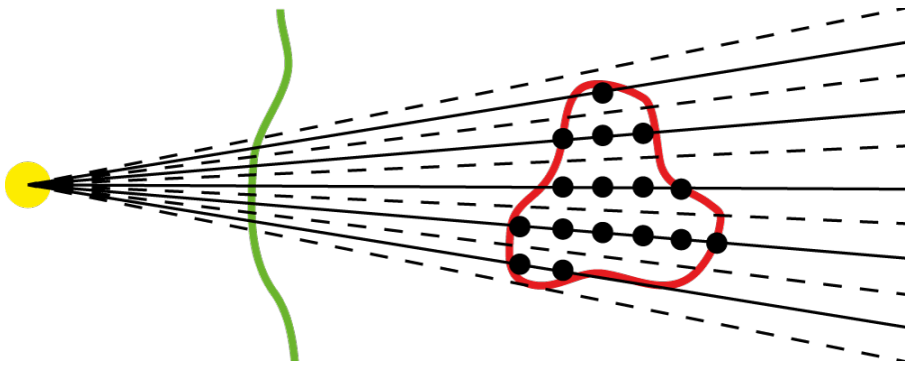

Figure II.11: A schematic visualization of the ray and bixel concept. (●) is the point source of radiation, ▬ represents the surface of the patient, (▬) represents the contour of the target volume and (●) represents the spot (Bragg peak) placement for particle therapies. Accessed from `https://github.com/e0404/matRad/wiki/Dose-influence-matrix-calculation`

angles that avoid OARs. Figure II.11 is a schematic of a point source of irradiation (●) delivering a single beam to the target volume (▬) after entering the patient surface (▬). Here the dashed lines (- - - -) represents the edges of the photon pencil beam and the black

dots (● on ——) represent the spot (Bragg peak) placement for particle therapies. As mentioned in II.1.3.2, particle therapy has three degrees of freedom with regards to spot placement: (1) control of range of beam by regulating the energy of the beam and (2) lateral deflection and positioning of the beam in a plane perpendicular to the beam direction, also known as an energy layer. In this thesis, the term *bixel* will be used to describe the individual pencil beams for photon therapy and particle therapy (bixels or spots). Once the beam and patient geometry is formalized, the dose calculation and optimization processes are possible.

II.3.3 Dose Calculation

The dose calculation engine of the treatment planning system is the algorithm used to estimate the absorbed dose in the patient. They can be classified into three main categories:

1. Grid Based Boltzmann equations Solvers (GBBS): The linear Boltzmann transport equation (LBTE) describes the macroscopic behaviour of ionizing particles as they pass through and interact with matter. GBBS is an analytical method that directly solves the Boltzmann transport equation through descretized space, angle and energy (Vassiliev et al., 2010).

2. Monte Carlo methods: The stochastic approach to solving the LBTE, where the paths and individual interactions of packets of particles are simulated to calculate the absorbed dose. Monte Carlo engines are considered as the gold standard in dose calculation. However, they are computationally intensive, time consuming methods.

3. Convolution Based Methods: dose is calculated based on precalculated models of absorption of dose in water that act as impulse response kernels to beam intensities.

For the thesis in hand, the focus will be on convolution based dose calculation, i.e., the pencil beam algorithm. Pencil beam dose calculation algorithms are two step processes where, first, the energy deposited by the primary particles is calculated. Then, the energy transported by secondary particles is calculated using dose kernels.

In photons, the energy deposited by the primary particles is given by the TERMA as presented in equation (II.6). The dose deposited by secondary particles is modelled using a point spread kernel as shown in the figure. The photon energy deposition kernels can be generated using Monte Carlo simulations (MacKie et al., 1988). The TERMA and the dose kernel are combined using a convolution superposition operation to calculate the absorbed dose (Ahnesjö and Aspradakis, 1999;

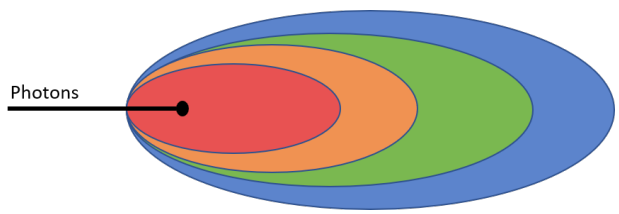

Figure II.12: Graphical representation of a photon point spread kernel

Bortfeld et al., 1993). The absorbed dose d at point (x, y, z) from interaction points (x', y', z') is given as

$$d(x,y,z) = \int_E \int_{z'} \int_{y'} \int_{x'} \text{TERMA}(x',y',z',E) k_{PSF}(x-x', y-y', z-z', E) dx'dy'dz'dE \quad \text{(II.25)}$$

where $k_{PSF}(x-x', y-y', z-z', E)$ is the translation invariant point spread kernel. Compared to Monte carlo methods and GBBS methods, the convolution dose calculation reduces the dose calculation time down to a few seconds.

In the case of heavy ion therapy, the integral dose ID from primary particles and the width of beam as a function of water equivalent path length (WEPL) are tabulated from Monte Carlo simulations and measurements into a look up table. The dose at a point $d(x, y, z)$ by a pencil beam along the z-axis positioned at (x_0, y_0) is assumed to be the product of a depth component ID and two lateral gaussian scatter components (Schaffner et al., 1999) given by

$$d(x,y,z) = N_p ID(z_{WEPL}) \frac{1}{2\pi\sigma_x\sigma_y} \left(e^{-(x_0-x)^2/2\sigma_x^2}\right) \left(e^{-(y_0-y)^2/2\sigma_y^2}\right) \quad \text{(II.26)}$$

where N_p is the number of primary particles at the beam spot, z_{WEPL} is the WEPL along the z-axis and σ_x, σ_y are the standard deviations of the Gaussians in x and y direction that include contributions of the overall beam divergence and Coulomb scatter in the patient. This model however does not fully represent the wider low dose bath from strongly scattered particles. Therefore, a superposition of two weighted normal distributions is used for each lateral direction (Parodi et al., 2013).

II.3.4 Treatment Plan Optimization

Optimization or "inverse planning" is one of the cornerstones of treatment planning for radiotherapy. The dose prescribed to a patient is decided by the radiation oncologist based on knowledge and experience of Tumour Control Probability (TCP) and Normal Tissue Complication Probability (NTCP). The aim of treatment plan optimization is to identify a set of parameters, beam angles and pencil beam intensities, that results in a fluence distribution that would best realize these clinical objectives. In modern radiotherapy with intensity modulated treatment modalities, optimization for beam intensities is a highly dimensional problem with the number of variables being in the range of thousands. The characterisation of optimality of the treatment plan is based on a scoring function, also known as the objective function and the optimal solution is derived by minimizing this objective function. Naturally, the obvious choice for framing this objective function would be in the context of TCP and NTCP. However, due to the lack of validated and accepted models of tumour response, the optimization problem is conventionally phrased in the context of dose and dose volume criteria.

II.3.4.1 Physical dose based optimization

Within the treatment plan optimization process, the dose is required to be recalculated for each iteration. Therefore, to save on time and computation, the dose contribution to each voxel in the patient from each pencil beam (photon or heavy ion) for fixed beam geometry is precalculated and stored in a dose influence matrix. The elements of the dose influence matrix, D_{ij}, represents the dose to voxel i from pencil beam (bixel) j with unit intensity. Absorbed dose d_i is calculated by accumulating dose contributions from all intensity weighted w_j elementary pencil beams. Individual treatment goals are formulated as a set of objective functions f_m. The inverse planning process estimates a set of pencil beam weights w that result in a dose distribution that minimizes the overall objective function $\mathcal{F}$

$$\begin{aligned} \underset{w}{\text{minimize}} \quad & \mathcal{F}(\boldsymbol{d}) = \sum_m p_m \, f_m(\boldsymbol{d}) \\ \text{subject to} \quad & c_k^l \leq c_k(\boldsymbol{d}) \leq c_k^u && \forall k \\ & d_i = \sum_j D_{ij} \, w_j && \forall i \\ & w_j \geq 0 && \forall j \end{aligned} \tag{II.27}$$

The objective function $\mathcal{F}(\boldsymbol{d})$ is the sum of the individual objectives $f_m(\boldsymbol{d})$ weighted by an importance or *penalty* factor p_m. c_k^l, c_k^u are the lower and upper bounds for constraint $c_k(\mathbf{d})$. The optimization is subject to a positivity constraint on pencil beam weights w. The individual objective functions are usually defined separately for each of the Volumes of Interest (VOIs), i.e., target structures and OARs. Common types of objective functions applied in radiotherapy are given in table II.3.4.1 (Oelfke and Bortfeld, 2001; Wieser et al., 2017; Wu and Mohan, 2000). Assuming the treatment plan objective function to be a combination of these objectives, the desired dose distribution is found by solving a convex non-linear objective function (Llacer et al., 2003). Typically a large-scale quasi Newton method is used to compute the optimal solution using explicit gradient computations and Hessian approximations. The gradient is given by

$$\nabla_w \mathcal{F} = \frac{\partial \mathcal{F}}{\partial w} = \frac{\partial \mathcal{F}}{\partial d} \frac{\partial d}{\partial w} \tag{II.28}$$

The most common method to ensure that clinical prescribed dose is achieved in the target volume is by treating it as a reference dose d_{ref} and penalizing any deviation in dose in the voxel d_i, given by the squared deviation objective ($d_{sq\ deviation}$). This objective drives the optimizer to achieve a uniform dose distribution in the volume S. The squared deviation objective can be split into the squared underdosage objective ($f_{sq\ underdosage}$) for target volumes and squared overdosage objectives ($f_{sq\ overdosage}$) for OARs, each affected only on positive values of the Heaviside function Θ. The mean dose objective f_{mean} is generally used to reduce dose to the normal tissues as the mean dose directly contributes to the overall objective function value. This must be used cautiously as it does not differentiate between the possible shapes of dose fall off, i.e., high dose with steep gradient or lower dose with low gradient.

Table II.1: Dose based objectives commonly used in radiotherapy. d_i dose in voxel i, d_{ref} is the prescribed or reference dose level in VOIs S with N_S number of voxels. a is the equivalent uniform dose parameter and Θ is the unit step Heaviside function. (Wieser et al., 2017)

Squared overdosing	$f_{sq\,overdoseage} =$	$\frac{1}{N_S}\sum_{i\in S}\ \Theta(d_i - d_{ref})(d_{ref} - d_i)^2$
Squared underdosing	$f_{sq\,underdoseage} =$	$\frac{1}{N_S}\sum_{i\in S}\ \Theta(d_{ref} - d_i)(d_{ref} - d_i)^2$
Squared deviation	$f_{sq\,deviation} =$	$\frac{1}{N_S}\sum_{i\in S}\ (d_{ref} - d_i)^2$
Mean dose	$f_{mean} =$	$\frac{1}{N_S}\sum_{i\in S} d_i$

In literature, there are many other kinds of dose objectives presented such as dose-volume objectives that are more similar to clinical dose objectives which are presented as maximum or minimum dose acceptable in a subvolume of the structure and the Equivalent Uniform Dose (EUD) objectives that translate inhomogenous doses in OARs to equivalent uniform dose distributions in order to evaluate the dose-volume criteria.

II.3.4.2 Effect Based Optimization

For proton radiotherapy, considering a constant RBE of 1.1, the optimization process can be identically defined as RBE weighted dose criteria (Oelfke and Bortfeld, 2001; Wu and Mohan, 2000). This is not the case for carbon ions as the RBE varies along the beam trajectory. Furthermore, in this thesis, as the intent is to combine different modalities, the optimization problem is framed in the context of biological effect (equation (II.13)) reiterating the assumption that the endpoints of tumour control or normal tissue response result from the death of a percentage of population of cells, irrespective of modality used to irradiate. The biological effect $\varepsilon_i(w)$ in voxel i is given by

$$\varepsilon_i(w) = \alpha_i \sum_j D_{ij} w_j + \beta_i \left(\sum_j D_{ij} w_j \right)^2 \tag{II.29}$$

where the α_i and β_i are the effective LQ model parameters in voxel i. For protons and photons, this corresponds to the intrinsic photon α and β parameters. For carbon ion beams, the biological effect in the voxel results from an accumulation of effects from different radiation qualities, e.g. ions of different energy in the same beam or from a different beam angle in a multifield plan. The effective α_i and β_i in voxel i are determined by a dose weighted average given by

$$\alpha_i = \frac{\sum_j \alpha_{ij}\, D_{ij}\, w_j}{\sum_j D_{ij}\, w_j} \qquad \text{and} \qquad \sqrt{\beta_i} = \frac{\sum_j \sqrt{\beta_{ij}}\, D_{ij}\, w_j}{\sum_j D_{ij}\, w_j} \tag{II.30}$$

where α_{ij} and β_{ij} are the LQ model parameter contributions in voxel i from pencil beam j (Wilkens and Oelfke, 2005, 2006; Zaider and Rossi, 1980). Substituting equation (II.30) into equation (II.29) gives

$$\varepsilon_i(w) = \sum_j A_{ij} w_j + \left(\sum_j B_{ij} w_j \right)^2 \tag{II.31}$$

where $A_{ij} = \alpha_{ij} D_{ij}$ and $B_{ij} = D_{ij}\sqrt{\beta_{ij}}$. The A_{ij} and B_{ij} matrices can be precalculated for a given beam setup and are used to speed up the process of biological effect calculation for optimization.
The optimization problem is then defined as (Wilkens and Oelfke, 2005):

$$\begin{aligned} \underset{w}{\text{minimize}} \quad & \mathcal{F}(\boldsymbol{\varepsilon}) = \sum_m p_m \, f_m(\boldsymbol{\varepsilon}) \\ \text{subject to} \quad & c_k^l \leq c_k(\boldsymbol{\varepsilon}) \leq c_k^u && \forall k \\ & \varepsilon_i = \alpha d_i + \beta d_i^2 && \forall i \\ & d_i = \sum_j D_{ij} \, w_j && \forall i \\ & w_j \geq 0 && \forall j \end{aligned} \tag{II.32}$$

As the prescribed doses are primarily defined in the context of photon irradiation, the reference prescribed dose objectives are converted to prescribed biological effects ε_{ref} with with photon α and β parameters.

Table II.2: Objectives considering biological effect ε_i in voxel i, ε_{ref} is the prescribed or reference biological effect level in VOIs S with N_S number of voxels. Θ is the unit step Heaviside function. (Frese, 2011; Oelfke and Bortfeld, 2001)

Squared overdosing	$f_{sq\,overdoseage} =$	$\frac{1}{N_S}\sum_{i\in S} \Theta(\varepsilon_i - \varepsilon_{ref})(\varepsilon_{ref} - \varepsilon_i)^2$
Squared underdosing	$f_{sq\,underdoseage} =$	$\frac{1}{N_S}\sum_{i\in S} \Theta(\varepsilon_{ref} - \varepsilon_i)(\varepsilon_{ref} - \varepsilon_i)^2$
Squared deviation	$f_{sq\,deviation} =$	$\frac{1}{N_S}\sum_{i\in S} (\varepsilon_{ref} - \varepsilon_i)^2$
Mean dose	$f_{mean} =$	$\frac{1}{N_S}\sum_{i\in S} \varepsilon_i$

II.3.4.3 Spatio-temporal Optimization

The effect based optimization approach is at the core of treatment planning for carbon ions and from the perspectives of photons and protons, effect or BED based treatment planning strategies presented in literature offer new opportunities to optimize the overall treatment (the concept of effect based optimization can easily be extended to a BED based optimization as the shown in equation (II.15)). The method of non-uniform spatio-temporal optimization presents the possibility to deliver distinct fraction dose distributions that potentially improve the overall treatment plan quality. This is achieved by hypofractionating subregions of the tumour while hyperfractionating normal tissue (Adibi and Salari, 2018; Gaddy et al., 2018; López Alfonso et al., 2017; Unkelbach et al., 2016; Unkelbach and Papp, 2015; Unkelbach et al., 2013). Spatio-temporally optimized plans add an additional degree of freedom in the temporal domain allowing for a superposition of distinct fractional biological effects that yields a uniform overall biological effect in the tumour that is more conformal, hence sparing more healthy tissue. For an n fraction single modality treatment, the effect based

spatio-temporal optimization problem can be given as

$$\begin{aligned}
\underset{w}{\text{minimize}} \quad & \mathcal{F}(\boldsymbol{\varepsilon}) = \sum_m p_m \, f_m(\boldsymbol{\varepsilon}) \\
\text{subject to} \quad & c_k^l \leq c_k(\boldsymbol{\varepsilon}) \leq c_k^u && \forall k \\
& \varepsilon_i = \sum_{t=1}^{n} \alpha d_{ti} + \beta d_{ti}^2 && \forall i \\
& d_{ti} = \sum_j D_{ij} \, w_{tj} && \forall i, \forall t \\
& w_{tj} \geq 0 && \forall j, \forall t
\end{aligned} \tag{II.33}$$

where d_{ti} is the dose delivered to voxel i and w_{tj} is the intensity of pencil beam j in fraction t. The objectives presented in II.3.4.2 can be used to codify the clinical prescriptions.
The conventional dose based optimization problem mentioned in the previous chapter is a convex problem and therefore the optimal solution can be found using gradient descent methods. The effect and BED based optimization problem may be non-convex due to quadratic definition of biological effect. For objective function $\mathcal{F}$ the weighted sum of convex functions f_1, f_2 are convex if the weights p_1, p_2 are non-negative

$$\mathcal{F} = p_1 f_1 + p_2 f_2 \quad \Rightarrow \quad \mathcal{F} \text{ is convex} \tag{II.34}$$

hence the overall objective function $\mathcal{F}$ is convex if its base component objective functions are convex. The squared overdosage objective and mean objective are inherently convex. The critical term here is the effect based squared underdosage objective. Evaluated at voxel i for an n fraction treatment and prescribe effect ε_{ref}. With domain restricted to $0 \geq d_i \geq d_{ref}$ the Heaviside function can be ignored and the under dosage objective objective f_i^U and its first derivative $f_i'^U(d_i)$ are given as

$$\begin{aligned}
f_i^U(d_i) &= \left(\frac{\varepsilon_{ref}}{n} - \alpha_i d_i - \beta_i d_i^2\right)^2 \\
f_i'^U(d_i) &= 2(\frac{\varepsilon_{ref}}{n} - \alpha_i d_i - \beta_i d_i^2)(-\alpha_i - 2\beta_i d_i)
\end{aligned} \tag{II.35}$$

and the second derivative $f_i''^U$ is given as

$$f_i''^U(d_i) = 2\left[6\beta_i^2 d_i^2 - 2\alpha_i \beta_i d_i + (\alpha_i^2 - 2\beta_i \frac{\varepsilon_{ref}}{n})\right] \tag{II.36}$$

Therefore $f_i^U(d_i)$ is convex if the inequality

$$\frac{\alpha_i^2}{2\beta_i} \geq \frac{\varepsilon_{ref}}{n} \tag{II.37}$$

is satisfied. This goes to show that the biological parameters and prescribed effects are intrinsic variables of the effect based optimization problem that determin the convexity of the objective function. Furthermore, if the objective function is non-convex, a range of dose d_i can be derived

$$d_i > \frac{1}{6}\frac{\alpha_i}{\beta_i} + \frac{1}{6}\sqrt{\left(\frac{\alpha_i}{\beta_i}\right)^2 - 6\left[\left(\frac{\alpha_i}{\beta_i}\right)^2 + \frac{2\,\varepsilon_{ref}}{n\beta_i}\right]} \tag{II.38}$$

where the second derivative is positive and $f_i^U(d_i)$ is convex. The squared underdosage objective is not always convex however in the domain of the target volume, for clinically relevent prescribed doses the objective function is convex. A heuristic solution to this problem of convexity in practice would be a careful selection of the starting point of the optimization such that it is situated in the convex region of the objective function. The issue of convexity is presented in further detail by Gaddy et al. (2018); Unkelbach and Papp (2015), in the context of BED based spatio-temporal optimization, and by Frese (2011), in the context of effect based optimization for carbon ions.

II.4 Mixed Modality Treatments

Radiotherapy today has several modalities in its arsenal, each with its distinct physical and biological characteristics and associated costs. Therefore the natural question of the beneficial combination of two or more modalities arises. A review of literature into the techniques that have been proposed to combine radiotherapy modalities is presented in the following subsections. This section also highlights the knowledge gap in photon–carbon ion mixed treatments and presents the motivation for this thesis.

II.4.1 Clinical Practice

As there is a strong base of evidence for single modality treatments in radiotherapy, the clinical approach to mixed modality treatments is to separately optimize individual modalities and simply combine them based on the total physical and RBE weighted doses to correspond with the existing knowledge from photon therapy treatment response.

The combination of photons and electrons is motivated by the ability of electrons (light particles) to reduce dose to deep seated tissue. The delivery of such a treatment is quite convenient as electron irradiation can be carried out with minor alterations to clinical LINACs. There have been a number of early publications presenting this with the general recommendation that IMRT may be superior to using both modalities (Gupta et al., 2009; Krayenbuehl et al., 2007). This disadvantage may be attributed to the very low range and larger scatter from electron irradiations.

Protons on the other hand, have a considerably greater range in tissue which motivated

some studies to consider mixed modality treatments to improve on existing photon therapies. Proton-photon treatments have been primarily explored for indications with adjacent critical structures like Meningiomas, Chordomas, Chondrosarcomas and neuroendocrine carcinomas where the ability of particle therapy to create steep dose fall-offs is exploited. These studies report that combined treatments have a conformity inferior yet similar to only proton therapy treatments and report well tolerated normal tissue effects (Adeberg et al., 2017; Boskos et al., 2009; Feuvret et al., 2007; Fitzek et al., 2002; Noël et al., 2001; Wenkel et al., 2000). The combined plans were found to be comparable to conventional photon therapy but are expected to be beneficial in terms of reduction of post irradiation side effects. Apart from the highly conformal dose distribution possibilities the use of carbon ions is also motivated by its higher RBE, therefore studies investigated treatments with a carbon ion boost to photon irradiations. These studies show promising results for indications like Adenoid Cystic Carcinomas (ACC) (Akbaba et al., 2019a,b; Jensen et al., 2015; Schulz-Ertner et al., 2005, 2003), spinal and base of skull chordomas (Schulz-Ertner et al., 2003), for prostate cancer (Nikoghosyan et al., 2011) and Glioblastomas (Combs et al., 2010).
A possible extension of this strategy is the sequential optimization of the two modalities, where the second dose distribution compensates for the previous dose distribution in order to achieve the specified overall objectives (Wu and Mohan, 2000). This approach was retrospectively studied by (Krämer et al., 2014; Schuppert et al., 2020), where the IMRT plan was optimized taking into account the previously delivered carbon ion dose distribution. The study reported possible benefits from bias dose optimization due to favourable dose distribution characteristics. Such combinations of radiation modalities are not based on any unified optimization criterion and thus may not fully exploit the full potential of combined treatments.

II.4.2 Joint optimization of mixed modality treatments

The question of ideal combination of radiation modalities may be answered by a simultaneous optimization of the modalities within a framework that models the overall treatment. The approach has been put forward in several papers regarding simultaneous optimization of intensity modulated photon-electron fields based on a cumulative dose criteria (Alexander et al., 2012; Míguez et al., 2017; Mueller et al., 2017, 2018; Palma et al., 2012; Renaud et al., 2017, 2019; Xiong et al., 2004). The rationale being that electron beams would be used to reduce the integral dose to deeper healthy tissues and photons to improve the plan quality and conformity.
One motivation behind proton-photon combination treatments is the optimal utilization of limited proton fractions. Gao (2019) presents a joint optimization strategy for protons and photons based on physical dose that imposes a uniform dose regularization for each modality. The following proton-photon joint optimization strategies make no restrictions on the dose

shape delivered by each modality. Fabiano et al. (2020a) considers the joint optimization of a horizontal fixed proton beamline with photons based on a physical dose criteria. The joint optimized plans use photons to improve on the reduced plan quality of protons and protons are used to reduce the integral dose to normal tissue. Kueng et al. (2020) present a triple modality combination of photons, electrons and protons optimized on the overall physical dose. As an example, the general joint optimization problem based on cumulative physical dose $\mathbf{d}$ for photon–proton treatments can be written as

$$\begin{aligned} \underset{w^\gamma, w^p}{\text{minimize}} \quad & \mathcal{F}(\mathbf{d}) = \sum_m p_m \, f_m(\mathbf{d}) \\ \text{subject to} \quad & c_k^l \leq c_k(\mathbf{d}) \leq c_k^u && \forall k \\ & d_i = \sum_r D_{ir}^\gamma w_r^\gamma + \sum_s RBE \; D_{is}^p w_s^p && \forall i \\ & w_r^\gamma \geq 0 && \forall r \\ & w_s^p \geq 0 && \forall s \end{aligned} \tag{II.39}$$

where p_m are the penalties for individual objectives $f_m(\mathbf{d})$ based on the cumulative dose. w_r^γ, w_s^p are the intensities for pencil beams r , s for photons and protons, and dose influence matrix elements D_{ir}^γ and D_{is}^p represent the dose contributions of pencil beams r,s to voxel i for unit intensity respectively. RBE for protons is assumed to be constant (1.1).

Some joint optimization approaches have been suggested based on an overarching BED based criterion as defined in equation (II.15). Fabiano et al. (2020b); Unkelbach et al. (2018) approach the joint optimization problem assuming a predetermined number of photon and proton fractions. Here the joint optimization process is similar to the problem described in equation (II.39), but considers the cumulative BED $\mathbf{b}$. The implication of employing the cumulative BED is that the optimization considers the physical dose distribution and the temporal distribution of dose, i.e., fractionation. Therefore, OARs are spared not just by improved conformity of the dose but also by the uniform distribution of dose contributions over all fractions of the combined treatment. This is based on the concept of *spatio-temporal optimization* as described in section II.3. For a treatment of n^γ fractions of photons and n^p

fractions of protons, the joint optimization problem can be given as

$$
\begin{aligned}
\underset{w^\gamma, w^p}{\text{minimize}} \quad & \mathcal{F}(\mathbf{b}) = \sum_m p_m \, f_m(\mathbf{b}) \\
\text{subject to} \quad & c_k^l \leq c_k(\mathbf{b}) \leq c_k^u && \forall k \\
& b_i = n^\gamma d_i^\gamma \left[1 + \frac{d_i^\gamma}{(\alpha/\beta)_i}\right] + n^p \, RBE \, d_i^p \left[1 + \frac{RBE \, d_i^p}{(\alpha/\beta)_i}\right] && \forall i \\
& d_i^\gamma = \sum_r D_{ir}^\gamma w_r^\gamma && \forall i \\
& d_i^p = \sum_s D_{is}^p w_s^p && \forall i \\
& w_r^\gamma \geq 0 && \forall r \\
& w_s^p \geq 0 && \forall s
\end{aligned}
\tag{II.40}
$$

where $(\alpha/\beta)_i$ is the intrinsic photon α/β ratio in voxel i. The use of BED based optimization results in a BED distribution where protons deliver most of the dose to target volume, thereby hypofractionating the tumour and therefore reduce the integral dose to healthy tissue from photons. Ten Eikelder et al. (2019) approach the joint optimization problem without predefined number of fractions for either modality. The approach is an amalgamation of the optimization on cumulative BED and the optimal fractionation problem presented by Mizuta et al. (2012a,b); Saberian et al. (2016).

Looking into heavy ion therapy, the preliminary results of combination of different ion species was presented by Krämer et al. (2014) and Kopp et al. (2020) presents a combination of carbon ion - proton and carbon ion - helium ion therapy with the aim of delivering a uniform LET distribution in addition to the physical dose.

II.5 Motivation and Research questions

The presented theoretical background should equip the reader with a broad understanding of the physical and biological characteristics of photon and carbon ion beams in the context of radiotherapy. To broadly summarize, compared to photons, carbon ions can be used to generate dose distributions that are much more conformal to the tumour volume and greatly reduce the integral dose to healthy tissue due to their dose deposition characteristics. Carbon ions are also biologically more effective than photons and are unfazed by effects such as the OER. Although this increased effectiveness is favourable in the tumour, it comes at the cost of a proportionally increased cell kill in healthy tissue. Photons on the other hand are able to exploit the fractionation effect in order to spare healthy cells.

The aim of this thesis is to develop a framework to simultaneously optimize photon–carbon ion treatment plans to exploit each modality's strengths in combination treatments. To accomplish this, the physical dose contributions from photons and carbon ions must be translated into a common frame of reference and this is done using the RBE predictions from the LEM model. The evaluation of the overall biological effect, considering fractionation effects, is done using the LQ model for a predetermined number of fractions. Although an assessment of the sensitivity to the number of assigned fractions was carried out, the question of optimization to find the ideal fractionation schedule for photons and carbon ions is outside the scope of this thesis. The approach taken in this thesis is related to earlier work on joint optimization of photons–protons by Fabiano et al. (2020b); Unkelbach et al. (2018), but extends it to complex biological considerations required for carbon ions. Previous work in carbon ion combined treatments rely on a simple RBE based dose summation (Schuppert et al., 2020), or use LET as a surrogate for biological effects (Kopp et al., 2020). The approach presented here directly incorporates the radiobiological considerations for carbon ions into the joint optimization framework. This thesis also investigates the influence of the underlying parameters of joint optimization like: (1) the choice of fractionation schedules on joint optimized treatments and the impact on the individual dose contributions for photons and carbon ions. (2) The choice of tumour radiosensitivity parameters, as the decision to fractionate dose depends on the relative radiosensitivity of the tumour and the healthy tissue around it. (3) The choice of RBE prediction model for carbon ions on the overall treatment.

Finally, these concepts are applied to develop a mixed modality treatment strategy for infiltrative tumours where the CTV is composed of a mixture of tumour and healthy tissue. In this scenario the healthy tissue could ideally be spared by fractionating the dose using photons while utilizing carbon ions to irradiate the GTV. In order to achieve this, a composite objective function was developed to consider the biological effect in both tumour and healthy cells located at the same spatial location. This strategy is demonstrated for Glioblastoma cases where the clinical approach was a carbon ion boost to photon irradiation.

"To a man with a hammer
everything looks like a nail"
Mark Twain, 1835 - 1910

III
Materials and Methods

III.1 Joint optimization framework for photon–carbon ion treatments

This section lays out the mathematical framework for joint optimization of photon–carbon ion treatments and the intricacies associated with the incorporation of variable RBE models. The theoretical implications of joint optimization with differential LQ model parameters are illustrated using a one dimensional prototype. This serves to help understand the dependency of optimal combination of photons and carbon ions on the radiobiological characteristics of the two modalities. This section also highlights the implementation of the joint optimization work-flow and the technical complexities associated with combined treatment optimization. Finally, methodology for the application of combined treatments to spinal metastases, base of skull chordoma and glioblastoma are presented.

III.1.1 Formulation of the joint optimization problem

Unimodal radiotherapy treatment plan optimization is based on the physical dose for photons, or dose weighted by a constant RBE for protons (as described in section II.3.4.1). Carbon ions are optimized based on RBE weighted dose to account for the varying biological effectiveness along the beam path (as described in section II.3.4.2). Conventional mixed modality treatment planning is based on the sum of separately optimized unimodal treatments. In order to achieve a truly optimal combination, the two modalities must be considered simultaneously within the optimization. Therefore, the first step is to establish a common frame of reference for both modalities to evaluate the cumulative effects of treatment. Alexander et al. (2012); Míguez et al. (2017); Mueller et al. (2017, 2018); Palma et al. (2012); Renaud et al. (2017, 2019); Xiong et al. (2004) consider physical dose delivered as the constant frame of

reference to accumulate dose for photon–electron treatments, however such a method is not useful for photon–carbon ion combinations as carbon ions exhibit a high RBE compared to photons. Gao (2019), Fabiano et al. (2020a) and Kueng et al. (2020) optimize based on the RBE weighted dose for photon–proton combined treatments, this approach however does not model fractionation effects seen for inhomogenous dose distributions. One approach to solve this challenge is to use a biological dose quantity, such as BED, to accumulate dose as presented by (Fabiano et al., 2020b; Unkelbach et al., 2018). Such an approach is based on the spatio-temporal optimization strategy described in section II.3.4.3. The implementation of this BED based model to combined treatments with carbon ions is challenging due to the difficulty in computing dose averaged effective α^C/β^C from multiple beams.
The joint optimization of photon–carbon ion treatments presented in this thesis employs the *biological effect* to model non-linear effects arising from not only the variable RBE of carbon ions as described in section II.3.4.2, but also from the fractionation of dose. Such a formulation is similar to the BED based approach and can be trivially extended to include protons treatments. The biological effect is modelled with the basic LQ model (as presented in section II.2.1) and does not consider the time schedule of irradiation using photons or carbon ions. With a fixed biological effect based frame of reference for both modalities, the treatment can be optimized to prescription that has been also translated into biological effect. Assuming a photon–carbon ion treatment with n^γ fractions of photons and n^C fractions of carbon ions, the optimization problem can be written as

$$\begin{aligned}
\underset{w}{\text{minimize}} \quad & \mathcal{F}(\boldsymbol{\varepsilon}^{Total}) = \sum_m p_m \, f_m(\boldsymbol{\varepsilon}^{Total}) \\
\text{subject to} \quad & \varepsilon_i^{Total} = n^\gamma \varepsilon_i^\gamma + n^C \varepsilon_i^C && \forall i \\
& \varepsilon_i^\gamma = \alpha^\gamma \sum_j D_{ij}^\gamma \, w_j^\gamma + \beta^\gamma \left(\sum_j D_{ij}^\gamma \, w_j^\gamma \right)^2 && \forall i \\
& \varepsilon_i^C = \sum_k \alpha_{ik}^C D_{ik}^C \, w_k^C + \left(\sum_k \sqrt{\beta_{ik}^C} D_{ik}^C \, w_k^C \right)^2 && \forall i \\
& w_j^\gamma \geq 0 && \forall j \\
& w_k^C \geq 0 && \forall k
\end{aligned} \tag{III.1}$$

where the objective function $\mathcal{F}(\boldsymbol{\varepsilon}^{Total})$ is the sum of the individual objectives $f_m(\boldsymbol{\varepsilon}^{Total})$, based on the total biological effect $\boldsymbol{\varepsilon}^{Total}$, weighted by a penalty factor p_m. The total biological effect in voxel i is the sum of the fraction biological effects from photons and carbon ions, ε_i^γ and ε_i^C respectively, weighted by the number of predetermined fractions, n^γ and n^C. w_j^γ is the intensity of photon pencil beam j, and D_{ij}^γ is its dose contribution in voxel i for a unit intensity. α^γ, β^γ are the LQ parameters for photons which are constant for a given type of tissue. w_k^C is the intensity of the carbon ion pencil beam k and D_{ik}^C is its physical dose contribution in voxel i for a unit intensity. α_{ik}^C and β_{ik}^C are the effective LQ model parameters for carbon ions that depend on the spatial location of the voxel i within the beam path of beam k. The given

objective function is solved to obtain a set of pencil beam intensities for photons w_j^γ and carbon ions w_k^C that yields the optimal total biological effect distribution.
The effect based objective functions $f_m(\boldsymbol{\varepsilon}^{Total})$ considered in this thesis are given in table III.1. Namely, squared underdosage objectives are used to achieve target coverage. Whereas squared overdosage and mean dose objectives are used to incentivize the reduction of dose to healthy tissue by redistributing fluence spatially and between photon or carbon ion fractions. The prescribed effect is calculated using the clinical dose prescription and photon α/β ratio of the tissue.

Table III.1: Objectives considering biological effect ε_i in voxel i, ε_{ref} is the prescribed or reference biological effect level in VOIs S with N_S number of voxels. Θ is the unit step Heaviside function. (Frese, 2011; Oelfke and Bortfeld, 2001)

Squared overdosing	$f_{sq\,overdoseage} =$	$\frac{1}{N_S}\sum_{i\in S}\ \Theta(\varepsilon_i - \varepsilon_{ref})(\varepsilon_{ref} - \varepsilon_i)^2$
Squared underdosing	$f_{sq\,underdoseage} =$	$\frac{1}{N_S}\sum_{i\in S}\ \Theta(\varepsilon_{ref} - \varepsilon_i)(\varepsilon_{ref} - \varepsilon_i)^2$
Squared deviation	$f_{sq\,deviation} =$	$\frac{1}{N_S}\sum_{i\in S}\ (\varepsilon_{ref} - \varepsilon_i)^2$
Mean dose	$f_{mean} =$	$\frac{1}{N_S}\sum_{i\in S}\varepsilon_i$

An extension to the aforementioned joint optimization configuration is the hypothetical case of dual irradiation where both modalities can be delivered in each fraction. This can be achieved by a change to the formulation of total biological effect in voxel i, given by

$$\varepsilon_i^{Total} = n(\varepsilon_i^\gamma + \varepsilon_i^C) \qquad \forall\, i \tag{III.2}$$

where the objective functions are evaluated for an n fraction treatment. Such a hypothetical treatment strategy is motivated by the idea of giving the optimizer complete control on the choice of modality given the option of uniform fractionation with either modality.
The joint optimization formulation presented here can be flexibly extended to utilize additional modalities and alternative variable RBE models.

III.1.2 Fractionation in combined photon–carbon ion treatments

The concept of fractionation is driven by the underlying radiosensitivity characteristics of different types of tissue. When the tumour is more has a higher α/β ratio than healthy tissue the LQ model predicts better normal tissue sparing by fractionating the dose. However, if there is no difference in the α/β ratios or if healthy tissue is more radiosensitive, the treatment is motivated to hypo fractionate dose as there is no benefit from fractionating dose (II.2). Within a given fraction allocation between photons and carbon ions, the joint optimization implicitly considers the fractionation decision within the target volume. The decision to hypofractionate or hyperfractionate local regions of the target volume are implicitly considered by the joint optimization formulation.

As mentioned in section II.2.1, carbon ions are more effective than photons and therefore report a higher α/β ratio for both tumour tissue and healthy tissue. This leads to the question of the ideal dose contributions from carbon ions and photons when there is a need to fractionate dose and whether carbon ions allow for any fractionation at all.

In radiotherapy, the tumour boundary (GTV) is defined by the anomalous volume visible in imaging modalities, however in reality, this interface between tumour and healthy tissue is not necessarily so well defined. In order to assess the optimal fractionation of photons and carbon ions, consider a voxel on such an interface with the assumption that both tumour and healthy tissue exist within this voxel. The objective function evaluated for this voxel consists of an underdosage objective for tumour tissue considering a tumour α/β ratio ($\alpha^\gamma/\beta^\gamma = 0.5/0.05$ Gy) and an overdosing objective considering normal tissue α/β ratio ($\alpha^\gamma/\beta^\gamma = 0.1/0.05$ Gy). Consider a treatment where 4 Gy is prescribed in 2 independent fractions, translating to a prescribed biological effect to tumour cells $\varepsilon^T_{ref} = 2.4$ and effect limit in the healthy cells $\varepsilon^{NT}_{ref} = 0.8$. The optimal combination of both modalities may be now defined as the minimum of the following objective function $\mathcal{F}(\boldsymbol{\varepsilon}_i)$, which penalizes underdosage to the tumor and overdosage to the healthy tissue in voxel i.

$$\begin{aligned}\mathcal{F}(\boldsymbol{\varepsilon}_i) = \quad & \Theta\left(\varepsilon^T_{ref}(\alpha^\gamma_T,\beta^\gamma_T) - \varepsilon_i(\alpha^\gamma_T,\beta^\gamma_T)\right)\left[\varepsilon_{ref}(\alpha^\gamma_T,\beta^\gamma_T) - \varepsilon_i(\alpha^\gamma_T,\beta^\gamma_T)\right]^2 \\ & + \Theta\left(\varepsilon_i(\alpha^\gamma_{NT},\beta^\gamma_{NT}) - \varepsilon^{NT}_{ref}(\alpha^\gamma_{NT},\beta^\gamma_{NT})\right)\left[\varepsilon_{ref}(\alpha^\gamma_{NT},\beta^\gamma_{NT}) - \varepsilon_i(\alpha^\gamma_{NT},\beta^\gamma_{NT})\right]^2\end{aligned} \tag{III.3}$$

where $\varepsilon_i(\alpha^\gamma_T,\beta^\gamma_T)$, $\varepsilon_i(\alpha^\gamma_{NT},\beta^\gamma_{NT})$ are the cumulative biological effects from the 2 independent fractions d_1 and d_2, considering an α^γ, β^γ for tumour and healthy cells respectively. For a photon-photon combination the total biological effect $\varepsilon_i(\alpha^\gamma,\beta^\gamma)$ is given as

$$\varepsilon_i(\alpha^\gamma_s,\beta^\gamma_s) = (\alpha^\gamma_s d^\gamma_1 + \beta^\gamma_s (d^\gamma_1)^2) + (\alpha^\gamma_s d^\gamma_2 + \beta^\gamma_s (d^\gamma_2)^2) \qquad \forall s \in \{T, NT\} \tag{III.4}$$

For a photon- carbon ion combination, the total biological effect is given by

$$\varepsilon_i(\alpha^\gamma_s,\beta^\gamma_s) = (\alpha^\gamma_s d^\gamma_1 + \beta^\gamma_s (d^\gamma_1)^2) + (\alpha^C_{i,s} d^C_2 + \beta^C_{i,s} (d^C_2)^2) \qquad \forall s \in \{T, NT\} \tag{III.5}$$

where $\alpha^C_{i,s}$, $\beta^C_{i,s}$ are the effective carbon ion α, β parameters that depend on tissue specific $\alpha^\gamma_s, \beta^\gamma_s$ and the location of the voxel i in the carbon ion beam.
Figure III.1 shows the objective function values of equation (III.3) for a range of fractional doses d_1 and d_2 of a photon-photon combination and a photon–carbon ion combination sampled at three different locations along the carbon ion beam. (- - - -) shows the lower bound of isoeffective dose combinations that satisfy the tumour underdosage objective, i.e., $\varepsilon^T_i \geq 2.4$. (——) shows the upper bound of isoeffective dose combinations that satisfy the healthy tissue overdosage objective, i.e., $\varepsilon^{NT}_i \leq 0.8$. For the independent photon-photon combination there exists a dose combination of dose $d_1 = d_2 = 2Gy$ (o) that satisfies both the underdosage and overdosage objectives ($\mathcal{F}(\boldsymbol{\varepsilon}_i) = 0$). On the other hand with photon–carbon ion combinations, it is not possible to satisfy both objectives simultaneously. Furthermore, for the carbon ion α^C, β^C sampled at the entrance and tail region of the beam, there exists an optimal combination of photon–carbon ion doses d_1, d_2 that suggests a non-zero dose contribution of carbon ions. This implies that a marginal fractionation gain can be observed in these regions for carbon ions. The high values of α^C, β^C at the Bragg peak suggest no gain in fractionation and therefore the optimal solution is to deliver the prescribed dose solely using photons that would minimize the violation of the overdosage objective for normal tissue. The carbon ion α^C, β^C were predicted using the LEM IV model.

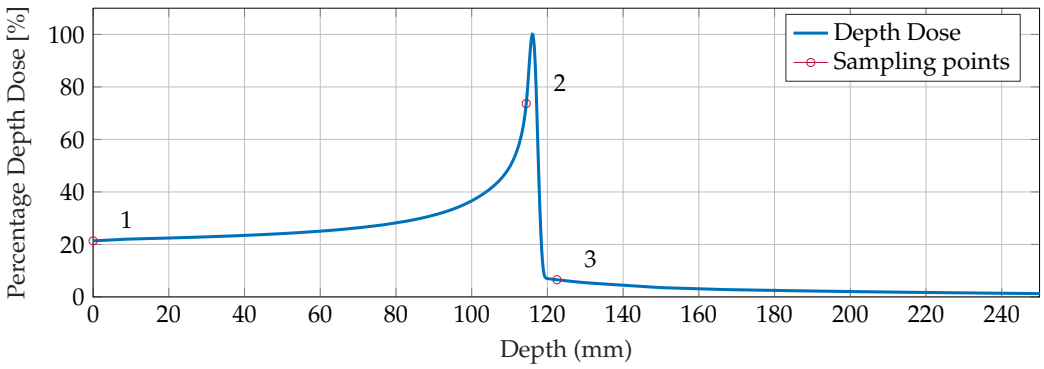

(a) Carbon ion beam, E = 241.03 MeV

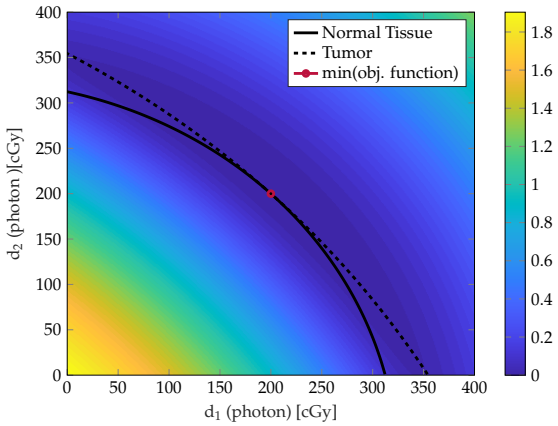

(b) Optimal photon-photon combination (two independent fractions)

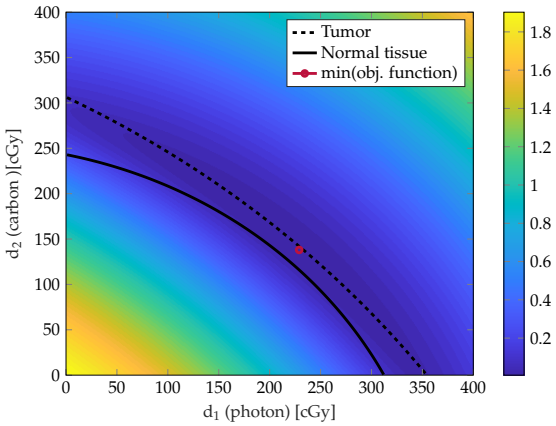

(c) Optimal photon–carbon ion combination (in the entrance region)

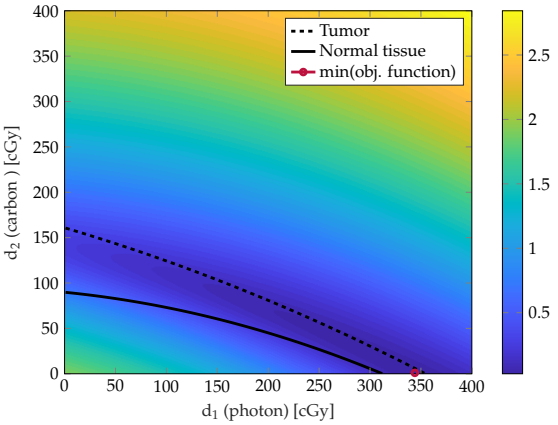

(d) Optimal photon–carbon ion combination (at the Bragg peak)

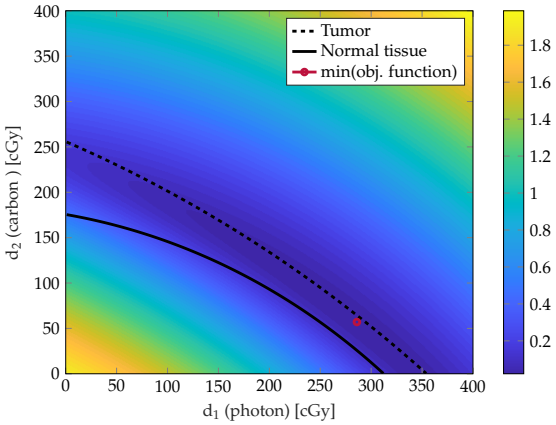

(e) Optimal photon–carbon ion combination (in the fragmentation tail)

Figure III.1: Iso-effective dose combinations that result in a total biological effect of 0.8 in normal tissue (▬▬) and 2.4 in tumour tissue (▪▪▪▪). (a) show the α^C, β^C sampling points along a carbon ion beam of 241.03 MeV for a photon–carbon ion combination. Objective function value is shown in the colourwash. ○ indicates the minimum of the objective function, i.e., the optimal combination of effect from two fractions d_1, d_2. (b) shows a photon-photon dose combination, and (c), (d), (e) show ideal photon–carbon combinations for carbon α^C,β^C sampled at points 11.6 cm before the Bragg peak, 0.2 cm before the Bragg peak, and 0.65 cm behind the Bragg peak, respectively.

III.1.3 Implementation

III.1.3.1 Software framework

The implementation of the combined treatment planning approach was developed on the existing framework for robust unimodal treatment planning in the open-source treatment planning platform matRad in the Matlab programming environment (Cisternas et al., 2015; Wieser et al., 2017, 2018). matRad provides the tools for dose calculation and optimization of intensity modulated radiation therapy with photons, protons and carbon ions. The generic treatment machine base data for each modality are stored as Matlab structures that model the physical beam characteristics. The photon machine base data provided with matRad, models a 6MeV SIEMENS Artiste 3 based on the single value decomposed pencil beam algorithm presented by Bortfeld et al. (1993). The particle base data for protons and carbon ions are generic treatment machines as presented by Wieser et al. (2018) with tabulated LET. For carbon ions, the dose-averaged LQ model parameters, based on LEM IV, are also provided for RBE based treatment planning (Wieser et al., 2017, 2018). Despite matRad not being a clinical treatment planning system, all computations have been validated against the clinical treatment planning system Syngo and can therefore be considered to be of clinically relevant accuracy.
In the matRad environment, the dose influence matrices are stored as compressed sparse matrices and the dose calculation is done by an internally parallelized matrix-vector product with pencil beam intensities. matRad uses the interior point optimizer package (IPOPT) (Wächter and Biegler, 2006) to solve the fluence optimization problem. IPOPT requires a set of initial pencil beam weights and function call-backs to evaluate the objective function and the gradient of the objective functions, while the Hessian is approximated by L-BFGS.

III.1.3.2 Spatio-temporal optimization

The implementation of the joint optimization framework was preceded by an implementation of a spatio-temporal optimization foundation where the optimized plan is based on the cumulative biological effect from multiple, possibly distinct, fractions. Unlike conventional treatment planning, which is optimized for the fraction dose, spatio-temporal optimization is carried out on the cumulative biological effect of the treatment over all fractions. Therefore the prescribed dose objectives are translated into prescribed total biological effects based on the tissue specific LQ model parameters to account for fractionation. In practice, the distinct fraction doses are handled using a matrix of pencil beam intensity vectors thus simplifying the dose calculation to a matrix-matrix product resulting in a matrix of dose vectors for each fraction that can then be transformed to biological effects to be accumulated. This implementation takes advantage of internal parallelization in matrix operations of Matlab to simultaneously calculate dose distributions over all distinct fractions.

III.1.3.3 Implementation of effect based joint optimization

The joint optimization framework was created with a modular approach in mind to facilitate the combination of multiple radiation modalities. The dose calculation was modified to serially accumulate the fractional biological effects from each modality into the overall biological effect of the treatment, which is then used to evaluated the objective function. In order to achieve this, the dose influence matrices for multiple modalities were consolidated into a single dose influence matRad structure which is then used to calcuate the cumulative biological effect. This implementation retains the functionality of spatio-temporal optimization within the modalities, i.e., the hypothetical situation of delivering multiple modalities each with a set of distinct dose distributions. The current bottleneck is memory management for the large dose influence matrices from multiple radiation modalities. A photon–carbon ion plan can be jointly optimized in matter of hours, where the matrix-vector product for dose calculation and gradient computation are the most computationally intensive tasks.

III.1.4 Convergence

III.1.4.1 Convergence considerations

The mixed modality joint fluence optimization problem, as described in section II.3.4.2, is generally a convex problem in the domain of therapeutic doses. Within this range of doses the optimization problem can be solved using gradient descent methods. However convergence is a practical problem that refers to the ability of the optimizer to come to consistent optimal solutions while traversing this convex space. Convergence is a challenge particularly interesting in the joint optimization scenario. The optimizer assesses the optimality of a joint optimized solution by evaluating the change in objective function value. If this change in objective function value is less than a predefined tolerance/threshold the solution is deemed to be acceptable/optimal. On varying the objective function value change tolerance for optimized unimodal treatments, the variation seen in dose distribution is small. Further analysis on the degeneracy of the radiotherapy optimization problem were presented by Alber et al. (2002). However for combined treatments, a small variation in objective function value may be reflected as a widely different individual fluence distribution of photons and carbon ions.

Initial experiments showed that the rate of convergence in late stages of optimization for jointly optimized plans is low as the driving factor is the reduction of mean biological effect to the external healthy tissue. Multiple arbitrary dose distributions may satisfy the squared underdosage objectives to the target. However the optimal combined treatment must also limit the dose to adjacent critical structures and minimize mean dose to external healthy tissue. The late stages of the optimization are characterized by a redistribution of fluence between the two modalities to reduce the mean biological effect to healthy tissue, which is reflected by a relatively small reduction in the objective function value, when compared to the

other square effect difference objectives seen by evaluating treatment plans at various time points, shown in figure III.2, of the optimization. This reduced gradient not only results in different overall biological effect distributions but also different individual dose contributions of each modality. Therefore the reduced gradient motivates the need for defining a smaller threshold on tolerance for change in objective function values to reach the optimal solution.

III.1.4.2 Preconditioning

The slow convergence may also be attributed to the differences in dose influence matrices for photons and carbon ions. The underlying magnitude of dose influence of each pencil beam is different between the two modalities within matRad, resulting in a large initial difference in gradients between the two modalities within the overarching cumulative dose influence matrix consisting of both modalities. This difference in turn causes a slower initial convergence rate. Preconditioning is a method used to reduce the condition number of the matrix, i.e., ratio of the largest singular value of the matrix to the smallest singular value. Intuitively, preconditioning is an approach to modify the quadratic form of the pencil beam dose influence space between the two modalities to a more spherical form (Shewchuk, 1994; Wathen, 2015). In this thesis a *Jacobi preconditioner* (diagonal preconditioner) was implemented that transforms the dose influence matrices of photons and carbon ions using a diagonal matrix, which is trivial to invert. The preconditioning diagonal matrix is composed of the reciprocal of the total dose contribution of each pencil beam.

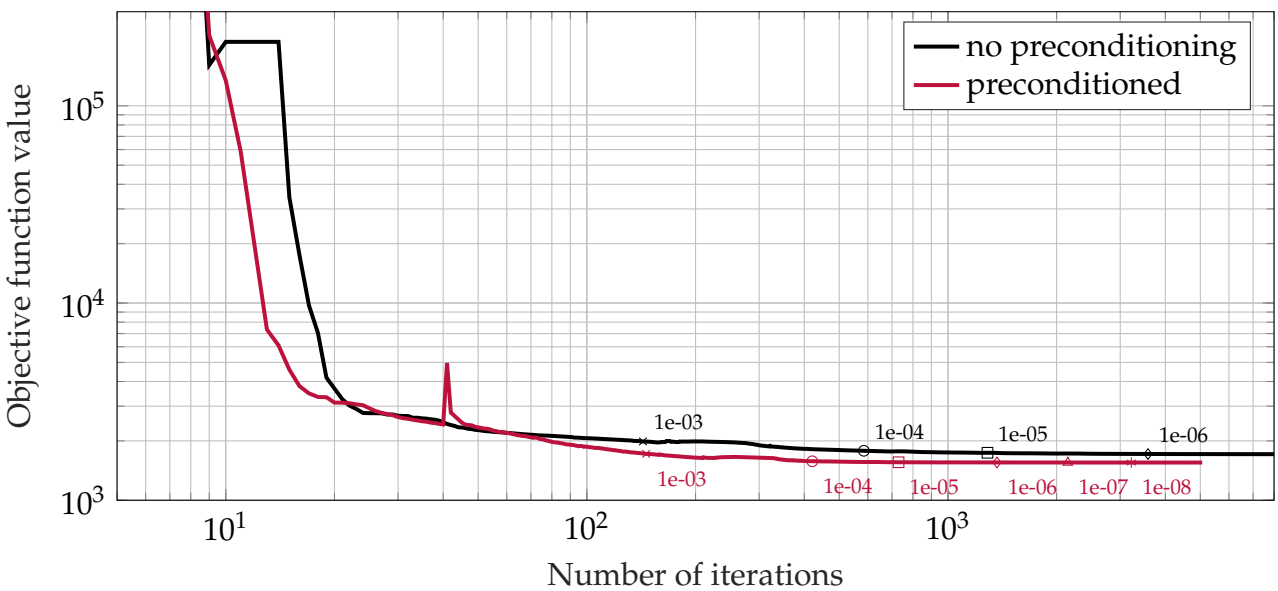

Figure III.2: Evolution of the objective function values with (—) and without (—) preconditioning. Markers present optimization end conditions considering different tolerances for changes ($1e^{-03}$, $1e^{-04}$, $1e^{-05}$, $1e^{-06}$, $1e^{-07}$, $1e^{-08}$).

The result of preconditioning on convergence is illustrated with figure III.2, that shows the objective function value over the course of an optimization for a sample case without a preconditioner (——) and with a preconditioner (——). The marks plotted on the curves represent the points where the optimization would satisfy the objective change tolerance threshold of various values. The jumps in objective function values in early steps of the optimization suggest an suboptimal choice of starting point for the optimizer as both optimizations converge to a similar starting point seen at iteration #15. As mentioned earlier, the rate of convergence of joint optimization is low in the later stages of optimization requiring a smaller objective function value change tolerance, and the use of a preconditioner demonstrably speeds up convergence.

III.2 Proof of concept

In order to validate the joint optimization framework the first step was to reproduce results previously presented in literature. Unkelbach et al. (2018) present a spinal metastasis case to illustrate the potential benefit of such jointly optimized photon–proton treatments and fractionated treatments in the situation of epidural involvement. Jointly optimized photon–proton plans were generated to qualitatively compare the matRad implementation of joint optimization to results published in the aforementioned publication. Following this comparison, photon–carbon ion plans was generated to quantitatively study the implications of joint optimized plans with the backdrop of unimodal treatments and the clinical work flow of a simple combination of separately optimized treatment plans.

III.2.1 Spinal Metastasis

The spine is the most common location for bone metastases. They have been treated with conventional palliative radiation which is associated with low rates of complete response with respect to pain management and local control (Husain et al., 2017). Stereotactic Body Radiotherapy (SBRT) was developed with the intent to improve pain control and local control and achieves this by delivering a considerably higher BED than conventional radiotherapy. In the case of spinal metastases, high fraction dose SBRT protocols are used, for example, single fraction SBRT of approximately 20 Gy (Husain et al., 2017; Yáñez et al., 2017). Figure III.3 shows a spinal metastasis patient where the cauda (——) is situated within the target volume (——). A dose limiting margin was considered surrounding the cauda as a 3 mm expansion of the cauda (——), additionally a dose fall-off region (——) was defined around the target volume to ensure conformity of the high dose. For tumours with epidural involvement, a larger number of fractions is required to spare the nearby OARs like the spinal cord. The use of particle therapy was predicted to improve this sparing of OARs (Yáñez et al., 2017).

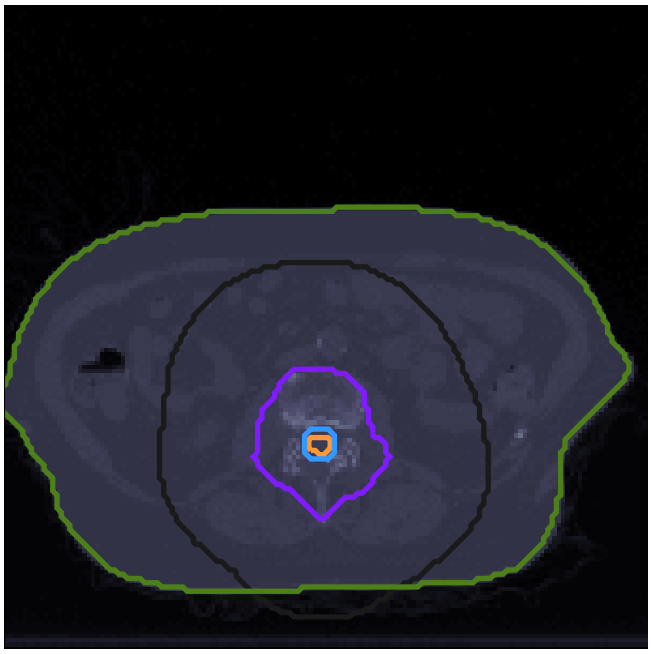

Figure III.3: Shows a spinal metastasis patient case where the target volume surrounds the critical structure, the cauda.

III.2.2 Treatment planning

The treatment plan was generated for a 5 fraction treatment delivering a total of 35 Gy to the target volume (CTV) (Gill et al., 2012). The LQ model parameters were assumed to be $\alpha^\gamma/\beta^\gamma = 10$ Gy for the tumour and $\alpha^\gamma/\beta^\gamma = 2$ Gy for healthy tissue. This differential $\alpha^\gamma/\beta^\gamma$ between tumour and healthy tissue implies a fractionation gain in terms of sparing healthy tissue. To maintain consistency, particle therapy modalities were planned with two dorsal oblique beams (140°, 220°) and photon (IMRT) plans were generated using 9 equispaced beams. The treatment planning objectives are given in table III.2.

Table III.2: Defines the treatment planning objectives for spinal metastases with involvement of the dura considering a 5 fraction treatment.

VOI	Objective function	$\alpha^\gamma/\beta^\gamma$ [Gy]	Dose objective [Gy]	Effect objective
CTV	sq. underdosing	0.5/0.05	35.2	29.99
CTV	sq. overdosing	0.5/0.05	36.45	31.51
Cauda	sq. overdosing	0.1/0.05	20	6
Cauda + 3mm	sq. overdosing	0.1/0.05	28.8	11.17
Fall-off	sq. overdosing	0.1/0.05	17.7	4.9
External	mean dose	0.1/0.05	-	-

Firstly, a proton-photon joint optimized plan was generated, similar to the treatment plan presented by Unkelbach et al. (2018). Distinct sequentially delivered fractions of photons (4 fractions) and carbon ions (1 fraction) are simultaneously optimized. The intent behind this plan was to validate the matRad implementation of joint optimization against previously published results and to establish the reproducibility of jointly optimized plans. Protons were considered with the clinically used constant RBE model ($RBE = 1.1$). The proton contribution to total effect ε_i^P in voxel i is given as

$$\varepsilon_i^P = \alpha^\gamma \; RBE \sum_k D_{ik}^P w_k^P + \beta^\gamma \left(RBE \sum_k D_{ik}^P w_k^P \right)^2 \qquad \forall i \tag{III.6}$$

where w_k^P is the intensity of pencil beam k and D_{ik}^P is its dose contribution to voxel i for unit intensities. The biological effect of photon-equivalent proton dose (RBE weighted dose) is computed using the photon LQ model parameters $\alpha^\gamma, \beta^\gamma$. The effect based formulation for photon–proton combined treatments is equivalent to the BED formulation presented in equation (II.40) when scaled by $1/\alpha^\gamma$.

To study the implications of jointly optimized photon–carbon ion combined treatments, five treatment plans are presented. The reference plans for this study are a 5 fraction photon only treatment, a 5 fraction carbon ion only treatment and the combination of RBE weighted dose of separately optimized photon treatment of 4 fractions and 1 fraction of carbon ion treatment which follows the clinical work flow for combined treatments. The jointly optimized treatments presented consider two strategies: first, the joint optimization of 1 fraction of carbon ions along with 4 fractions of photons. Second, the jointly optimized concurrent

irradiation strategy where both photons and carbon ions are applied in all fractions, to afford the optimizer the maximum freedom to exploit any possible fractionation gain.

III.3 Impact of treatment parameters

III.3.1 Impact of fraction allocation

Particle therapy is a limited resource and it is essential to understand the variations in plan quality over different photon and carbon ion fraction allocation sets. Therefore treatment plans were generated over varying number of carbon ion fractions and their complementary photon fractions for a 5 fraction treatment for the spinal metastasis case, presented in the previous section. To this end, six treatment plans were generated varying from an only photon treatment plan through jointly optimized photon–carbon ion plans to an only carbon ion treatment plan. These plans were evaluated based on the objective function value and clinically used treatment plan quality indicators based on the EQD2.
To take this further, photon–carbon ion plans were compared to photon–proton plans, for varying distributions of fractions, to understand broader relative differences between carbon ions and protons for mixed modality treatments. Treatment plans for photon–carbon ions and photon–protons were optimized considering the objectives presented in table III.2.

III.3.2 Impact of Linear Quadratic model parameter selection

The spinal metastasis cases described until now have been optimized assuming an increased radiosensitivity of the tumour compared to healthy tissue reflected by a tumour $\alpha^{\gamma}/\beta^{\gamma} = 0.5/0.05$ Gy and an $\alpha^{\gamma}/\beta^{\gamma} = 0.1/0.05$ Gy for healthy tissue. This naturally leads to a question regarding the optimal combination when there is no gain from fractionation, i.e., $\alpha^{\gamma}/\beta^{\gamma} = 0.1/0.05$ Gy for tumour and healthy tissue. In the interest of continuity with the example spinal metastasis patient case, a hypothetical mixed modality treatment plan was generated using the treatment objectives mentioned in table III.2, where the CTV $\alpha^{\gamma}, \beta^{\gamma} = 0.1/0.05$ Gy, equal to that of healthy tissue. This plan was qualitatively compared against a jointly optimized plan assuming a fractionation gain as presented in section III.2.2.

III.3.2.1 Base of skull chordoma

A base of skull chordoma was used to illustrate this concept in a more clinical context and lay out the importance of the differential $\alpha^{\gamma}/\beta^{\gamma}$ parameters. Chordomas are slow-growing, infiltrative tumours often located at the skull base (Debus et al., 2000). This is a challenging indication due to the close proximity of critical structures like the brain stem and due the low α/β ratio of chordomas which corresponds to a reduced response to radiation (Schulz-Ertner et al., 2004). The superior physical dose characteristics of proton therapy has established it as a standard treatment for chordomas of the skull base (Feuvret et al., 2007; Fossati et al., 2016; Nikoghosyan et al., 2010). Combined photon–proton treatments were investigated and although they achieved dose conformation similar to an only proton treatment, the unimodal approach presents the advantage of a reduced integral dose to healthy tissue (Feuvret et al., 2007; Noël et al., 2001). More recently, the application of carbon ion therapy is being investigated due to its higher RBE in addition to the improved dose deposition characteristics (Nikoghosyan et al., 2010; Schulz-Ertner et al., 2002, 2007, 2003, 2004; Takagi et al., 2018; Uhl et al., 2014).

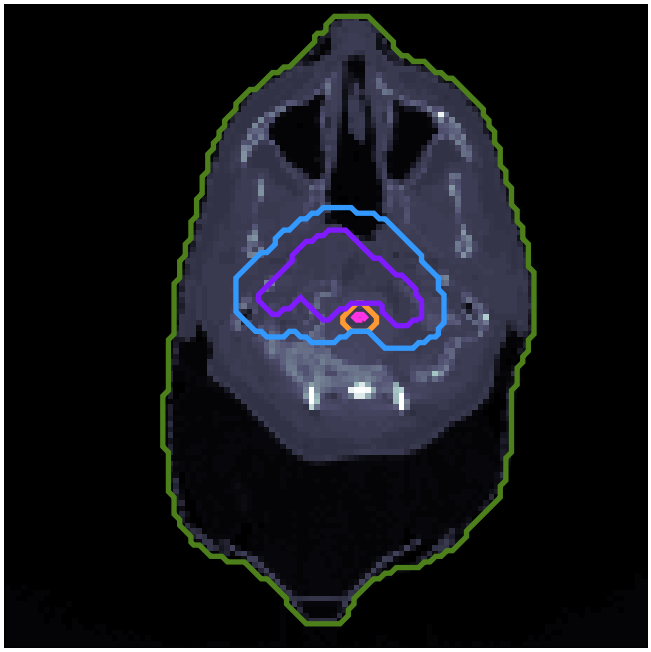

Figure III.4: Shows a base of skull chordoma patient case where the target volume is abutting the critical structure, the brainstem. The structures considered for the optimization are CTV (—), brainstem (—), center of brainstem (brainstem ct : —), dose fall-off volume (—) and external healthy tissue (—)

III.3.2.2 Treatment planning

The treatment plan was generated using the objectives presented in table III.3 for a 37 fraction treatment delivering 66.6 Gy to the target volume (CTV)(Debus et al., 2000; Fossati et al., 2016; Noël et al., 2001). The 37 fractions are divided into 25 fractions of photons and 12 fractions of carbon ions that are simultaeneously optimized. The mixed modality plan was generated using 4 beams of carbon ions (90°, 120°, 240°, 270°) and 9 equispaced photon (IMRT) beams. The LQ model parameters were assumed to be $\alpha^{\gamma}/\beta^{\gamma} = 2$ Gy for tumour and healthy tissue (Henderson et al., 2009; van Leeuwen et al., 2018). Without a fractionation gain, the 37 fraction photon–carbon ion jointly optimized treatment plan is expected to utilize superior carbon ion physical characteristics to achieve target coverage. Therefore the jointly optimized plan is compared against a unimodal 12 fraction carbon ion plan delivering the same prescribed effects.

Table III.3: Defines the treatment planning objectives for base of skull chordoma with 37 fraction treatment.

VOI	Objective function	$\alpha^{\gamma}/\beta^{\gamma}$ [Gy]	Dose objective [Gy]	Effect objective
CTV	sq. underdosing	0.1/0.05	66.6	12.65
CTV	sq. overdosing	0.1/0.05	68	13.05
Brainstem	sq. overdosing	0.1/0.05	60	10.86
Brainstem center	sq. overdosing	0.1/0.05	54	9.34
Fall-off	sq. overdosing	0.1/0.05	60	10.86
External	mean dose	0.1/0.05	-	-

III.4 Mixed modality treatments for Infiltrative disease

As mentioned before, carbon ions are radiobiologically more effective than photons and may be quite well suited to treating the GTV. However, this comes at a cost of a higher effect in healthy tissues from a reduced fractionation effect. Therefore carbon ions may not be ideal for treating infiltrative tumours where there is a combination of tumour tissue and healthy tissue in the CTV and the healthy tissue is to be protected by fractionating the dose, i.e., uniform distribution of biological effect. The application of mixed modality treatments to infiltrative disease is illustrated in the context of treatment for glioblastoma where, clinically, the photon–carbon ion plans are separately generated and manually combined (Combs et al., 2010).

III.4.1 Glioblastoma

Glioblastomas are one of the most common primary brain tumours in adults and have a poor prognosis with median survival times of 9-12 months (Delgado-López and Corrales-García, 2016; Fernandes et al., 2017). The current standard of care is a multidisciplinary treatment of maximal resection of the tumour followed by concurrent chemotherapy (Temozolomide) and radiotherapy (IMRT, up to 60 Gy in 2 Gy fractions) (Combs et al., 2010, 2008; Fernandes et al., 2017; Stupp et al., 2005). The use of carbon ions is motivated by the rapid progression and radioresistance of glioblastomas Malouff et al. (2019). Furthermore, compared to photons, carbon ions have a higher cytotoxic effect in glioblastoma cell lines (Combs et al., 2009).
Glioblastomas are also known to infiltrate the brain tissue far beyond the GTV boundary which necessitates a large CTV that is created with a 2 cm margin expansion around the GTV not including overlapping tissue interfaces (Hochberg and Pruitt, 1980). This CTV, consisting of mixed tumour and healthy tissue, presents a need for mixed modality treatments which would exploit the higher RBE of carbon ions in the GTV and utilize photons to fractionate dose to the CTV.

III.4.2 Fractionation in joint optimization

As seen in figure II.8, carbon α^C and β^C vary along the carbon ion beam path and intrinsically depend on the LET. Generally, α^C rises when approaching the Bragg peak and β^C decreases when approaching the Bragg peak. Therefore increasing α^C towards the Bragg peak which is always greater than the photon α^γ implies a higher biological effect for unit intensity. Here photon α^γ and β^γ are used to model the dependence of carbon α^C and β^C on the tissue type. This can be seen in figure III.5, which shows that for isoeffective doses delivered to tumour tissue by photons and carbon ions, the photon $EQD2^\gamma_{NT}$ (——) is always less than the carbon ion $EQD2^C_{NT}$ (——) for equal tumour EQD2 of carbon ions $EQD2^C_T$ and photons $EQD2^\gamma_T$. The "dip" seen at approximately 115 mm is an effect of the LEM based α^C, β^C prediction results from a difference in peak positions of α^C_T, β^C_T and $\alpha^C_{NT}, \beta^C_{NT}$ predicted by LEM IV. It is further compounded by the underlying inverted dose profile used to achieve a uniform EQD2 in tumour tissue at different depths of the carbon beam.

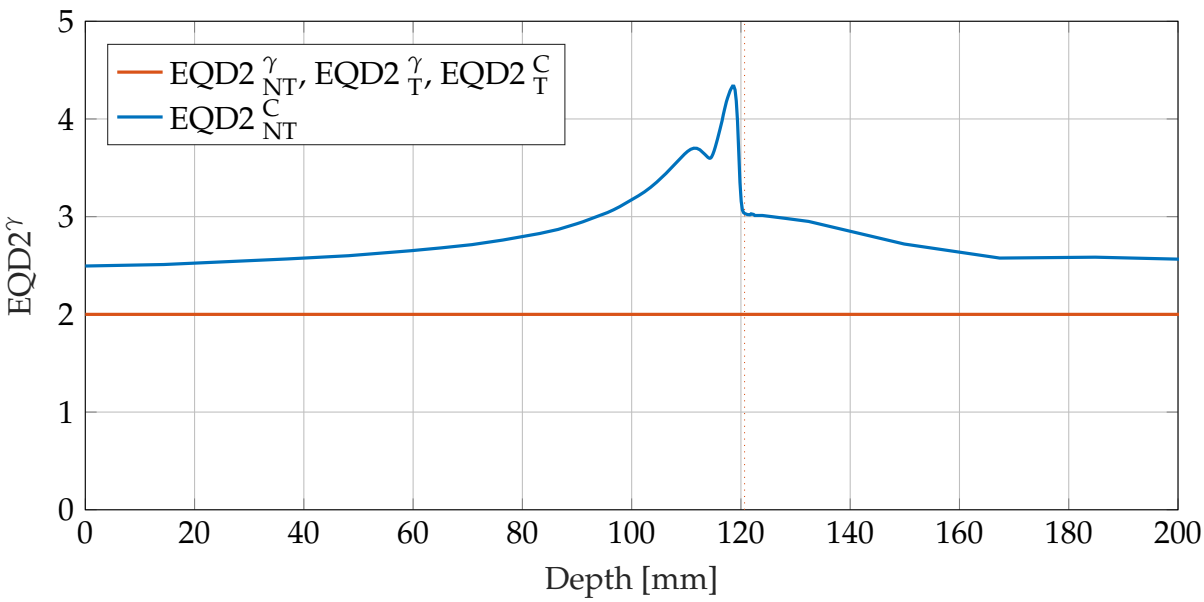

Figure III.5: Comparison of EQD2 in healthy tissue from carbon ions ($EQD2^C_{NT}$, ——) and photons ($EQD2^\gamma_{NT}$, ——) for isoeffective $EQD2^C_T$ (——) and $EQD2^\gamma_T$ (——) doses in tumour tissue in mixed tissue considering a 241.03 MeV carbon ion beam with Bragg peak at 120.6mm (·····).

In terms of treatment planning for Glioblastomas there are two levels of trade-offs: (1) the general conflict between target converge and sparing surrounding healthy tissue of the critical structures such as the brainstem, chiasm, optic nerves and external healthy brain. (2) the conflict between delivering therapeutic dose to tumour cells in the CTV and sparing healthy tissue in the CTV at the same spatial location, i.e., same voxel. The first trade-off can be addressed by the spatial conformity of the dose to the target volume, however the second trade-off can only be addressed by a fractionation of dose that can be modelled using the LQ model. The conflicting goals within the CTV can be mathematically expressed as a combination of an effect based quadratic underdosage objective considering tumour tissue

$(\alpha_T^\gamma/\beta_T^\gamma)$ and an effect based overdosage objective for healthy tissue $(\alpha_{NT}^\gamma/\beta_{NT}^\gamma)$. These can be written as:

$$\begin{aligned} f_{CTV,T}\left[\varepsilon_i^{Total}(\alpha_T^\gamma/\beta_T^\gamma)\right] &= \Theta(\varepsilon_{ref}(\alpha_T^\gamma,\beta_T^\gamma)-\varepsilon_i(\alpha_T^\gamma,\beta_T^\gamma)) \\ &\quad (\varepsilon_{ref}(\alpha_T^\gamma,\beta_T^\gamma)-\varepsilon_i(\alpha_T^\gamma,\beta_T^\gamma))^2 \\ f_{CTV,NT}\left[\varepsilon_i^{Total}(\alpha_{NT}^\gamma/\beta_{NT}^\gamma)\right] &= \Theta(\varepsilon_i(\alpha_{NT}^\gamma,\beta_{NT}^\gamma)-\varepsilon_{ref}(\alpha_{NT}^\gamma,\beta_{NT}^\gamma)) \\ &\quad (\varepsilon_{ref}(\alpha_{NT}^\gamma,\beta_{NT}^\gamma)-\varepsilon_i(\alpha_{NT}^\gamma,\beta_{NT}^\gamma))^2 \end{aligned} \tag{III.7}$$

The implementation of this objective required a considerable alteration to the handling of dose influence structures in matRad. The evaluation of effect based objectives considering different $\alpha^\gamma/\beta^\gamma$ parameters required the computation of two distinct biological effect matrices which implied an additional biological effect calculation and gradient estimation step for each iteration.

III.4.3 Glioblastoma patient cases

Treatment plans were generated for six patient cases. Two of whom received conventional photon radiotherapy while four patients received a carbon ion boost treatment. The GTV was delineated as the observable tumour volume on T1 weighted MR-images, and the CTV was generated by a 2 cm expansion of the GTV corrected for anatomical barriers to microscopic tumour infiltration. Two patients are highlighted in figure III.6: (1) Patient I characterized by a large GTV (143 cc) where due to the location of the target volume, the CTV volume outside of the GTV is moderate (256.2 cc). (2) Patient II with a smaller GTV (68.9 cc) which does not abut critical structures except normal brain. The CTV volume outside of the GTV is comparatively large (193.5 cc).

III.4.4 Treatment plan setup

Plans were generated using 9 equi-spaced photon (IMRT) beams and 2-3 carbon ion beams depending on the tumour location and volume. This analysis compares a reference treatment plan based on the CLEOPATRA glioblastoma trial protocol (Combs et al., 2010) and a simultaneously optimized photon–carbon ion plan. The reference plan is generated by a manual combination of a photon (IMRT) plan delivering 50 Gy in 25 fractions and a carbon ion plan delivering 18 Gy in 6 fractions and the treatment plan obejctives are given in tables III.4 and III.5 respectively.

The jointly optimized plan of 31 fractions was optimized to achieve a total biological effect in the tumour identical to that of the combined reference plan. For biological effect based optimization, the tumour $\alpha^\gamma/\beta^\gamma$ was assumed to be 10 (0.5/0.05 Gy), an approximation of the high $\alpha^\gamma/\beta^\gamma$ for glioblastoma presented by (Henderson et al., 2009). The $\alpha^\gamma/\beta^\gamma$ for

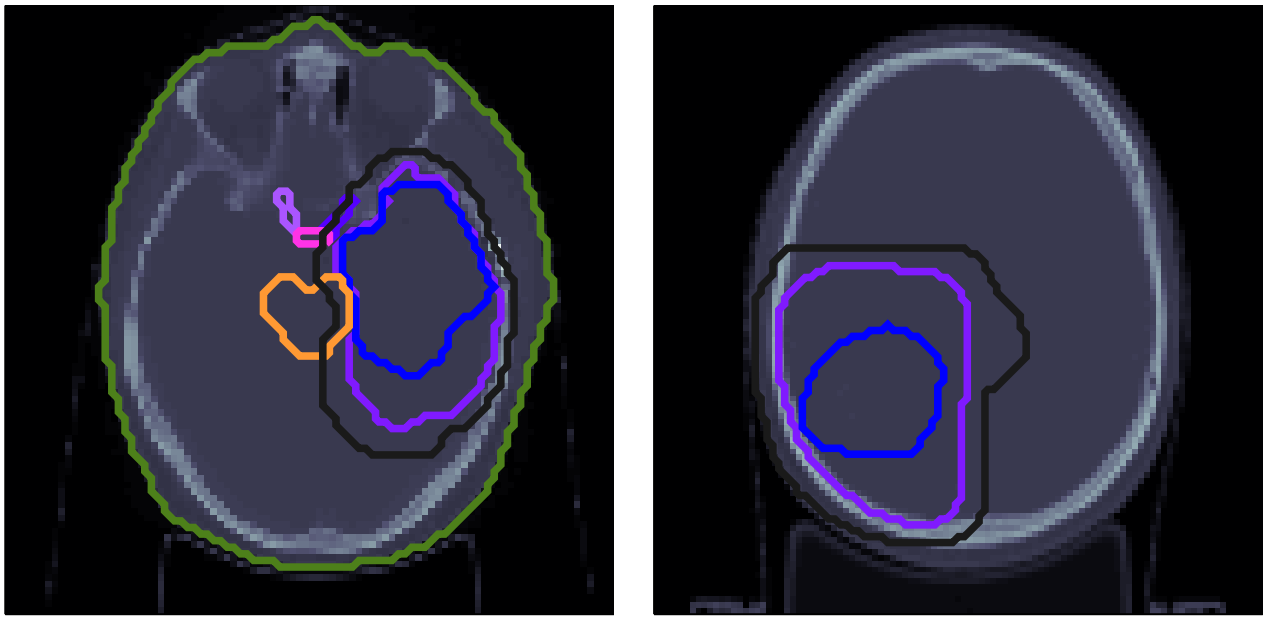

(a) Patient I (b) Patient II

Figure III.6: The highlighted glioblastoma patient cases. (a) Patient I (b) Patient II presents with no critical structures in the immediate vicinity of te target structures . The structures considered are theGTV (—) and CTV(—) along with critical structures like the brainstem (—) optic chiasm (—), optic nerve (—) and a synthetic dose fall off structure (—).

Table III.4: Glioblastoma reference photon treatment planning objectives for 25 fractions

VOI	Objective function	$\alpha^{\gamma}/\beta^{\gamma}$ [Gy]	Dose objective [Gy]	Effect objective
CTV	sq. underdosing	0.5/0.05	50	30
CTV	sq. overdosing	0.5/0.05	50	30
Brainstem	sq. overdosing	0.1/0.05	48	9.41
Optic Nerve	sq. overdosing	0.1/0.05	30	4.8
Chiasm	sq. overdosing	0.1/0.05	48	9.41
Fall-off	sq. overdosing	0.1/0.05	48	9.41
External	sq. overdosing	0.1/0.05	10	1.2
External	mean dose	0.1/0.05	-	-

Table III.5: Glioblastoma reference carbon ion treatment planning objectives for 6 fraction boost

VOI	Objective function	$\alpha^{\gamma}/\beta^{\gamma}$ [Gy]	Dose objective [Gy]	Effect objective
GTV	sq. underdosing	0.5/0.05	18	11.7
GTV	sq. overdosing	0.5/0.05	18	11.7
Brainstem	sq. overdosing	0.1/0.05	17	4.11
Chiasm	sq. overdosing	0.1/0.05	17	4.11
Optic Nerve	sq. overdosing	0.1/0.05	15	3.38
Fall-off	sq. overdosing	0.1/0.05	17	4.11
External	sq. overdosing	0.1/0.05	10	1.83
External	mean dose	0.1/0.05	-	-

healthy tissue was assumed to be 2 Gy (0.1/0.05). The detailed treatment plan objectives are presented in table III.6. The plans were generated on the GTV and CTV directly, and no margin expansion was considered. Naturally, the exact treatment plan and the relative dose

Table III.6: Glioblastoma photon–carbon ion jointly optimized treatment planning objectives over 31 fractions

VOI	Objective function	$\alpha^{\gamma}/\beta^{\gamma}$ [Gy]	Dose objective [Gy]	Effect objective
GTV	sq. underdosing	0.5/0.05	68	41.46
GTV	sq. overdosing	0.5/0.05	72	44.36
CTV	sq. underdosing	0.5/0.05	51.46	30
CTV	sq. overdosing	0.1/0.05	52	9.83
Brainstem	sq. overdosing	0.1/0.05	50	9.03
Chiasm	sq. overdosing	0.1/0.05	48	8.52
Optic Nerve	sq. overdosing	0.1/0.05	30	4.45
Fall-off	sq. overdosing	0.1/0.05	48	8.52
External	sq. overdosing	0.1/0.05	10	1.16
External	mean dose	0.1/0.05	-	-

contributions of each modality depend on the relative weighting of each individual objective (table III.6). In order to highlight this, an additional plan was generated that has an increased weight of the mean dose objective sparing the external healthy brain, and a reduced weight of the squared underdosage objective sparing the healthy tissue in the CTV. It is expected that, this change would motivate the optimizer to utilize more carbon ions, that would reduce the integral dose to the healthy tissue at the cost of a lower penalty within healthy tissue in the CTV.

III.4.5 Proton–carbon ion treatment

The results presented for combined photon–carbon ion treatments for glioblastoma arise from a complex interplay of the physical dose characteristics and radiobiological characteristics of the modalities used. Naturally one of the questions that would arise is the relative importance of biological fractionation objective with respect to the effects seen from physical dosimetric superiority of carbon ions over photons. To investigate this importance of the radiobiological aspect of joint optimization a proton–carbon ion plan was generated. Protons, in physical dose characteristics, are quite similar to carbon ions exhibiting a strong albeit, stretched out Bragg peak. However, radiobiologically they are assumed to be similar to photons, with a constant RBE as applied in the clinic. Therefore, it can be argued that the individual dose contributions seen in proton–carbon ion jointly optimized plans arise from a radiobiological trade off between the two modalities. The proton- carbon ion plan was generated using the same treatment objective presented in table III.6 and compared against a photon–carbon ion plan.

III.5 Impact of Local Effect Model version selection

As presented in section II.2.3, the LEM models for carbon ions have gone through a number of iterations. The LEM I predicts a higher RBE, i.e., greater magnitude of the α^C and β^C parameters at non-Bragg peak regions, this implies a larger biological effect in tissue compared to LEM IV for equal physical doses. The implications of the choice of LEM model version on joint optimization are illustrated with treatment plans generated for a glioblastoma case. The LEM I base data used for this optimization models the machine used at the Heidelberg Heavy Ion Therapy (HIT) facility as opposed to the LEM IV based generic machine base data available with matRad. The treatment plans are generated using the treatment protocol specified in III.4.4. The LEM I based jointly optimized plan is compared to the LEM IV based jointly optimized plan as described in section III.4.4

"Exceptional claims demand exceptional evidence."

Christopher Hitchens, 1949-2011

IV Results

IV.1 Validation

In order to qualitatively validate this implementation of joint optimization, an initial treatment plan was generated to reproduce results presented by Unkelbach et al. (2018). Figure IV.1, shows a simultaneously optimized photon–proton treatment plan. There are three striking features of this plan:

1. Photon fractions (Figure IV.1a) and proton fractions (Figure IV.1b) deliver distinct dose distributions.
2. The difference in fraction allocation between the two modalities results in parts of the target volume are differently fractionated.
3. The plan cumulatively delivers a uniform biological effect in the target volume, as shown in Figure IV.1c.

The four photon fractions deliver a bulk of the dose to the target volume surrounding the cauda, whereas, the single carbon ion fraction delivers dose to the rest of the target volume. In regions of the target volume surrounding the cauda, almost equal fraction doses are delivered over the entire treatment suggesting uniform fractionation to protect the cauda. However, for other regions the dose is delivered predominantly by carbon ions within one fraction, here the optimizer is essentially selecting a hypofractionation scheme. This is in line with the results presented by Unkelbach et al. (2018).

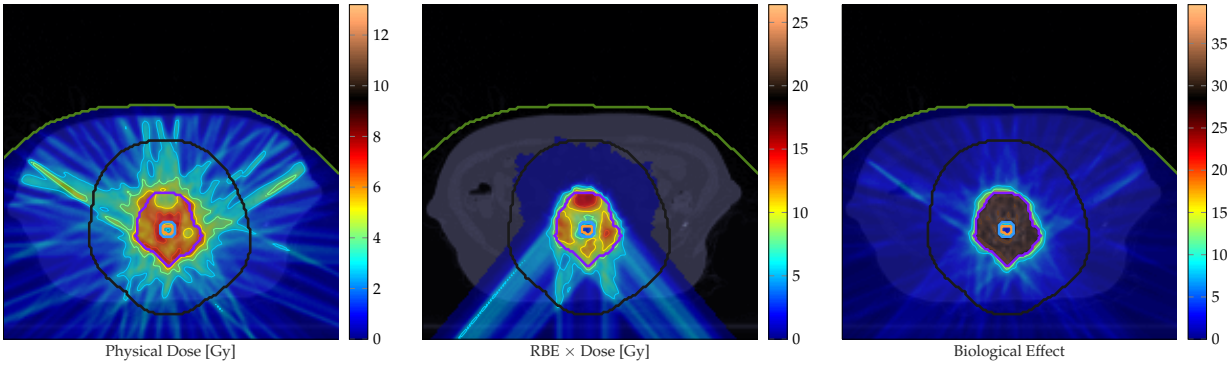

(a) Photon fraction dose (b) Proton fraction dose (c) Total biological effect

Figure IV.1: Dose per fraction and cumulative biological effect of a jointly optimized plan for a spinal metastasis case. The plan consists of (a) 4 photon fractions, (b) 1 proton fraction, and delivers (c) a uniform cumulative biological effect. Here the target volume (——) surrounds the cauda (——). A dose limiting margin was considered surrounding the cauda as a 3 mm expansion of the cauda (——), additionally a dose fall-off region (——) was considered to enforce conformity of dose.

IV.2 Spinal Metastasis

The result presented is a spinal metastasis patient case as described in section III.2. An initial proof of concept study was carried out with a photon–proton plan to emulate results previously presented in literature. Photon–carbon ion plans for the same case are presented to lay out the fundamental outcomes of a joint optimization strategy in comparison to the clinical status quo.

IV.2.1 Photon–carbon ion combined treatments

This section presents a qualitative and quantitative analysis of photon–carbon ion jointly optimized plans for the same spinal metastasis case. The treatment protocol is laid out in section III.2.1. To provide a wider picture, the jointly optimized plans are compared to three reference plans:

1. unimodal photon treatment of 5 fractions. The corresponding fraction physical dose is shown in Figure IV.2a.

2. unimodal carbon ion treatment of 5 fractions. The fraction RBE × dose is shown in figure IV.2c.

3. A simple mixed modality treatment where four fractions of photons and one fraction of carbon ions was independently optimized, i.e., as unimodal plans described above. These plans were then simply combined and evaluated based on total RBE × dose, following clinical procedure. The cumulative EQD2 is presented in figure IV.2e.

With the backdrop of these clinical plans, two types of jointly optimized photon–carbon ion plans are presented: (1) photons and carbon ions are intended to be delivered sequentially in distinct fractions presented in section IV.2.1.1, (2) photons and carbon ions are applied concurrently in each fraction. The latter will henceforth be referred to as the concurrent irradiation strategy. The results of the concurrent irradiation plan are presented in section IV.2.1.2. A quantitative study of these plans is presented in sections IV.2.1.3.

IV.2.1.1 Joint optimization with fixed fraction allocation

The cumulative EQD2 of the photon fraction (physical dose shown in figure IV.2b) and carbon ion fraction (RBE$\times$ dose shown in figure IV.2d) are given in figure IV.2f. The dose "corona" seen around the target volumes in figures of the cumulative EQD2 arises from the discontinuity in the assumed α^{γ} and β^{γ} between healthy tissue ($\alpha^{\gamma}/\beta^{\gamma} = 0.1/0.05$ Gy) and tumour tissue ($\alpha^{\gamma}/\beta^{\gamma} = 0.5/0.05$ Gy).

The reference plans and the jointly optimized plan achieve a comparable level of overall target coverage, but they do so in very different ways. The three reference plans deliver a uniform dose of 7 Gy to the target volume in each fraction. The jointly optimized photon–carbon ion treatment, however, delivers a highly inhomogeneous fraction dose distribution which sums up to a uniform total biological effect. Carbon ions deliver most of the dose to the target volume in a single fraction, whereas photon dose is limited to regions surrounding the cauda and the proximal edges of the target volume.

Figure IV.3a shows the difference in cumulative EQD2 between the simple combination plan and the jointly optimized plan. The yellow colour wash illustrates regions where the simple combination plan delivers a greater biological effect compared to the jointly optimized plans. The large areas of the external healthy brain with the yellow colour wash show the reduction in integral dose to external healthy tissue as a result of an increased dose contribution from carbon ions in the jointly optimized plan. Furthermore the joint optimization shows an improvement in conformity of dose to the target volume seen by the dose differences surrounding the target volume.

Dose to the regions of the target volume immediately adjacent to the cauda are delivered almost uniformly across all fractions by both photons and carbon ions. This can be seen as the white washed regions in figure IV.3b which shows the difference in fraction doses delivered by photons and carbon ions for the jointly optimized plans.

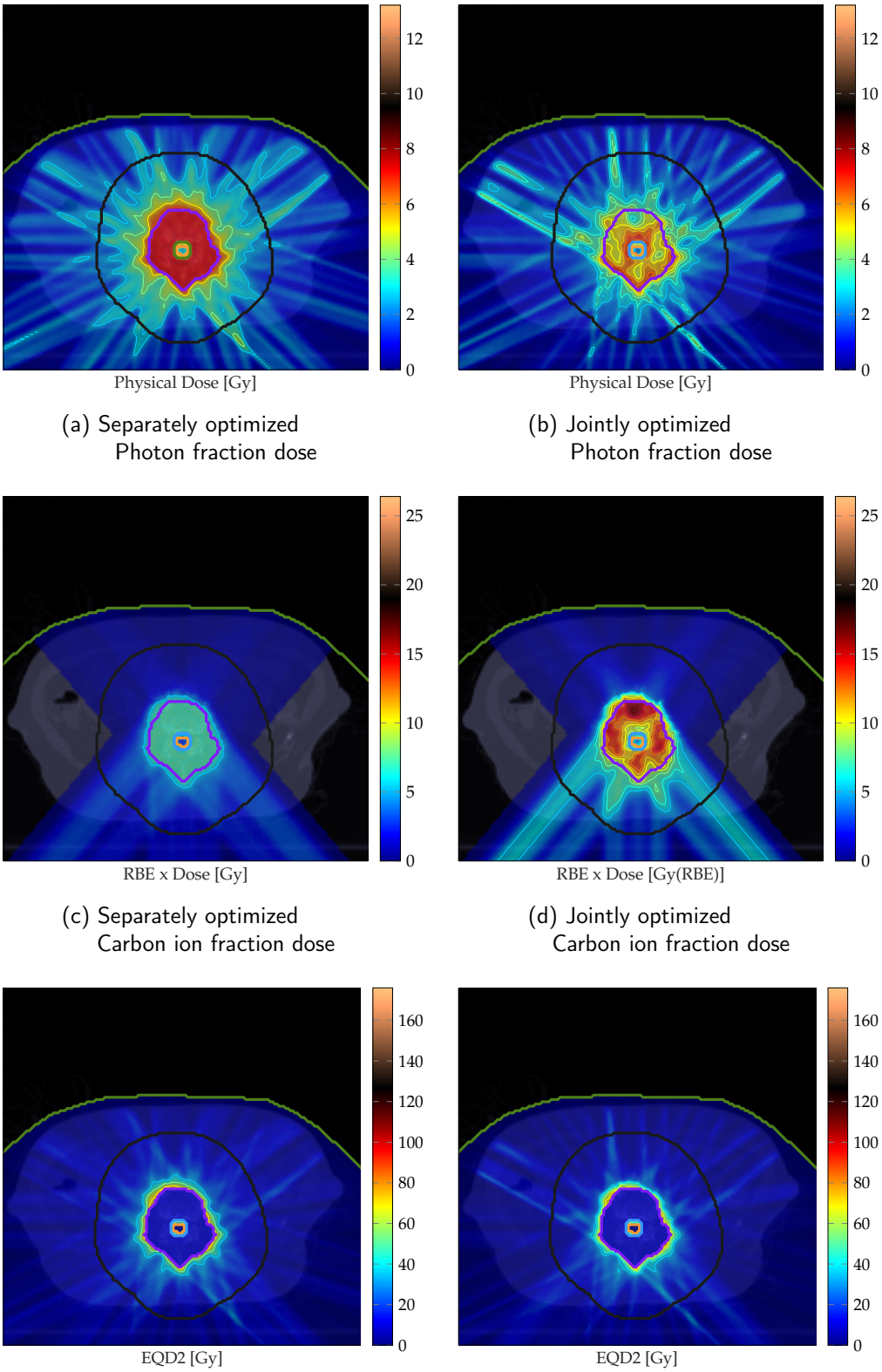

(a) Separately optimized Photon fraction dose

(b) Jointly optimized Photon fraction dose

(c) Separately optimized Carbon ion fraction dose

(d) Jointly optimized Carbon ion fraction dose

(e) Separately optimized Cumulative EQD2

(f) Jointly optimized Cumulative EQD2

Figure IV.2: Fraction doses for separately optimized and jointly optimized treatment of 4 fractions of photons and 1 fraction of carbon ions. (a) Photon fraction dose of the separately optimized treatment (b) Photon fraction dose of the jointly optimized treatment (c) Carbon ion fraction RBE $\times$ dose of the separately optimized treatment (d) Carbon ion fraction RBE $\times$ dose of the jointly optimized treatment (e) Cumulative EQD2 of the separately optimized treatment (f) Cumulative EQD2 of the jointly optimized plan.

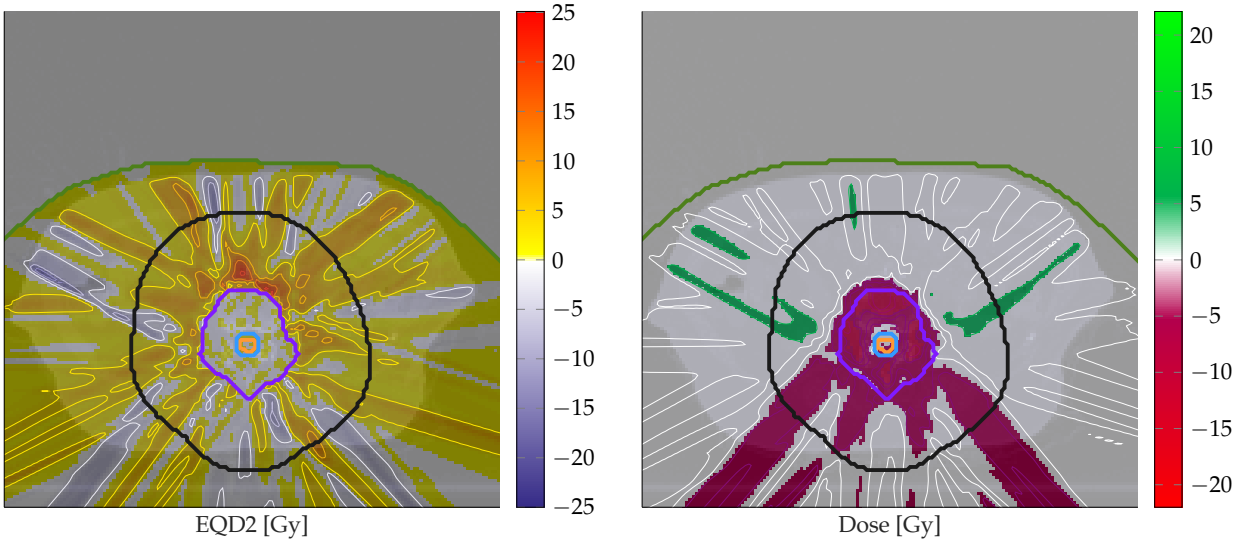

(a) EQD2 difference
(Simple combination – Jointly optimized plan)

(b) Difference in fraction dose
(Photon fraction – Carbon ion fraction)

Figure IV.3: (a) Difference in cumulative EQD2 between separately optimized plans and jointly optimized with a fixed fractionation schedule (b) Difference between the fraction photon physical dose and carbon ion RBE $\times$ dose for carbon ions for the fixed fraction joint optimization strategy

IV.2.1.2 Concurrent Irradiation

The concurrent irradiation strategy presents a hypothetical scenario where both modalities can be delivered within a single fraction, i.e., the time between carbon ion and photon irradiations is less than 6 hours. The fraction allocated joint optimization strategy limits the use of carbon ions, the predominant contributor to dose, to a single fraction. The concurrent irradiation strategy in contrast facilitates an additional degree of freedom where carbon ions can exploit their limited fractionation capabilities. The cumulative EQD2 of the photon fraction effects (physical dose shown in figure IV.4a) and carbon ion fraction effects (RBE $\times$ dose shown in figure IV.4b) are shown in figure IV.4c. The concurrent irradiation strategy shows a better cumulative EQD2 conformity illustrated by the larger differences seen in regions nearest to the target volume. This is especially noticeable in figure IV.4d. Figure IV.4e shows the difference in fraction doses of photons and carbon ions. Here photons and carbon ions deliver the equal effective fraction doses surrounding the cauda and at the perimeter of the target volume.

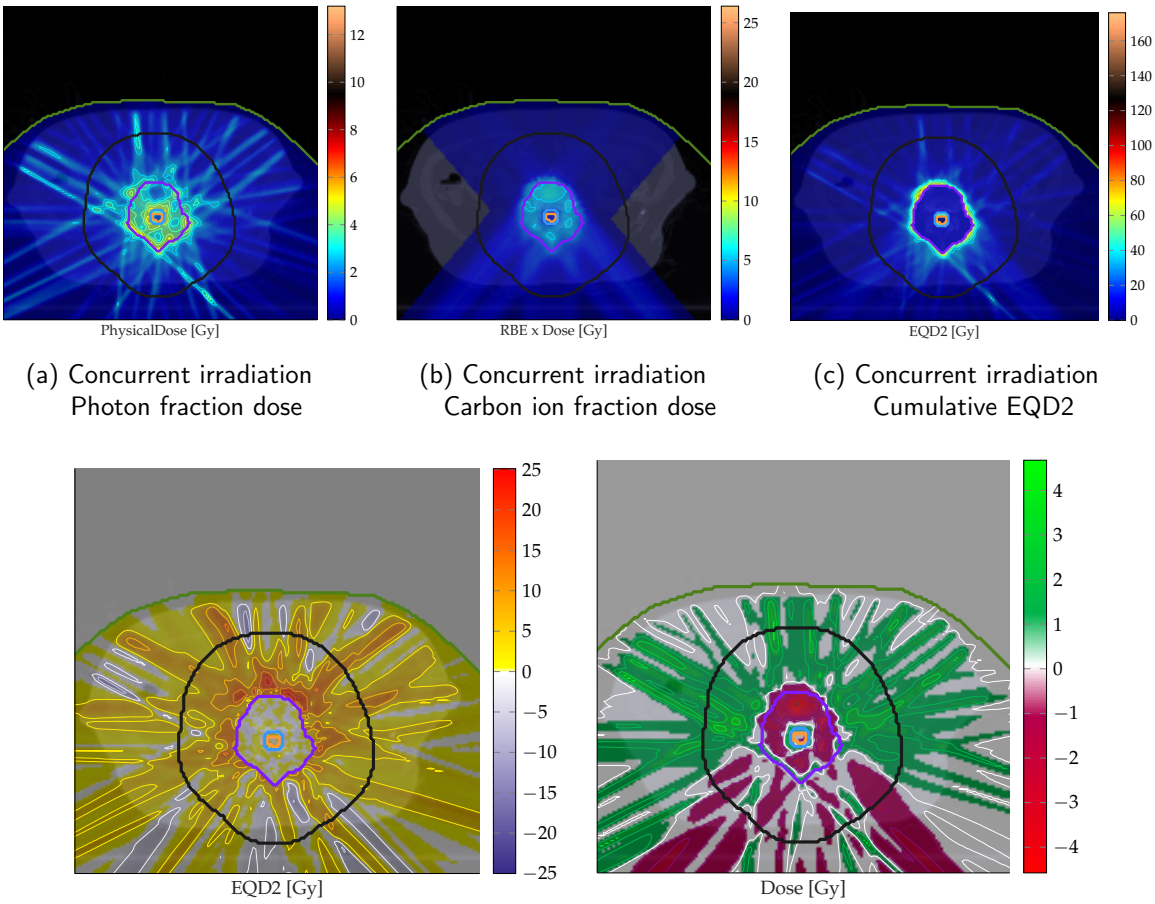

(a) Concurrent irradiation Photon fraction dose

(b) Concurrent irradiation Carbon ion fraction dose

(c) Concurrent irradiation Cumulative EQD2

(d) EQD2 difference (Simple combination - Concurrent irradiation)

(e) Difference in fraction doses (Photon fraction - Carbon ion fraction)

Figure IV.4: Dose distributions of the concurrent irradiation strategy (a) photon fraction physical dose (b) Carbon ion fraction RBE $\times$ dose (c) cumulative EQD2 of the concurrent irradiation strategy. (d) Difference in cumulative EQD2 between the simple combination plan and the concurrent irradiation strategy (e) Difference between the fraction photon physical dose and carbon ion RBE $\times$ dose for carbon ions

IV.2.1.3 Quantitative analysis

This section provides a quantitative analysis of the joint optimization strategy against the backdrop of separately optimized reference plans. Table IV.1 presents the EQD2 based treatment plan quality indicators for all plans and Figure IV.5 shows the Biological Effect Volume Histogram (EVH) of all plans for each of the VOIs.

The improved conformity of the jointly optimized strategies is reflected as a reduction in mean EQD2 in the dose fall-off region by 1.2 Gy and 2.02 Gy with the use of the fixed fraction jointly optimized plan and the concurrent irradiation strategy, respectively, compared to the simple combination strategy. The jointly optimized plans and the concurrent irradiation strategy also achieve a mean EQD2 reduction of 0.1 Gy and 0.18 Gy, respectively, in the external healthy tissue (excluding the dose fall-off region).

The improved redistribution of fluence also results in a reduction of cumulative EQD2 to adjacent critical structures. The jointly optimized plan and the concurrent irradiation strategy achieve a EQD2 reduction of 0.99 Gy and 3.07 Gy in near maximum dose to 3 mm margin around the cauda and a reduction of 1.59 Gy and 1.34 Gy in near maximum dose to the cauda, as compared to the simple combination treatment. Naturally the unimodal carbon ion treatment is best at reduction of integral dose in external healthy tissue, however this comes at the cost of a higher near maximum dose to the cauda. To summarize, for a comparable target coverage, joint optimization strategies show an improvement in sparing of adjacent critical structures such as the cauda and external healthy tissue.

Table IV.1: EQD2 based treatment plan quality indicators comparing 5 fraction treatments: (1) unimodal photon, (2) unimodal carbon ion, (3) simple combination of independently optimized photon–carbon ion treatments (4) jointly optimized photon–carbon ion (with fixed fractions) and (5) jointly optimized concurrent irradiation photon–carbon ion plans.

VOI (QI)	Unimodal Photon	Unimodal Carbon ion	Separately optimized	Jointly optimized	Jointly optimized Concurrent irr.
CTV $D_{95\%}$	48.32	48.42	48.43	48.80	49.08
Cauda $D_{5\%}$	31.42	31.67	31.42	29.83	30.08
Cauda + 3mm $D_{5\%}$	61.69	63.59	61.88	60.89	58.81
Dose Fall-off D_{mean}	9.76	6.38	9.08	7.88	7.06
External D_{mean}	0.89	0.48	0.81	0.71	0.63

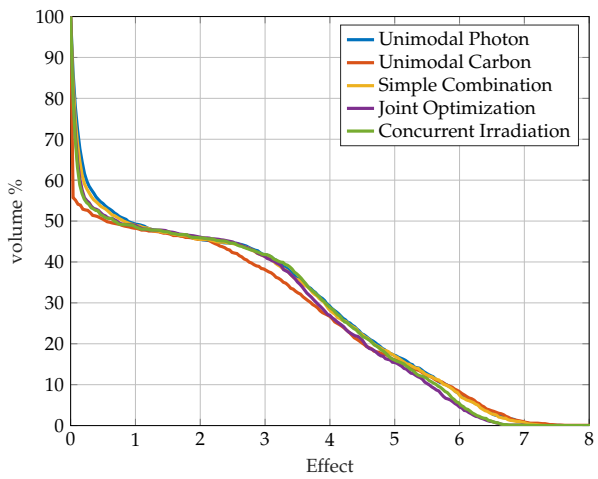

(a) Cauda

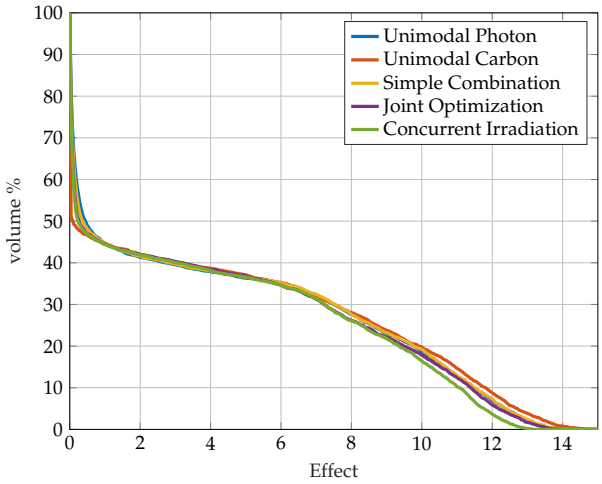

(b) Cauda + 3mm margin

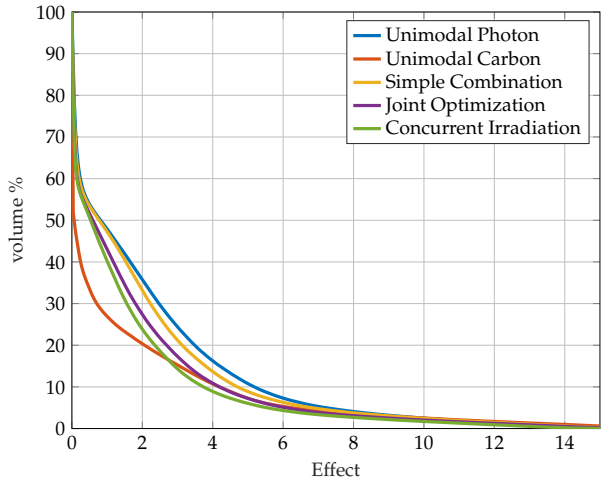

(c) Dose fall-off

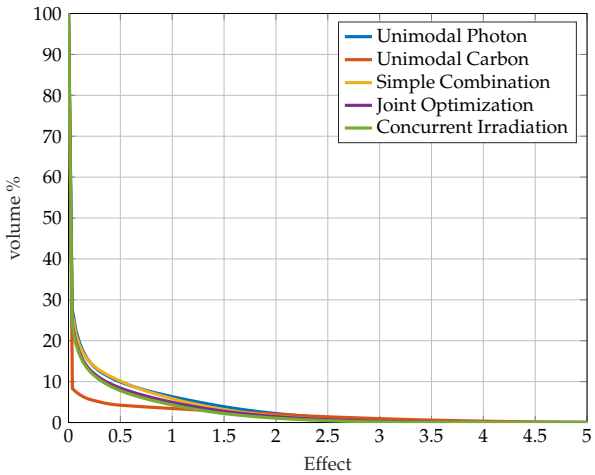

(d) External

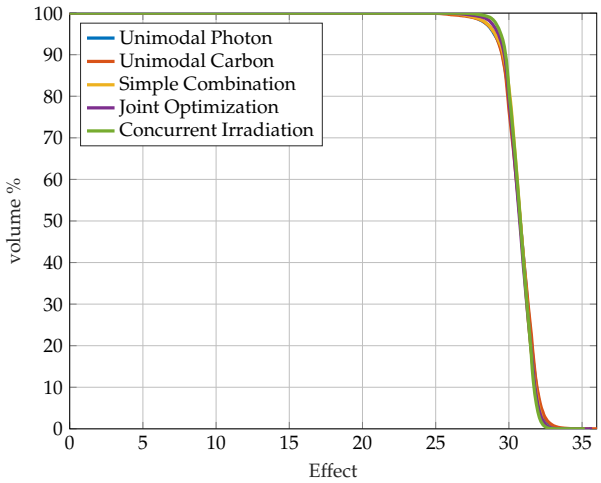

(e) CTV

Figure IV.5: The EVH comparing the unimodal carbon ion plan, unimodal photon plan, separately optimized photon–carbon ion combination, jointly optimized photon–carbon ion plan with fixed fractions and jointly optimized photon–carbon ion plan for concurrent irradiation for a spinal metastasis patient case. This is shown for the structures (a) Cauda, (b) Cauda + 3mm margin, (c) Dose fall-off margin around the target volume, (d) External healthy tissue and (e)CTV

IV.3 Impact of fraction allocation

The number of treatment fractions allocated to each modality is a treatment design parameter that is essential to the joint optimization problem definition in this study. This section presents the consequences of fraction distributions on the overall plan quality. In a 5 fraction treatment for a spinal metastasis patient case, the number of particle therapy fractions were varied from 0 to 5, i.e., the treatment plans vary from a unimodal photon treatment to mixed modality treatments, finally to a unimodal particle therapy treatment. Figure IV.6 shows the variation of treatment plan quality indicators in photon–carbon ion treatments and photon–proton treatments for the 6 fraction distribution scenarios. Apart from the dosimetric quantities, figure IV.6f shows the variation in objective function values for the six scenarios. In general, the mixed modality treatments are more desirable than unimodal treatments owing to the degree of freedom associated with the redistribution of dose between the two modalities. Figures IV.6a and IV.6b show that the variations in target coverage are small and, as expected, the unimodal carbon ion treatment fare worse than the unimodal proton treatment due to the sub optimal beam angle selection, increased RBE and reduced fractionation capacity of carbon ions. Furthermore, photon–proton combined treatments are better at sparing the cauda due to increased fractionation effect as compared to photon–carbon ion treatments and the absence of a fragmentation tail. For this given treatment setup, the objective function evaluation shows that for the photon–carbon ion combined treatment the ideal fraction distribution is one fraction of carbon ions and four fractions of photons. Whereas, for photon–proton combination the ideal fraction allocation is two fractions of protons and three fractions of photons. This result suggests that due to the reduced fractionation effect seen with carbon ions a very limited number of carbon ion fractions are necessary to generate the ideal photon–carbon ion combined treatment. It is important to note that, the ideal fractionation schedule for sparing of the cauda (2:3 fractions for photon–proton treatments and 3:2 fractions for photon–carbon ion treatments) does not correspond with the ideal fractionation schedule recommended by this study.

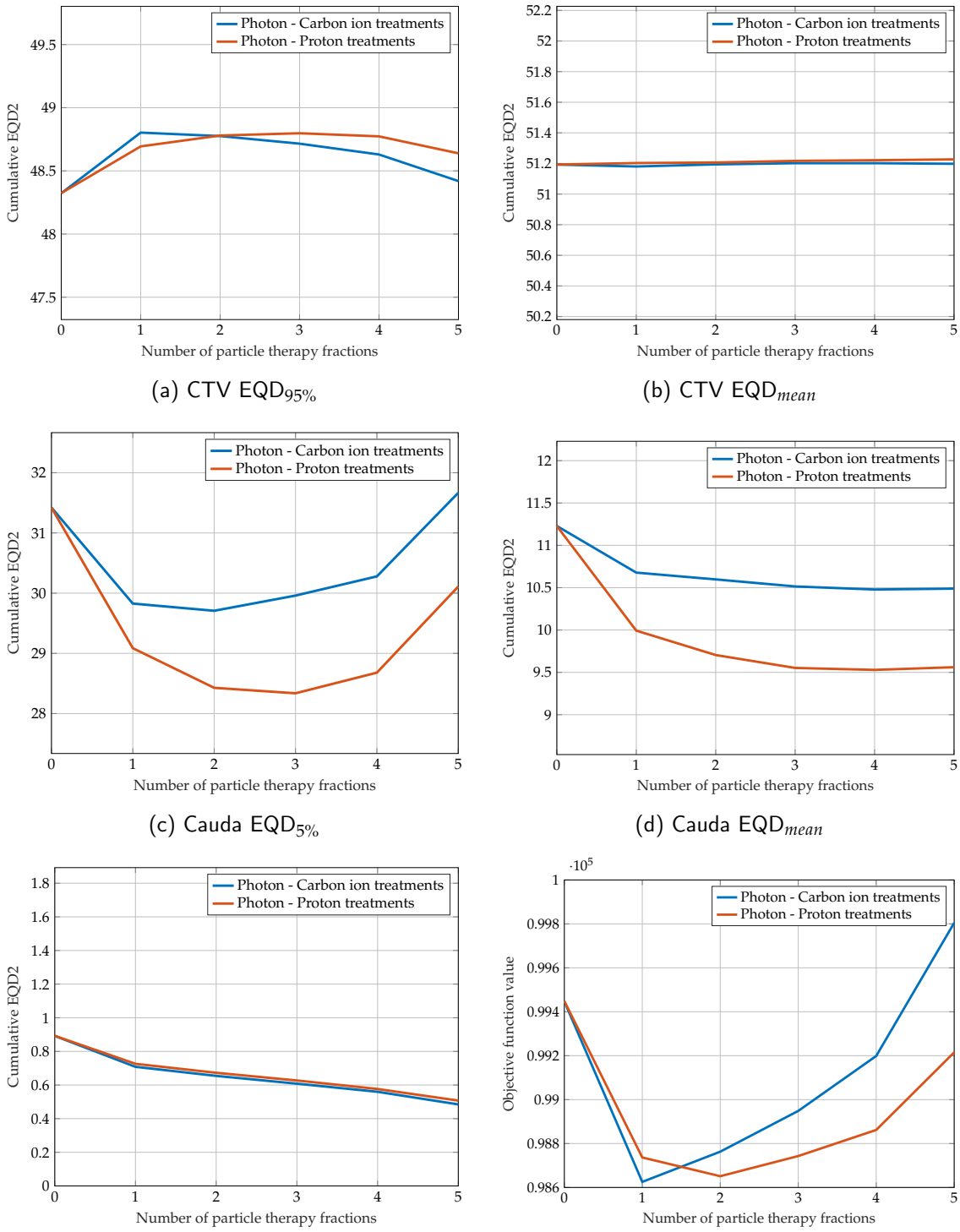

(a) CTV $EQD_{95\%}$

(b) CTV EQD_{mean}

(c) Cauda $EQD_{5\%}$

(d) Cauda EQD_{mean}

(e) External EQD_{mean}

(f) Objective function values

Figure IV.6: Comparison of treatment plan quality indicators and objective function values for 5 fraction photon–carbon ion and 5 fraction photon–proton jointly optimized treatments varying with the number of fractions allocated to particle therapy. EQD2 based treatment plan quality indicators for a series of photon–carbon ion treatments (▬) and a series of photon–proton treatments (▬): (a) CTV $EQD_{95\%}$ (b) CTV EQD_{mean} (c) Cauda $EQD_{5\%}$ (d) Cauda EQD_{mean} (e) External EQD_{mean} (f) variation of objective function value with fraction allocation to particle therapy.

IV.4 Impact of LQ model parameter selection

Within the bounds of the LQ model, a gain in sparing of healthy tissue by way of fractionation is only possible when the target volume is more radiosensitive, i.e., has a higher $\alpha^\gamma/\beta^\gamma$ ratio, than healthy tissue. In the context of joint optimization, such an assumption provides an impetus to the optimizer to distribute dose in and around critical structures uniformly over all available fractions.

IV.4.1 Spinal Metastasis

To see the impact of $\alpha^\gamma, \beta^\gamma$ selection on jointly optimized plans, a hypothetical treatment plan was generated for the spinal metastasis cases presented above. The treatment protocol was identical to that used in the previous sections, presented in Chapter III.2.2. For the used case of no fractionation gain the LQ model parameters for tumour and healthy tissue are assumed to be equal, $\alpha_T^\gamma/\beta_T^\gamma = \alpha_{NT}^\gamma/\beta_{NT}^\gamma = 0.1/0.05$ Gy. Figure IV.7 shows the comparison of photon–carbon ion jointly optimized treatments with a predicted fractionation gain ($\alpha_T^\gamma/\beta_T^\gamma > \alpha_{NT}^\gamma/\beta_{NT}^\gamma$) and without a predicted fractionation gain ($\alpha_T^\gamma/\beta_T^\gamma = \alpha_{NT}^\gamma/\beta_{NT}^\gamma$).
The previously seen, joint optimization result considering a fractionation gain is shown in figures IV.7b, IV.7d and IV.7f. Figure IV.7a and IV.7c show the photon fraction physical dose and carbon ion RBE $\times$ dose of a jointly optimized plan where $\alpha_T^\gamma/\beta_T^\gamma = \alpha_{NT}^\gamma/\beta_{NT}^\gamma$. There is a 39.9% increase in the RBE weighted carbon ion dose contribution to the target volume and a corresponding decrease in photon contribution. The photon contributions are downregulated and limited to regions that lie in the shadow of the cauda with respect to each carbon ion beam. This suggests that the photons are used to improve the physical dose conformity in regions of the target volume which are difficult to access with the predetermined carbon ion beam angles.

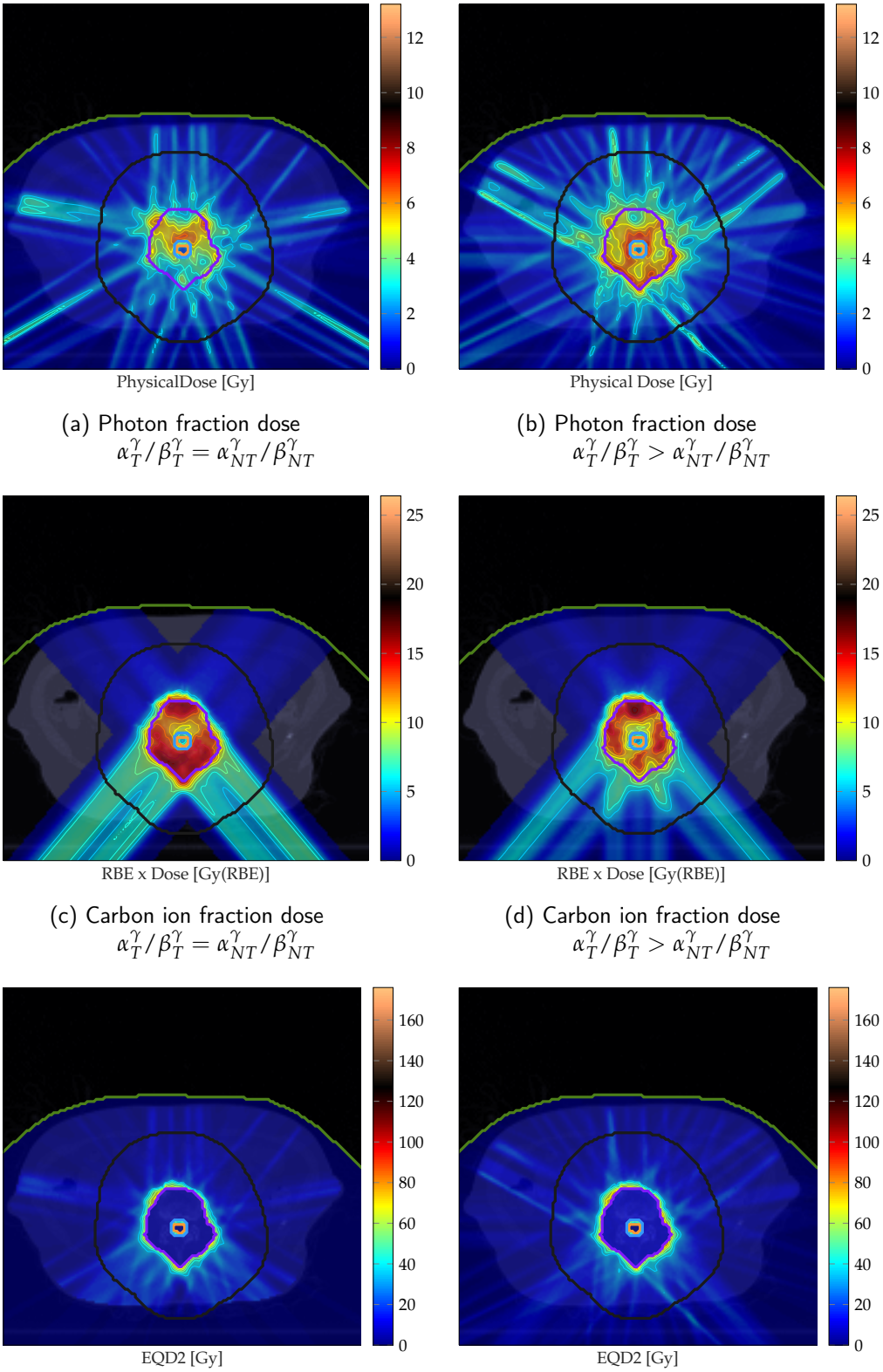

(a) Photon fraction dose $\alpha_T^\gamma/\beta_T^\gamma = \alpha_{NT}^\gamma/\beta_{NT}^\gamma$

(b) Photon fraction dose $\alpha_T^\gamma/\beta_T^\gamma > \alpha_{NT}^\gamma/\beta_{NT}^\gamma$

(c) Carbon ion fraction dose $\alpha_T^\gamma/\beta_T^\gamma = \alpha_{NT}^\gamma/\beta_{NT}^\gamma$

(d) Carbon ion fraction dose $\alpha_T^\gamma/\beta_T^\gamma > \alpha_{NT}^\gamma/\beta_{NT}^\gamma$

(e) cumulative EQD2 $\alpha_T^\gamma/\beta_T^\gamma = \alpha_{NT}^\gamma/\beta_{NT}^\gamma$

(f) Cumulative EQD2 $\alpha_T^\gamma/\beta_T^\gamma > \alpha_{NT}^\gamma/\beta_{NT}^\gamma$

Figure IV.7: The fraction dose and cumulative EQD2 distributions of jointly optimized plans with a fractionation gain ($\alpha_T^\gamma/\beta_T^\gamma > \alpha_{NT}^\gamma/\beta_{NT}^\gamma$) and without a predicted fractionation gain ($\alpha_T^\gamma/\beta_T^\gamma = \alpha_{NT}^\gamma/\beta_{NT}^\gamma$). For the jointly optimized plans (a) shows the photon fraction physical dose without a fractionation gain (b) shows the photon fraction physical dose with a fractionation gain (c) shows the carbon ion fraction RBE $\times$ dose without a fractionation gain (d) shows the carbon ion fraction RBE $\times$ dose with a fractionation gain. (e) Shows the cumulative EQD2 of a jointly optimized plan when there is no fractionation gain and (f) Shows the cumulative EQD2 of a jointly optimized plan when there is a fractionation gain.

IV.4.2 Base of skull chordoma

A 37 fraction base of skull chordoma treatment was optimized to showcase a more practical example. For this indication, clinical assumption of LQ model parameters is $\alpha_T^\gamma/\beta_T^\gamma = \alpha_{NT}^\gamma/\beta_{NT}^\gamma = 0.1/0.05$ [Gy]. The jointly optimized plan was compared to a unimodal carbon ion treatment of 12 fractions. The jointly optimized plan was predicted to have an almost only carbon ion dose distribution and therefore to assess the similarity to unimodal treatment the jointly optimized plan was compared against a unimodal carbon ion treatment of 12 fractions. Figure IV.8a and IV.8b show the jointly optimized photon and carbon ion fraction dose contributions and IV.8c shows the biological effect distribution of the 12 fraction unimodal carbon ion treatment. Figure IV.8b shows that almost all the dose to the target volume is delivered by carbon ions, however there is a small region in the shadowed edge of the brainstem which is irradiated by a single beam of photons. This photon contribution was motivated by a subtle reduction in the dose to the centre of the brainstem as seen in Table IV.2. The effect volume histogram shown in Figure IV.8f also confirms that the jointly optimized plan is almost identical to the unimodal 12 fraction carbon ion treatment. Comparing the objective function values, the jointly optimized treatment fares better with a lower objecitve function value (91.16) as compared to the unimodal carbon ion treatment (98.23).
This implies that when there is no fractionation gain observed the optimizer opts to use carbon ions in order to utilize the sharp dose gradient and reduce the integral dose to the healthy tissue in the external structure. The photon contribution seen at the brainstem interface is motivated by an improvement in dose conformity to the target volume in the shadow of the brain stem with respect to the carbon ion beams. This can be seen in figure IV.8e.

Table IV.2: Treatment plan quality indicators and treatment plan objectives, based on EQD1.8, of an isoeffective 12 fraction unimodal carbon ion plan and 37 fraction jointly optimized photon–carbon ion plan for base of skull chordoma

Treatment plan	CTV $D_{95\%}$	Brainstem $D_{5\%}$	Brainstem ctr. $D_{5\%}$	Fall-off D_{mean}	External D_{mean}
Only Carbon ions	65.8	52.5	41.4	30.1	0.54
Jointly optimized	65.8	52.7	41.3	30.06	0.55

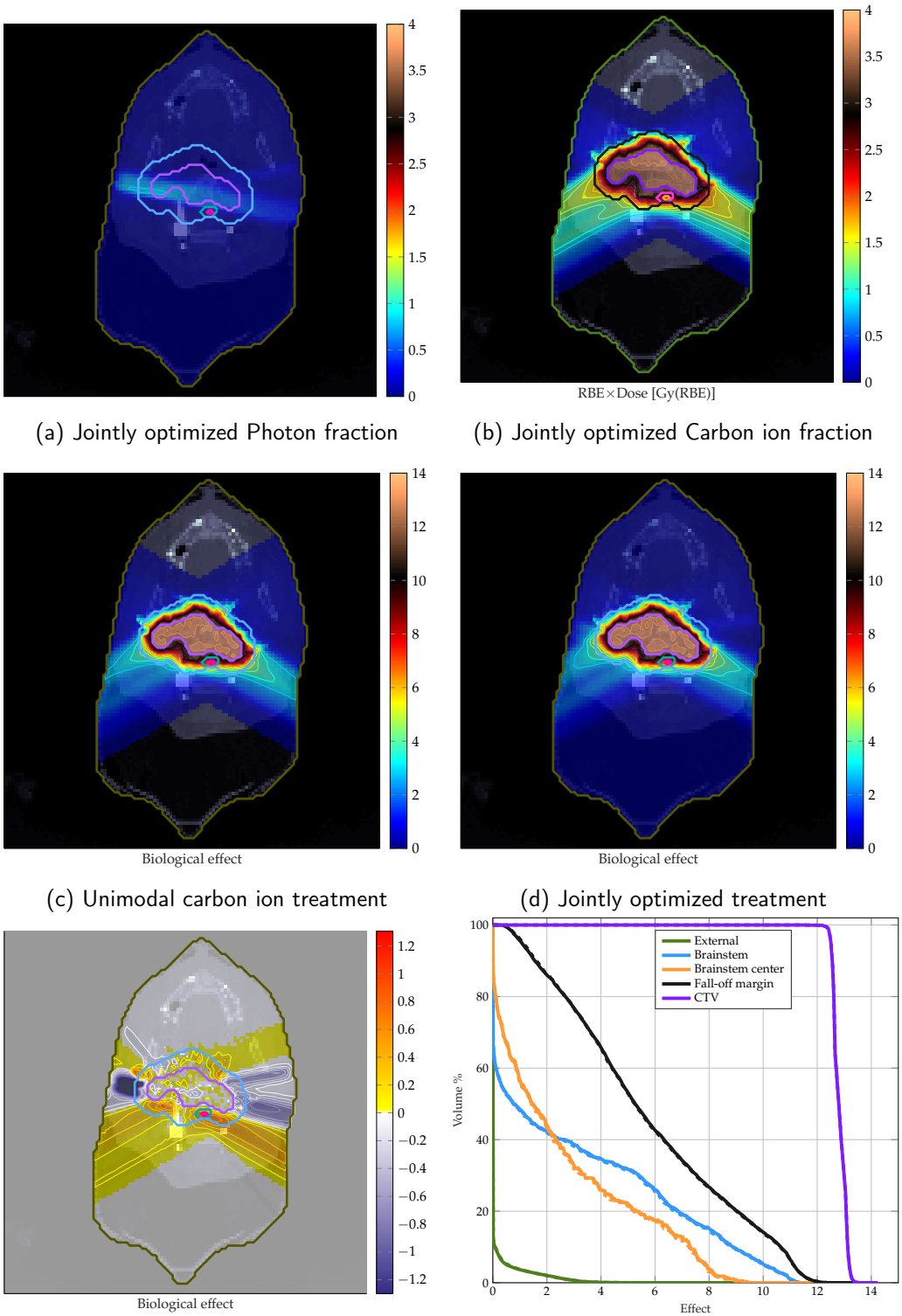

(a) Jointly optimized Photon fraction

(b) Jointly optimized Carbon ion fraction

(c) Unimodal carbon ion treatment

(d) Jointly optimized treatment

(e) Difference between unimodal carbon ion plan and jointly optimized plan

(f) Effect Volume Histograms of the joint optimized plan and unimodal carbon ion

Figure IV.8: fraction dose and cumulative effect difference between a 12 fraction unimodal carbon ion treatment and 37 fraction jointly optimized treatment ($n^{\gamma} = 25, n^{C} = 12$). (a) the jointly optimized photon contribution (b) the jointly optimized carbon ion contribution (c) cumulative biological effect of the unimodal carbon ion treatment (d) cumulative biological effect of jointly optimized photon–carbon ion treatment (e) difference in cumulative biological effect between the unimodal carbon ion plan and jointly optimized photon–carbon ion plan. (f) The EVH comparing a 37 fraction jointly optimized treatment ($n^{C} = 12, n^{\gamma} = 25$, dashed line ▪▪▪▪) and a 12 fraction carbon ion treatment (solid line ▬▬).

IV.5 Glioblastoma

This section presents the results of the investigation of the application of joint optimization for infiltrative tumours, focussing on glioblastoma. The cohort for this study consists of 6 glioblastoma patient cases, of which two patient cases have been highlighted for a qualitative insight into joint optimization. Treatment plan quality indicators for all plans are presented in section IV.5.3.
The specifics of the treatment planning protocol are presented in section III.4. Jointly optimized plans were generated by simultaneously optimizing 25 unimodal fractions of photons and 6 unimodal carbon ion fractions. The jointly optimized plans are compared against a reference plan of the simple combination of separately optimized unimodal treatments. The photon component of the reference plan delivers a uniform 2 Gy per fraction to the target volumes and the carbon ion component delivers 3 Gy(RBE) per fraction to the GTV. Such a boost treatment is motivated by the use of photons to protect infiltrated healthy tissue in the CTV through fractionation while using carbon ions to boost the dose to the GTV. Jointly optimized plans were designed to also follow this rationale.
The jointly optimized treatments are quite sensitive to the individual objective penalty settings. Such changes affect not only the overall treatment but also the contributions of each modality. Two types of jointly optimized treatments are presented in this section: (1) where sparing of healthy tissue in the CTV through fractionation is prioritized (2) where sparing of external healthy brain is prioritized with a reduced weight to sparing healthy tissue within the CTV. This plan is henceforth referred to as *jointly optimized plan #2*.

IV.5.1 Patient I

For Patient I, shown in figure IV.9 the target volumes abut the critical structures such as the brainstem, chiasm and optic nerves. Figures IV.9b and IV.9e show the fraction photon physical dose and the carbon ion RBE weighted dose produced by joint optimization. Carbon ion dose is restricted to the GTV, whereas photons deliver dose to the CTV and the outer edge of the GTV. Compared to the reference plan, the joint optimization strategy down regulates the overall carbon ion contribution. At the center of the tumour, jointly optimized carbon ion fraction delivers nearly twice the dose as the reference carbon ion fraction. This carbon ion contribution generally reduces when approaching the CTV - GTV interface. At this outer rim of the GTV, most of the dose is delivered by photons. In the CTV, as with the reference plan, almost all the dose is delivered by photons. At the interface of target volumes and critical structures, like the brainstem, both modalities in the joint optimizations strategy deliver equal fraction doses in order to maximally fractionate dose at this location. This can be seen in figure IV.10b, which shows the difference between the photon fraction physical dose and carbon ion fraction RBE $\times$ dose. The green areas signify regions where photons deliver a larger fraction dose and the red regions indicate the same for carbon ions. The white

regions shown in this figure are locations where both photons and carbon ions deliver equal fraction doses.
Overall, the jointly optimized plan improves high dose conformity (5 Gy reduction in mean dose to dose fall-off structure) and reduces cumulative the near maximum dose to the brainstem by 10.29 Gy and to the ipsilateral optic chiasm and nerves by 6.46 Gy and 16.57 Gy respectively. This reduction can be clearly seen in figure IV.10a that shows the difference in cumulative EQD2 between the reference plan and the jointly optimized plan. Furthermore the jointly optimized strategy also exhibits a more conformal high dose fall-off in the CTV around the GTV. The Biological Effect Volume Histogram (EVH) for Patient I are presented in Figure IV.14a.
Figures IV.9c, IV.9f and IV.9i show the photon fraction physical dose, carbon ion fraction RBE weighted dose and cumulative EQD2 for jointly optimized plan #2, which focusses on sparing of external healthy tissue. Here the carbon ion contribution is increased within the GTV as seen in the dose difference between the photon fractions and carbon ion fractions in figure IV.10d. However the photon fractions still deliver the bulk of dose to the CTV and the interfaces with abutting critical structures. The increased carbon ion contribution of jointly optimized plan #2 allows for a further improvement in external dose conformity (7.63 Gy reduction in mean dose to dose fall-off) which results in a further reduction of dose to adjacent critical structures. Figure IV.10c shows a reduction of cumulative near maximum dose of 17.7 Gy to the brainstem , 10.57 Gy to the chiasm and 16.72 Gy to the optic nerve. It also results in a 0.68 Gy reduction in mean dose to external healthy brain.
The highly modulated carbon ion beams of jointly optimized plans also result in highly heterogeneous LET distributions within the target volumes. Figure IV.11 shows the dose averaged LET distributions and the LET weighted fraction dose for the the reference plan and two jointly optimized plans. Figure IV.11e shows that the LET weighted carbon ion dose is concentrated at the center of the tumour where as for the reference plan the LET weighted dose is maximum at the distal edge of the target volume, adjacent to the brainstem. The external prioritized jointly optimized plan has an increased carbon ion contribution where a large proportion of the LET weighted dose is delivered to the center of the GTV.

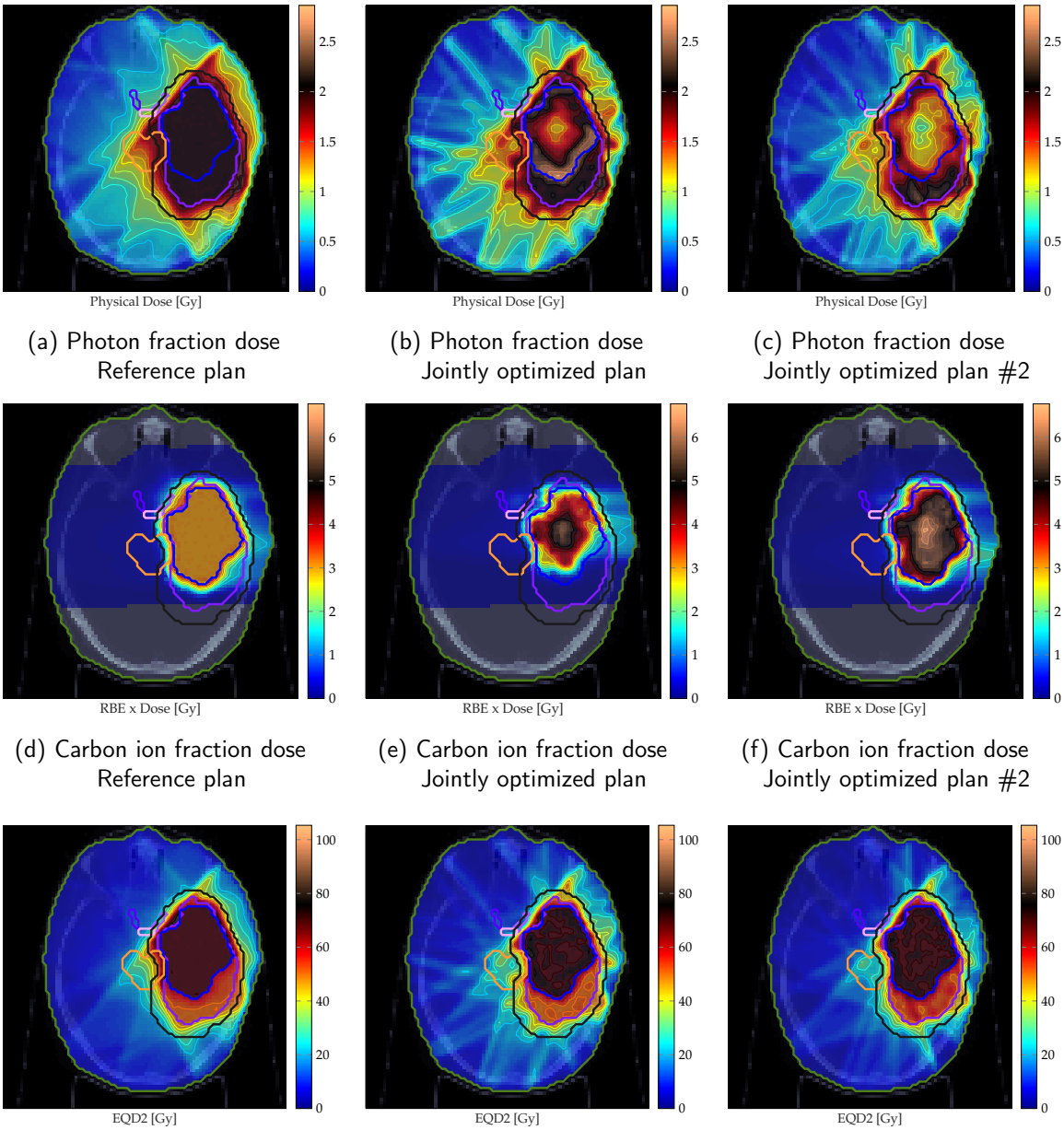

(a) Photon fraction dose Reference plan

(b) Photon fraction dose Jointly optimized plan

(c) Photon fraction dose Jointly optimized plan #2

(d) Carbon ion fraction dose Reference plan

(e) Carbon ion fraction dose Jointly optimized plan

(f) Carbon ion fraction dose Jointly optimized plan #2

(g) Cumulative EQD2 Reference plan

(h) Cumulative EQD2 Jointly optimized plan

(i) Cumulative EQD2 Jointly optimized plan #2

Figure IV.9: Dose distributions of the reference separately optimized simple combination plan and jointly optimized plans for Patient I. (a) Photon fraction physical dose of the reference plan (b) Photon fraction physical dose of the jointly optimized plan (c) Photon fraction physical dose of the jointly optimized plan #2 (d) Carbon ion fraction RBE $\times$ dose of the reference plan (e) Carbon ion fraction RBE $\times$ dose of the jointly optimized plan (f) Carbon ion fraction RBE $\times$ dose of the jointly optimized plan #2 (g) Cumulative EQD2 of the simple combination of the reference plan (h) Cumulative EQD2 of the jointly optimized plan (i) Cumulative EQD2 of the jointly optimized plan #2. The VOIs are the GTV (——), CTV (——) as target volumes, and critical structures like the brainstem (——), optic chiasm (——) and optic nerve (——).

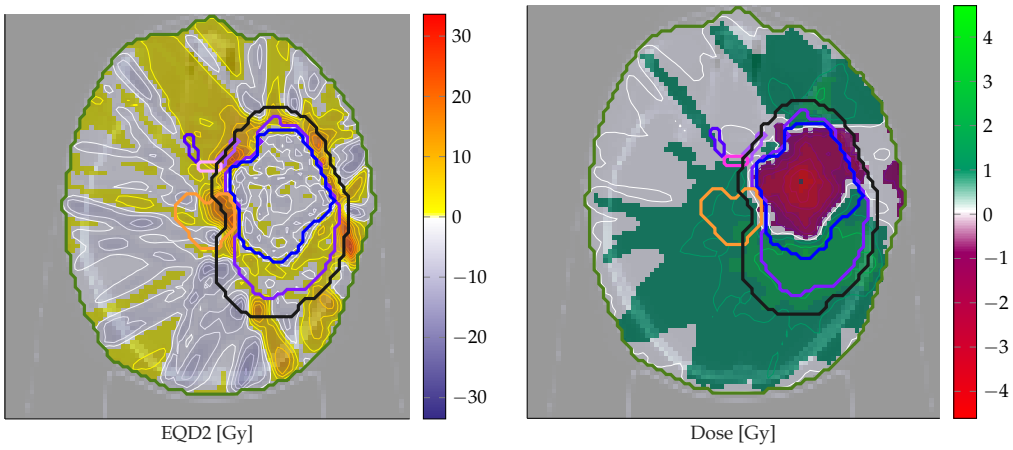

(a) EQD2 Difference
(Reference plan – Jointly optimized plan)

(b) Jointly optimized fraction dose difference
(Photon fraction – Carbon ion fraction)

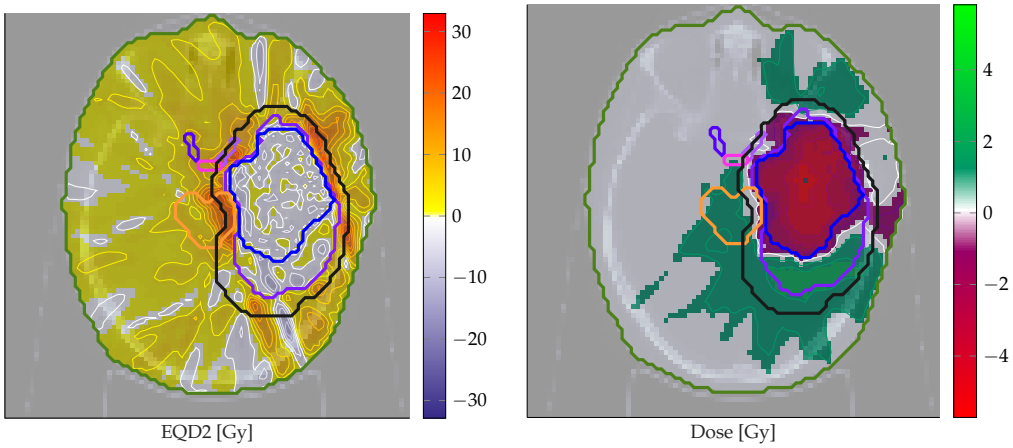

(c) EQD2 Difference
(Reference plan – Jointly optimized plan #2)

(d) Joint optimized #2 fraction dose difference
(Photon fraction – Carbon ion fraction)

Figure IV.10: Comparing the cumulative EQD2 distributions of the reference plan and the jointly optimized plans and fraction dose contributions of each modality for the jointly optimized treatments for Patient I (a) The cumulative EQD2 difference between the reference plan and jointly optimized plan (b) Difference in fraction dose contribution between photon fraction and carbon ion fraction for the jointly optimized plan (c) The cumulative EQD2 difference between the reference plan and jointly optimized plan #2, (d) Difference in fraction dose contribution between photon fraction and carbon ion fraction for the jointly optimized plan #2.

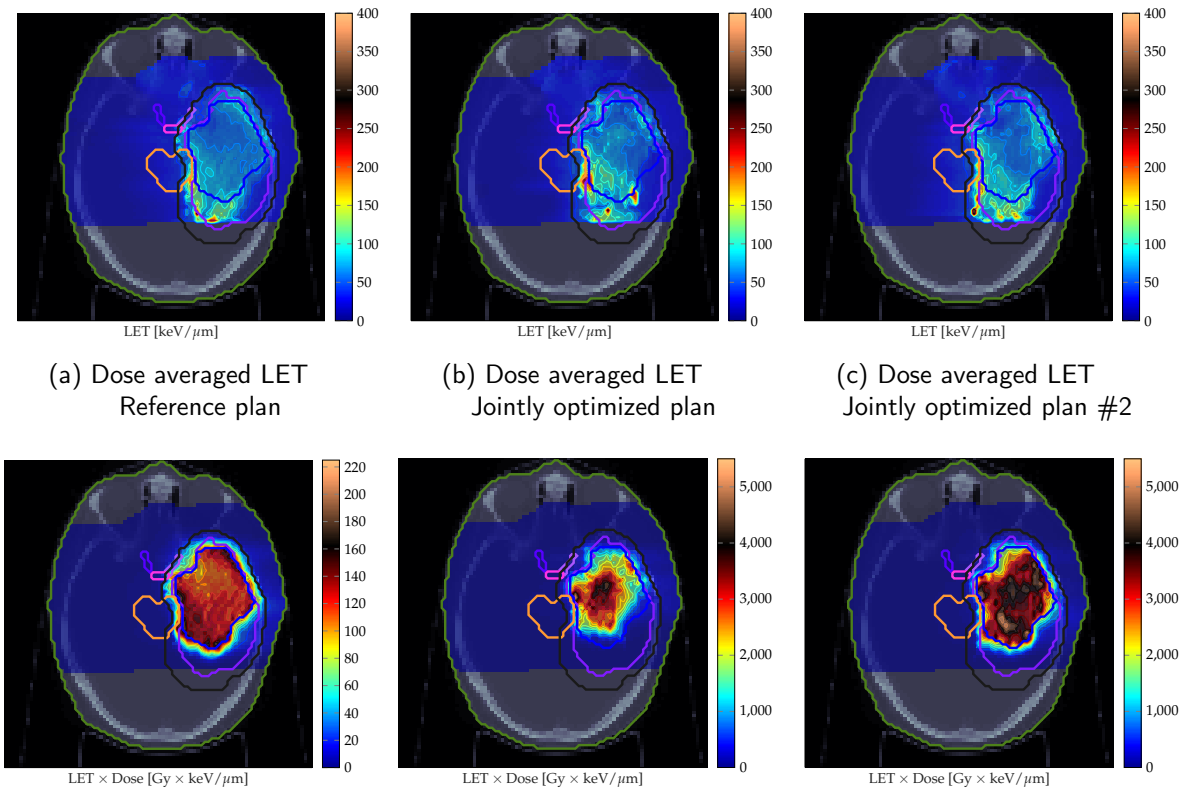

(a) Dose averaged LET Reference plan

(b) Dose averaged LET Jointly optimized plan

(c) Dose averaged LET Jointly optimized plan #2

(d) LET weighted dose Reference plan

(e) LET weighted dose Jointly optimized plan

(f) LET weighted dose Jointly optimized plan #2

Figure IV.11: Dose averaged LET distributions and LET weighted dose distributions for the reference separately optimized simple combination plan and jointly optimized plans for Patient I. (a) Dose averaged LET distribution of the reference plan (b) Dose averaged LET distribution of the jointly optimized plan (c) Dose averaged LET distribution of jointly optimized plan #2 (d) LET weighted dose distribution of the reference plan (e) LET weighted dose distribution of the jointly optimized plan (f) LET weighted dose distribution of the jointly optimized plan #2 .

IV.5.2 Patient II

Patient I showcases a large GTV (143 cm^3) with a relatively small CTV which is larger than the GTV by a factor of 2.7. Patient II shows a different scenario, one where the GTV is comparatively smaller (68.9 cm^3) but the CTV is larger than GTV by a factor of 3.8. There are no abutting critical structures apart from the external healthy brain. Figure IV.12 shows the photon fraction physical dose, carbon ion fraction RBE $\times$ dose and cumulative EQD2 of the reference and jointly optimized plan for the Patient II. For Patient II, most of the dose to the target volumes is delivered by photons. Here due to the increase in relative CTV volume the carbon ion contribution is downregulated in order to spare healthy tissue in the CTV. The impact of this down regulation can be seen in figure IV.13a, which shows the difference between the reference plan and the jointly optimized plan. The mean cumulative EQD2 to healthy tissue in the CTV is reduced by 4.24 Gy. Carbon ions are primarily utilized to improve dose conformity at the distal edge of the GTV, illustrated by a 1.17 Gy reduction in mean dose to the dose fall-off structure.
The jointly optimized plan #2 increases the carbon ion contribution in order to reduce the mean dose to the external healthy brain. This results in a more conformal plan reflected by a 2.91 Gy reduction in mean dose to the dose fall-off structure. The effect of this can be seen in figure IV.13c with an increased EQD2 contribution of the reference plan in the external tissue.

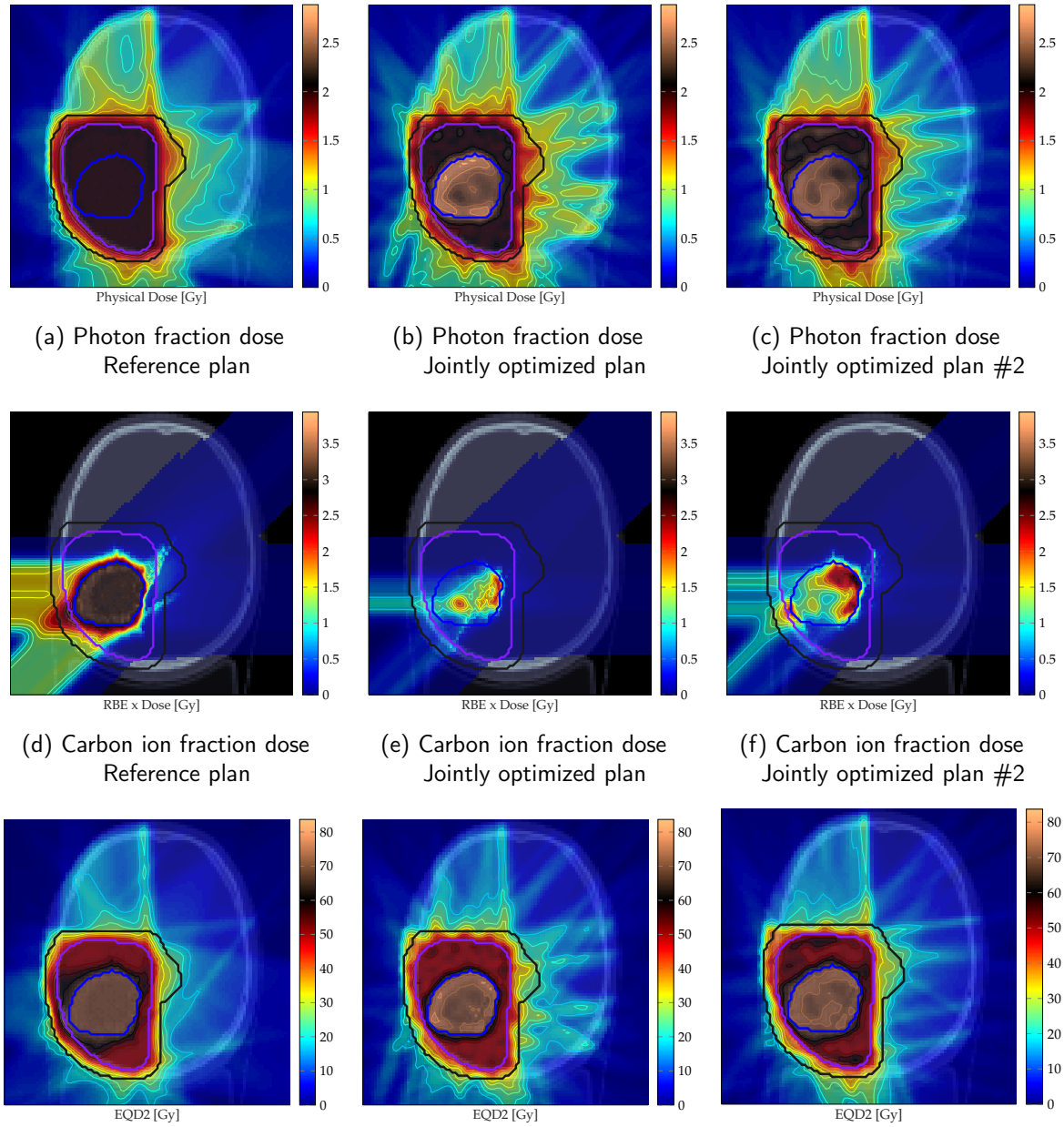

(a) Photon fraction dose Reference plan

(b) Photon fraction dose Jointly optimized plan

(c) Photon fraction dose Jointly optimized plan #2

(d) Carbon ion fraction dose Reference plan

(e) Carbon ion fraction dose Jointly optimized plan

(f) Carbon ion fraction dose Jointly optimized plan #2

(g) Cumulative EQD2 Reference plan

(h) Cumulative EQD2 Jointly optimized plan

(i) Cumulative EQD2 Jointly optimized plan #2

Figure IV.12: Dose distribution maps of the reference separately optimized simple combination plan and jointly optimized plan for Patient II. (a) Photon fraction physical dose of the reference plan, (b) Photon fraction physical dose of the jointly optimized plan, (c) Photon fraction physical dose of the jointly optimized plan #2, (d) Carbon ion fraction RBE $\times$ dose of the reference plan, (e) Carbon ion fraction RBE $\times$ dose of the jointly optimized plan, (f) Carbon ion fraction RBE $\times$ dose of the jointly optimized plan #2, (g) Cumulative EQD2 of the simple combination of the reference plan, (h) Cumulative EQD2 of the jointly optimized plan, (i) Cumulative EQD2 of the jointly optimized plan #2

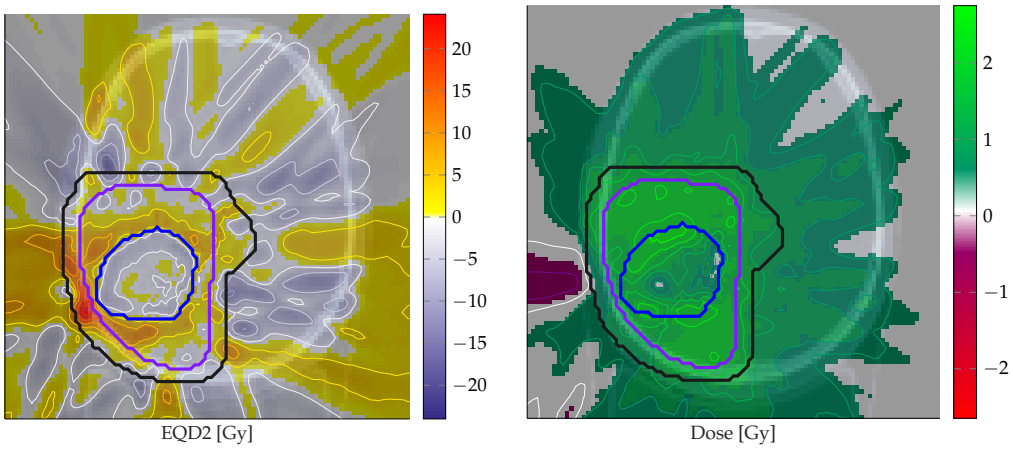

(a) EQD2 Difference
(Reference plan - Jointly optimized plan)

(b) Jointly optimized fraction dose difference
(Photon fraction - Carbon ion fraction)

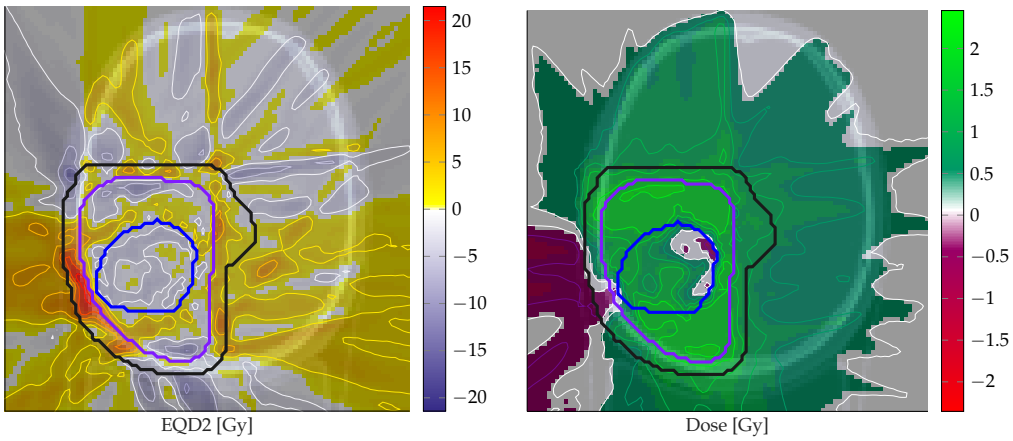

(c) EQD2 Difference
(Reference plan - Jointly optimized plan #2)

(d) Joint optimized #2 fraction dose difference
(Photon fraction - Carbon ion fraction)

Figure IV.13: Comparing the cumulative EQD2 distributions of reference plan and the jointly optimized plans and fraction dose contributions of each modality for the jointly optimized treatments for Patient II (a) The cumulative EQD2 difference between the reference plan and jointly optimized plan (b) Difference in fraction dose contribution between photon fraction and carbon ion fraction for the jointly optimized plan (c) The cumulative EQD2 difference between the reference plan and jointly optimized plan #2 (d) Difference in fraction dose contribution between photon fraction and carbon ion fraction for the jointly optimized plan #2

IV.5.3 Dose volume statistics

Table IV.3 presents EQD2 based dose quality indicators for the six considered cases. The prescribed dose in EQD2 differs from the prescribed dose by approximately 2%. For comparable target coverage the jointly optimized plans exhibit a better sparing of the critical structure at near maximum effect levels. Patient I, Patient III and Patient VI with the brainstem in proximity to the target volumes present a mean reduction in D5% of 4.58 ± 6.53 Gy. The chiasm was adjacent to the target volume for Patient I, Patient III, Patient IV and Patient VI and for these patients the jointly optimized plan presents a mean reduction in D5% of 7.81 ± 5.46 Gy. For the ipsilateral optic nerve in Patient I, Patient III and Patient VI the jointly optimized plan showed a reduction 11.12 ± 5.54 Gy in the near maximum dose. The effects of the spatio-temporal redistribution of fluence can be seen in conformity with 1.87 ± 1.65 Gy reduction in mean dose to the dose fall-off margin (used as an objective to enforce conformity) and in the reduction of mean dose to healthy tissue in the CTV by 4.27 ± 1.29 Gy averaged over all patients.

The jointly optimized plan prioritizing the sparing of external healthy brain (jointly optimized plan #2) generally increases the carbon ion contribution. This in turn results in a more conformal plan that reduces dose to critical structures at the cost of a higher dose to healthy tissue within the CTV. The improved conformity can be seen by a 2.42 ± 2.82 Gy reduction in mean dose to the dose fall-off structure compared to the reference plan. The near maximum dose in the brainstem is reduced by 8.45 ± 8.88 Gy, in chiasm by 10.29 ± 2.57 Gy and in the ipsilateral optic nerve by 13.64 ± 6.69 Gy, for the above mentioned patient cases. The mean dose in the healthy tissue within the CTV, however, is increased marginally by 0.17 ± 0.61 Gy.

Figure IV.14 shows the cumulative effect volume histograms of the reference plan, jointly optimized plan and jointly optimized plan #2 for all six patients. Here we see that within the jointly optimized plans it is possible to produce a spectrum of plans that, subject to the weight of objectives, reflect varying trade-offs between the competing objectives. The CTV-NT sparing curves in Figure IV.14 may be considered particularly important as it illustrates the gain in sparing of healthy tissue through fractionation although the underlying physical dose results in comparable coverage of the CTV. The differences seen in these two curves arise from assuming different LQ model parameters for tumour and healthy tissue propagated through the predicted effective carbon α^C, β^C from LEM IV for these two types of tissue.

Table IV.3: EQD2 [Gy] based glioblastoma treatment plan quality indicators for six patients comparing Reference plan, jointly optimized plan (JO) and the External brain sparing prioritized jointly optimized plan (NT prior.). Also given are the volumes of the target structures: GTV and CTV [cm^3].

	Patient I			Patient II			Patient III		
Vol. GTV (CTV) [cm^3]		143.0	(399.2)		68.9	(262.5)		74.7	(250.6)
VOI	Reference	JO	NT prior.	Reference	JO	NT prior.	Reference	JO	NT prior.
GTV $D_{95\%}$	69.03	67.71	68.78	68.93	68.19	68.98	69.20	67.96	68.88
CTV $D_{95\%}$	49.73	49.05	49.58	49.55	49.28	49.74	49.94	48.95	49.55
CTV D_{mean}	53.30	52.42	54.82	54.26	52.09	54.46	59.28	57.96	59.95
CTV NT D_{mean}	59.85	53.62	59.92	57.15	52.91	56.50	64.30	58.92	63.85
Dose Fall-off D_{mean}	42.55	37.54	34.92	35.16	33.98	32.25	48.14	46.21	45.96
External D_{mean}	4.37	4.37	3.69	1.64	1.72	1.58	4.82	4.77	4.46
Brainstem $D_{5\%}$	47.09	36.8	29.39	1.97	2.015	2.01	19.16	21.69	19.17
Chiasm $D_{5\%}$	34.02	27.56	23.46	1.52	0.45	1.51	53.51	43.128	42.82
Ipsi. Optic nerve $D_{5\%}$	40.17	23.6	23.45	-	-	-	50.37	39.09	32.13
Contra. Optic Nerve $D_{5\%}$	16.58	17.3	13.42	-	-	-	23.56	16.07	13.84
	Patient IV			Patient V			Patient VI		
Vol. GTV (CTV) [cm^3]		51.5	(345.6)		91.2	(332.7)		140.2	(395.3)
VOI	Reference	JO	NT prior.	Reference	JO	NT prior.	Reference	JO	NT prior.
GTV $D_{95\%}$	69.20	67.96	69.03	69.08	67.87	68.88	69.02	69.04	69.05
CTV $D_{95\%}$	49.51	48.82	49.63	48.90	48.78	49.29	50.89	49.52	49.83
CTV D_{mean}	54.99	54.69	56.73	57.16	57.17	59.07	63.03	62.24	63.52
CTV NT D_{mean}	59.00	55.43	59.74	60.65	57.75	61.26	66.90	63.59	67.63
Dose Fall-off D_{mean}	45.95	45.09	45.44	49.26	48.90	49.69	52.41	50.54	50.71
External D_{mean}	4.05	4.07	3.92	9.30	9.52	9.20	7.87	7.78	7.48
Brainstem $D_{5\%}$	3.06	2.90	2.65	0.14	0.14	0.14	24.91	18.92	17.26
Chiasm $D_{5\%}$	18.54	17.68	11.71	6.54	6.95	6.8	47.76	34.24	34.70
Ipsi. Optic nerve D_5	1.35	1.32	1.25	8.58	9.03	6.36	41.34	35.84	35.38
Contra Optic Nerve $D_{5\%}$	0.97	0.96	0.88	0.9	0.9	0.97	16.89	13.80	7.43

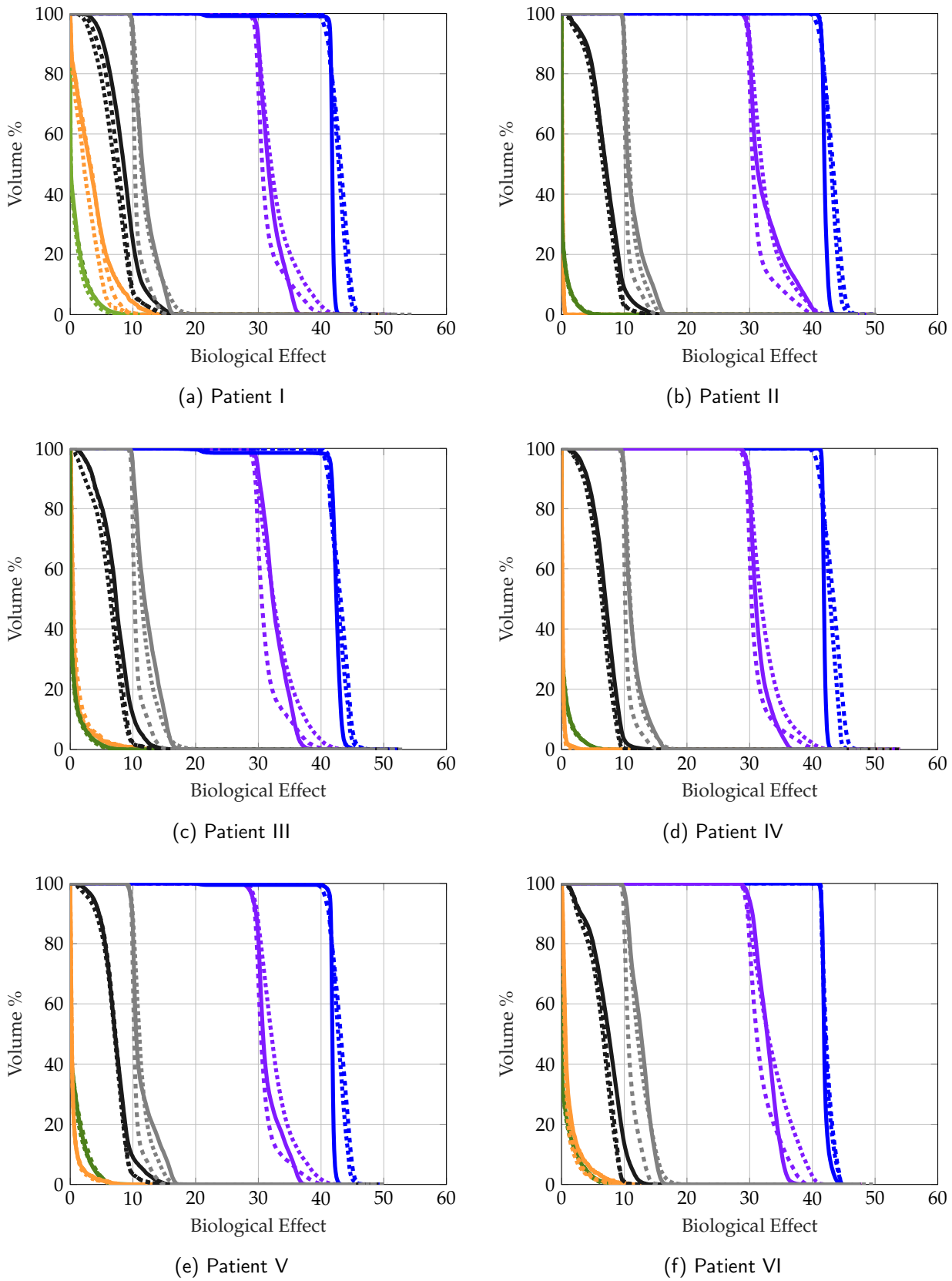

(a) Patient I

(b) Patient II

(c) Patient III

(d) Patient IV

(e) Patient V

(f) Patient VI

Figure IV.14: Cumulative effect volume histograms for all six patients the reference plan (solid line), jointly optimized plan (dashed line) and the jointly optimized external healthy tissue sparing prioritized plan (dotted line). The VOIs are the GTV (—), CTV(—) as target volumes, and critical structures like the brainstem (—), external healthy brain (—) and the conformity based dose fall-off margin (—). The effect to healthy tissue in the CTV is shown using the CTV-NT curve (—).

IV.6 Glioblastoma : Proton–carbon ion treatment

The jointly optimized plans shown above result from an interplay of two fundamental driving factors. Firstly, the spatial conformity of dose to the target volume in order to achieve adequate target coverage while minimizing the dose to healthy tissue. Secondly, the temporal distribution of biological effects to spare OARs and infiltrated healthy tissue through fractionation. This section presents an investigation of a proton–carbon ion treatment, where protons are presumed to be radiobiologically similar to photons considering a constant RBE. As protons and carbon ions have similar dose profiles and have a similar effect on physical conformity, the jointly optimized distribution of proton and carbon ion fluence is primarily driven by fractionation motivation. The optimizer then decides the modality to be used in order to reduce the cumulative biological effect to OARs based on radiobiology.
Figures IV.15b, IV.15d and IV.15f show the photon physical dose, carbon ion RBE weighted dose and cumulative EQD2, respectively, for a photon–carbon ion jointly optimized treatment, as shown in section IV.5. Figures IV.15a, IV.15c and IV.15e show the proton RBE weighted dose, carbon ion RBEweighted dose and cumulative EQD2, respectively, for a proton - carbon ion jointly optimized treatment. All the biological effect to the CTV is delivered using protons. Carbon ions are used to deliver a greater proportion of the prescribed biological effect to the centre of the GTV and an inner margin of the GTV is irradiated primarily with protons. Here, the proton contribution is limited to a prominent margin as seen in the photon–carbon ion jointly optimized combination. This is driven by the incentive to fractionate dose in the CTV. The two treatments presented above are qualitatively similar even though physical characteristics of the two modalities have been equalized. This results suggests that the optimization is primarily driven by biological objectives and supports the hypothesis that the fractionation objective is essential for modality selection in subregions of the target volume which contain healthy tissue.

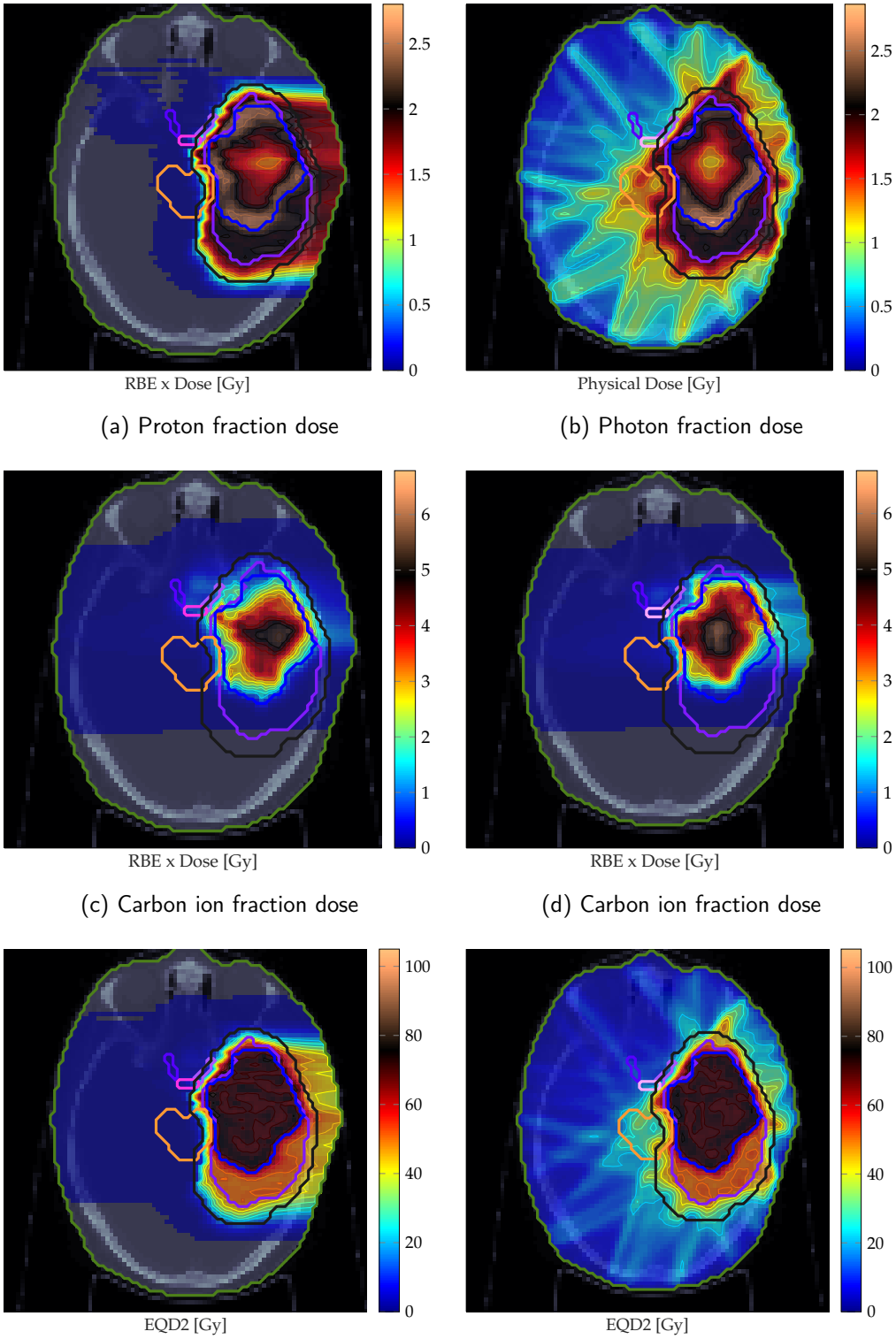

(a) Proton fraction dose

(b) Photon fraction dose

(c) Carbon ion fraction dose

(d) Carbon ion fraction dose

(e) Cumulative EQD2

(f) Cumulative EQD2

Figure IV.15: shows the fraction doses and cumulative EQD2 for a jointly optimized proton–carbon ion treatment and a jointly optimized photon–carbon ion treatment. (a) Proton RBE weighted fraction dose in a jointly optimized proton - carbon ion treatment, (c) Carbon ion RBE weighted fraction dose in a jointly optimized proton–carbon ion treatment, (e) Cumulative EQD2 over a jointly optimized proton–carbon ion treatment, (b) Photon fraction physical dose in a jointly optimized photon–carbon ion treatment, (d) Carbon ion fraction RBE weighted dose in a jointly optimized photon–carbon ion treatment, (f) Cumulative EQD2 in a jointly optimized photon–carbon ion treatment

IV.7 Impact of Local Effect Model version selection

An essential part of the joint optimization work flow is the estimation of the biological effectiveness of carbon ions. The results presented thus far were based on α^C, β^C predictions using LEM IV. However, currently in clinical practice for carbon ions, LEM I is used to predict the RBE. Compared to LEM IV, the LEM I model predicts a greater RBE for carbon ions in the entrance region and the fragmentation tail. This implies a larger collateral biological effect in surrounding OARs. This section shows a jointly optimized photon–carbon ion treatment where the RBE of carbon ions was estimated with LEM I. The LEM I based jointly optimized plan is compared to a jointly optimized plan considering LEM IV as described in section III.5. Figures IV.16a and IV.16c show the photon fraction and carbon ion fraction contribution to the LEM I based treatment. The carbon ion component is reduced as compared to the LEM IV based mixed modality plan, as seen in Figures IV.16d. Carbon ions are only utilized at the edges of the target volume in order to facilitate a sharp dose fall-off.
Although the physical motivation to use carbon ions is the same in both plans, the difference in carbon ion contributions stems from the difference in radiobiological assertions of the two LEM versions.

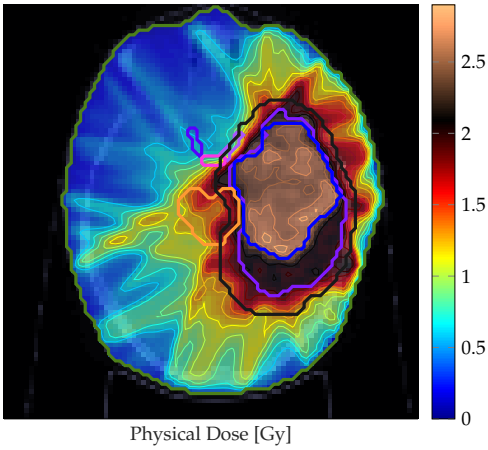

(a) Photon fraction dose
LEM I plan

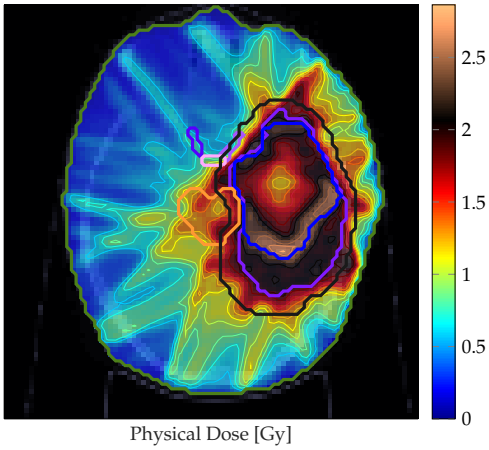

(b) Photon fraction dose
LEM IV plan

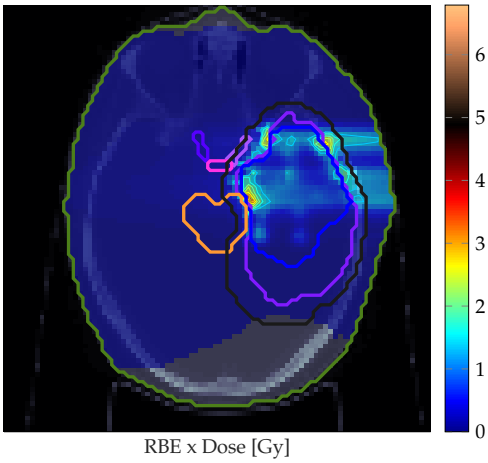

(c) Carbon ion fraction dose
LEM I plan

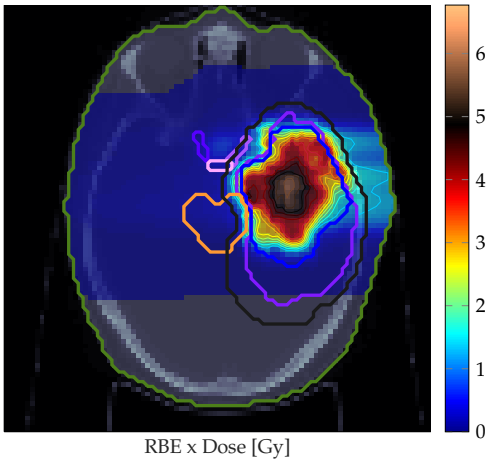

(d) Carbon ion fraction dose
LEM IV plan

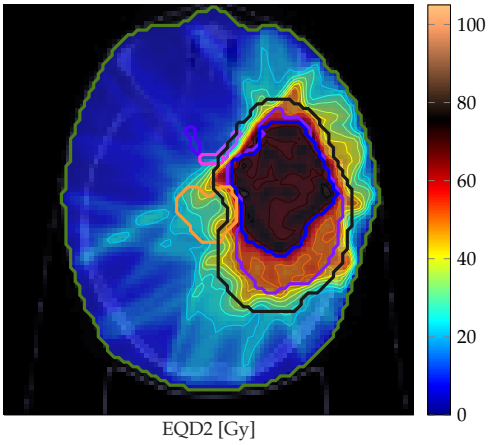

(e) Cumulative EQD2
LEM I plan

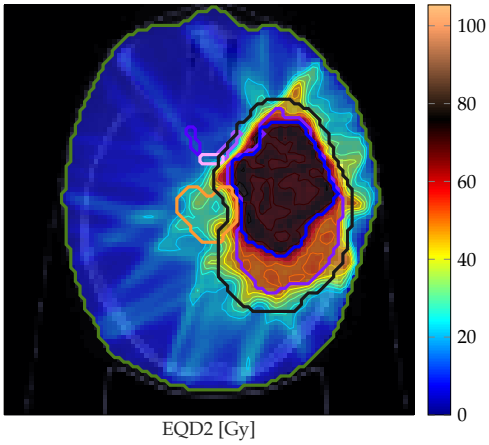

(f) Cumulative EQD2
LEM IV plan

Figure IV.16: shows the fraction doses and cumulative EQD2 for a jointly optimized photon–carbon ion treatment considering LEMI and LEM IV for carbon ions. (a) Photon fraction physical dose in a jointly optimized treatment considering LEM I, (b) Photon fraction physical dose in a jointly optimized treatment considering LEM IV, (c) Carbon ion RBE weighted fraction dose in a jointly optimized treatment considering LEM I, (d) Carbon ion fraction RBE weighted dose in a jointly optimized treatment considering LEM IV, (e) Cumulative EQD2 over a jointly optimized treatment considering LEM I, (f) Cumulative EQD2 in a jointly optimized treatment considering LEM IV

"The whole is greater than the sum of its parts."

Aristotle, 384 - 322 BC

V Discussion

This work studies a novel treatment strategy of synergistically optimized combined photon–carbon ion treatments. Photons and carbon ions are fundamentally different in terms of physical dose deposition characteristics and radiobiological effectiveness. Photon therapies rely on multiple beams whose superposition deposits therapeutic dose to the target volume. This, however, comes at the cost of delivering dose to a large volume of healthy tissue and critical structures surrounding the target volume. Radiobiologically, photons deliver a constant biological effect along the entire beam path, subject to the radiosensitivity of the traversed tissue. Carbon ions on the other hand exhibit an inverted dose deposition profile that allows for a highly conformal target dose delivery. Therefore carbon ions deliver a very low collateral dose to distally situated healthy tissue structures. Radiobiologically, carbon ions are much more effective than photons and exhibit a variable RBE along the beam path. This increased effectiveness is beneficial in treating the GTV, however, it is disadvantageous when considering the dose delivered to healthy tissue. Therefore combined treatments must take into account such fundamental characteristics of the two modalities. In current clinical trials and practice of combined treatments, photon fractions and carbon ion fractions are independently optimized and combined based on the RBE weighted dose. Also the temporal administration of dose is explicitly predefined by the fractionation schedule and is uniform for the entire target volume.

In a real-world treatment planning scenario, there are rare situations where a discrete decision for a single modality means the ideal solution for the patient. The optimization problems are highly complex with multiple conflicting objectives where an ideal solution may be a non-binary combination of spatial confinement and non-standard fractionation of dose using multiple modalities. The joint optimization framework presented in this thesis provides a method to arrive at such a solution.

An initial proof of concept is presented by the jointly optimized SBRT treatment of spinal metastasis with epidural involvement in section IV.2.1. Furthermore a brief investigation

was made into the implication of treatment parameter selection, specifically with regard to fraction allocation (section IV.3) and choice of intrinsic $\alpha^{\gamma}, \beta^{\gamma}$ parameters (section IV.4.1). Further, indications with heavily infiltrative tumours were found to be particularly suitable for the developed joint optimization technique and was demonstrated for glioblastoma in section IV.5. Here the large CTV volume consists of a mixture of healthy tissue and tumour tissue and would benefit from a fractionated irradiation scheme. Objective functions for this mixed tissue region were defined as a composite of a tumour underdosage objective and an overdosage objective for healthy tissue. The validity and importance of such a biological objective is highlighted with a proton - carbon ion treatment of a glioblastoma presented in section IV.6.
The selection of RBE estimation model for carbon ions is another fundamental decision required for joint optimization. In this work, The primary focus is placed on the LEM IV as it is a better fit to *in vitro* cell survival data as compared to LEM I. In order to investigate the implications of RBE model selection, jointly optimized plans were generated and compared in section IV.7 for both carbon ion RBE models, LEM I and LEM IV.

V.1 Validation of the joint optimization framework

The joint optimization implementation was validated through optimization of a photon–proton combination and compared against results from literature (Unkelbach et al., 2018). The jointly optimized treatment plan for the respective spinal metastasis patient case, presented in section IV.1, shows inhomogeneous unequal fraction dose contributions of each modality within the target volume that cumulatively deliver the prescribed biological effect. The result of this optimization shows that protons are best exploited by delivering higher doses per fraction than photons to parts of the tumour where hypofractionation is desirable, while delivering comparable doses per fraction to dose-limiting normal tissues in the vicinity of the target volume, hence successfully reproducing the results presented in literature.
The results presented in this thesis are optimized on the cumulative biological effect. As opposed to the cumulative BED approach presented in literature, the biological effect translation provides a convenient formulation to apply variable RBE models of carbon ions within the joint optimization framework. It also necessitates the translation of prescribed dose objectives to biological effect based treatment objectives. Furthermore, the novel preconditioning strategy described in this implementation reduces the number of iterations required to converge to an optimal jointly optimized plan.

V.2 Proof of concept: Spinal metastasis

The first application of the novel jointly optimized photon–carbon ion treatment strategy is presented for the same spinal metastasis patient case as in section IV.2.1.
Compared to unimodal fractions delivering uniform doses, the joint optimization strategy possesses the ability to redistribute fluence between the two modalities. This means that subregions of the target volume are irradiated by the modality that delivers a lower effect to OARs, which is generally carbon ions. Carbon ions are superior to photons in terms of reduction of the integral dose to healthy tissue and in terms of dose conformity, however, they also deliver a higher RBE weighted dose to the abutting critical structures like the cauda. This can be seen by comparing the unimodal photon plan (figure IV.2b) to the unimodal carbon ion plan (figure IV.2d). Even though the carbon ion plan has superior dose conformity compared to the photon plan, it delivers an excess of 0.24 Gy in near maximum EQD2 to the cauda and 1.9 Gy in near maximum EQD2 to the 3 mm margin around the cauda. This overdosage of the cauda is a result of two factors: the increased RBE of carbon ions and the carbon ion beam orientations selected for this treatment. In such regions it would be beneficial to utilize the less effective photons to deliver the required biological effect. The simple combination of separately optimized photon–carbon ion treatments implicitly achieves this goal to a reduced extent, however such a treatment planning method does not consider the cumulative effect in OARs.
The joint optimization with fixed fraction allocation strategy uses a combination of photons and carbon ions in regions surrounding the cauda in order to (1) reduce the fraction RBE weighted dose and (2) uniformly distribute the dose over all fractions. The RBE weighted dose to OARs is managed by a reduction in carbon ion contribution to the target volume adjacent to the critical structures and an increase in the photon contribution to make up the lacking dose in the target. Apart from the physical redistribution of fluence, another degree of freedom of the joint optimization strategy manifests in the redistribution of biological effects between fractions. Due to the difference in assumed α^{γ} and β^{γ} between healthy tissue and tumour tissue there is a predicted improvement in sparing of healthy tissue with fractionation. In the jointly optimized plan with unimodal fractions, large areas of the target volume receive most of the prescribed biological effect within the single carbon fraction. However, for regions surrounding the cauda, the biological effect is almost uniformly distributed between photon and carbon ion fractions, corresponding to, hyperfractionation of dose within the bounds of available fractions.
The joint optimization strategy could also be used to investigate the hypothetical setup of concurrent irradiation. In the concurrent irradiation strategy both modalities are delivered in every fraction. This allows for greater freedom to the carbon ion fractions to utilize its limited fractionation capabilities. The comparison of the presented joint optimization strategies, i.e., fixed fraction combined treatments and concurrent irradiation, yields novel insights into the ideal combination of photons and carbon ions. Even with a single carbon ion fraction in the

fixed fraction treatment, the optimized result chooses to utilize a greater proportion of carbon ions to deliver dose to the target volume in order to reduce integral dose to healthy tissue as seen in figure IV.2. The impact of this is most evident at the distal edge of the target volume in figure IV.3. Photons are utilized around the cauda to distribute effect between fractions. Even though the concurrent irradiation setup allows the use of carbon ions in all fractions, photons are still used in the target volume surrounding the cauda. This implies a preferential use of low RBE radiation in regions adjacent to critical structures.

In summary, joint optimization is able to exploit the many factors that affect the fraction biological effect contribution of each modality to sub-volumes of the target. Firstly, the physical conformity of biological effect to the target volume. Here carbon ions are desirable as they are superior to photons in reducing the integral dose to healthy tissue and critical structures. Secondly, the temporal distribution of biological effects when there is a predicted fractionation benefit. This can also be interpreted as the fractional contribution of "fraction" biological effects by each modality to the total biological effect. For the spinal case, most of the target volume is irradiated by carbon ions within one fraction, here the subvolumes are hypo fractionated, this implies a disparity in the fraction biological effects between the two modalities. At the interface with critical structures or healthy tissue, it is more beneficial to uniformly distribute the biological effects across all fractions.

For a fixed fraction jointly optimized treatment, physical conformity and fractionation are opposing ideals. As physical conformity generally motivates an upregulation of carbon ions, fractionation motivation incentivises the use of photons for a uniform fraction effect distribution over all fractions. A jointly optimized plan that utilizes this spatial and temporal redistribution of fluence is almost always more conformal than unimodal treatments and simple combination treatments.

Naturally, such a model-based approach critically depends on the underlying models of biological mechanisms. In the case of biological effect based joint optimization this concerns foremost the RBE prediction for carbon ions and the LQ model for the accumulation of biological effect over multiple fractions.

The LQ model is the dominant model in radiotherapy that relates dose to cell kill and is currently the best approximation for the cumulative effects of a multitude of underlying biological processes. It is a simple formulation that works under the assumption that clinical endpoints of tumour control and normal tissue response are driven by a biological effect in tissue, i.e. cell kill. In this study, the LQ model is used for biological effect accumulation over the entire treatment. Hence concerns regarding the validity of the LQ model are one fundamental source of uncertainty. There is evidence that suggests a low dose hypersensitivity (< 0.5 Gy) presented by Joiner et al. (2001) and a linearization of the curve at high dose ranges (> 7 Gy) presented by Astrahan (2008). Such corrections to the LQ model were not considered in this implementation of joint optimization. The accumulation of biological effects over as wide a range of fraction doses as that seen for joint optimization has not been thoroughly studied in literature. Although this dose limit for biological certainty is

not violated in conventional radiotherapy treatments, they might be significant for jointly optimized treatments. In practice optimization could be constrained to the valid domain of the biological model. In principle, future modifications to the biological effect computation could also be incorporated without invalidating the presented framework.
With regards to carbon ion therapy, the current strategy translates knowledge gained with photon treatments in order to apply it to charged ion therapies. There are several sources of uncertainties in the estimation of RBE values for carbon ion therapies which can be broadly classified into four categories (Böhlen et al., 2012):

1. Uncertainty in experimental data from cell survival and tissue response studies that are used to validate RBE models. Here the uncertainty arises from experiment design and statistical variance in experiments used to establish RBE values.

2. Uncertainty within the biophysical model itself that may stem from uncertainties in the input parameters given to the model or from fitting procedures to experimental data and radiobiological models.

3. Uncertainty from inter-tumour and inter-patient variability of tissue and tumour microenvironments. This includes differences in *in vitro* and *in vivo* data used for model verification.

4. Physical uncertainties in treatment such as the fragment fluence composition of the radiation fields.

The uncertainties in the $\alpha^{\gamma}/\beta^{\gamma}$ affect both the biological effect accumulation stage and the RBE estimation stage of a joint optimization strategy and may alter not only the delivered physical dose but also individual dose distributions of each modality. A first impression of the impact of uncertainties in $\alpha^{\gamma}/\beta^{\gamma}$ for jointly optimized treatments is presented in section IV.4.

V.3 Impact of fraction allocation

The concurrent irradiation strategy presented earlier is an "extreme" case where uniform fractionation is enforced for each modality over the 5 fractions. Such a treatment would only be possible in institutions that have both modalities of treatment, and even so would be logistically challenging to deliver within the one fraction. In terms of the current clinical practice of fixed fraction allocation, it is essential to estimate the ideal fraction distribution for photons and carbon ions that may optimally utilize both modalities. Section IV.3 presents results for the jointly optimized photon–proton combined treatments and photon–carbon ion combined treatment generated with a range of fraction allocation schemes for the spinal metastasis patient case presented earlier.
The results for an optimal fraction allocation for photon–carbon ion treatments are presented

with the background of optimal fraction allocations for photon–proton treatments. As expected, for a comparable target coverage, photon–carbon ion treatments over all fare worse at sparing of the cauda and are marginally better at reducing mean dose to the external healthy tissue, when compared to the photon–proton treatments. The fractionation study also suggests the optimal fraction allocations for jointly optimized treatments. For the evaluated case, the analysis suggest a combined treatment of 3:2 fractions to be the ideal combination for a photon–proton combined treatment, whereas for a photon–carbon ion treatment the ideal fraction ratio is predicted to be 4:1. This result suggests that due to the reduced fractionation effect, it may be beneficial to have a single fraction of carbon ions. Such a result challenges the current paradigm of fractionation for carbon ion treatments. The increased RBE and reduced fractionation capacity of carbon ions motivate a hypofractionated treatment schedule where fewer or one fraction would suffice.

The optimal jointly optimized treatment depends on many treatment decisions. Ideally the unimodal proton treatment is expected to be superior to the jointly optimized treatments as it exhibits superior dose deposition characteristics and similar radiobiological effectiveness compared to photons. However the unimodal proton treatment, presented in figure IV.6f, is estimated to be worse than the jointly optimized treatments. This tendency is due to suboptimal beam angle selection. The three posterior beam angles selected for this study can only deliver dose to the anterior region of the target volume by passing through the cauda. Therefore a Volumetric Arc Radiotherapy (VMAT) solution could be potentially better than particle therapy modalities with poor beam angle selection. In such situations the joint optimization strategy chooses “a path of least resistance” when selecting modalities to irradiate the difficult subvolumes, hence utilizing the additional degree of freedom interms of physical redistribution of dose.

In this study, the number of fractions for reference plans and jointly optimized photon–carbon ion plans was fixed and defined as unimodal fractions; possible trade-offs emerging from altered fractionation schemes were not exploited. In principle, however, the number of carbon ion fractions could be used as an additional degree of freedom in order to optimize the allocation of scarce carbon ion resources over multiple patients. The problem of optimal fraction allocation for combined treatments must be addressed in future research for photon–carbon ion treatments. Such an approach is shown by Ten Eikelder et al. (2019) for a photon–proton jointly optimized treatment assuming a constant RBE for protons.

V.4 Impact of LQ model parameter selection

The differential α/β ratios and their interfaces between tissue play an important role in driving joint optimization. As in the clinic, the viability of fractionation is dependent on a differential α/β ratio. Photons would be utilized as long as the α/β ratio of the target volume is larger than that of healthy tissue, therefore exploiting the possible gain in sparing healthy tissue with fractionation. In other cases carbon ions would be primarily used due to the more favourable physical dose characteristics and photons would only be utilized in cases of limitations in particle therapy delivery, e.g., for a fixed beamline (Fabiano et al., 2020b). With regards to implementation, the distribution of α/β ratios for different VOIs are tabulated as a spatial map used for carbon ion RBE estimation and photon effect calculation. Such an implementation leaves room for future considerations of spatial distributions of radiosensitivity parameters based on data from biopsies or imaging (Hawkins, 2017).
To maintain continuity, the implications of an assumed fractionation gain is presented using a photon–carbon ion treatment for the spinal metasatasis patient, described in section IV.4.1. Assuming a fractionation gain, the joint optimization has two competing factors: (1) conformity of biological effect to the target volume improved with the use of carbon ions and (2) sparing of the cauda and surrounding healthy tissue through fractionation using photons. Compared to a jointly optimized treatment assuming a fractionation gain ($\alpha_T^\gamma/\beta_T^\gamma > \alpha_{NT}^\gamma/\beta_{NT}^\gamma$), the joint optimization without a fractionation gain ($\alpha_T^\gamma/\beta_T^\gamma = \alpha_{NT}^\gamma/\beta_{NT}^\gamma$) has an increased carbon ion contribution. Also the buffer of photon dose seen around the cauda and at the posterior edge of the target volume are absent. This is because the only driving factor in this optimization is the physical conformity of biological effect, which is better achieved using carbon ions.
Furthermore, a clinical example is presented with the base of skull chordoma patient case in section IV.4.2 where the fractionation benefit is absent. Here again the physical conformity of biological effect to the target volume is the primary goal and almost all the prescribed dose to the target volume is delivered using carbon ion fractions. However this is also subject to carbon ion beam angles selected for treatment. In an ideal case, with optimal carbon ion beam angles and no fractionation gain, the jointly optimized plan will be an only carbon ion treatment. Evidence of this is seen in the comparison of the jointly optimized plan ($n^\gamma = 25$ and $n^C = 12$) to a unimodal carbon ion treatment of $n^C = 12$. The treatment plan quality indicators are almost identical. The use of a single photon beam for the jointly optimized treatment shown in figure IV.8a, is due to suboptimal irradiation of the target subvolume that is anterior and adjacent to the brainstem. This improvement although small in terms of clinical parameters is seen with the reduction in the cumulative objective function value.
Such a result suggests that joint optimization strategies can improve on treatment plans with suboptimal beam angles and the photon contributions seen are indicators of regions that are suboptimally irradiated by carbon ions.
The variability of $\alpha^\gamma, \beta^\gamma$ parameters is one of the main sources of uncertainty in jointly optimized treatments. LQ model parameters published in literature exhibit large variances due

to clinical and methodological inconsistencies in parameter estimation (Joiner and van der Kogel, 2009; van Leeuwen et al., 2018). Despite this heterogeneity some tendencies could be identified. In the context of joint optimization the uncertainty in LQ model parameters is propagated to the treatment plan through LQ model based accumulation of biological effects. Another issue to note is that $\alpha^{\gamma}, \beta^{\gamma}$ are also input parameters to LEM models and hence also affect the predicted RBE of carbon ions. A possible solution to mitigate this uncertainty is the optimization of combined treatments over a range of plausible α/β values in order to better visualize the expected variability in biological effect and, by extension, in predicted tumour response.

V.5 Mixed modality treatments for infiltrative disease: Glioblastoma

The application of the joint optimization strategy for infiltrative diseases is illustrated using a cohort of 6 glioblastoma patient cases. Here the CTV is defined as a 2 cm anisotropic margin, limited by anatomical barriers, which contains a mixture of healthy tissue and microscopic tumour infiltrations. The increased RBE and the reduced fractionation effect of carbon ions is sometimes considered an advantage over photons in treating the GTV. However, for the same reasons, carbon ions face limitations for treating such infiltrative tumours, where a large part of the target volume represents CTV rather than GTV, containing normal tissue that can only be protected through fractionation rather than dose conformity. This issue is generally acknowledged in carbon ion therapy and is reflected in clinical practice such as the CLEOPATRA glioblastoma trial combining photon fractions to treat the CTV with a carbon ion boost to the GTV (Combs et al., 2010). Currently, photon and carbon fractions are manually designed and separately optimized. By simultaneously optimizing both modalities, the combination that optimally takes advantage of the characteristics of each modality is determined.

There are two tradeoffs that must be realized for the optimal combination of photons and carbon ions: (1) a conflict between irradiating the target volume and sparing the surrounding healthy tissue in the external brain, brainstem, optic chiasm and optic nerves (2) a conflict between irradiating the tumour tissue in the CTV and the infiltrated healthy tissue at the same location.

In this treatment planning study, joint optimization results in a redistribution of the photon and carbon ion contributions within the overall treatment plan. The quality and extent of the reorganization depend on manifold factors, such as the volume of the GTV and CTV (and their volumes relative to each other), locations of adjacent critical structures, the choice of radiobiological parameters α, β, and the number of fractions. For Patient I with a large tumour volume with abutting critical structures (brainstem and chiasm), there is an observed

increase in carbon ion contribution to the core of the tumour when compared to the reference plan. Consequently, there is a pronounced buffer of photon dose at the edge of the GTV and adjacent to the critical structures in order to spare OARs and healthy tissue within the CTV by fractionation. Here, the CTV volume was larger than the GTV by a factor of 1.8. For Patient II with a smaller and isolated tumour, the carbon contribution was comparatively down regulated by joint optimization. This reduction in the carbon contribution is attributed to the size of the boost volume relative to the spared CTV (larger than the GTV by a factor of 2.8), the extent of the entrance channel and exit channel of the carbon ion beams and the effect fall-off from the carbon ion Bragg peak. This trade-off in turn lends itself very well to the treatment of large target volumes with typically more hypoxic cells at the centre of the tumour, which would be targeted by an increased carbon ion contribution.

The jointly optimized plan also exhibits better dose conformity in two aspects: 1) dose conformity around the CTV, as seen in dose characteristics of CTV margin structure; 2) the dose conformity of the boost dose to the GTV. Compared to reference plans for the patient cohort, the variations in mean dose to the external healthy tissue for the jointly optimized plan can be explained by a tradeoff between the mean dose objective sparing external healthy tissue and the overdosage objective for critical structures like the brainstem. This additional degree of freedom of joint optimization can be facilitated to articulate additional trade-offs, for example, sparing of healthy tissue in CTV versus sparing external healthy brain. The jointly optimized plan #2, the external healthy tissue prioritized plan, represents the other end of the spectrum, where the altered weights of the objectives result in not only a new overall treatment with lower external healthy tissue mean dose, but also in a different ratio of contributions of each modality. The increased carbon ion contribution results in a more conformal plan that in turn reduces the overall dose to adjacent critical structures and the external healthy brain. This flexibility of jointly optimized plans might make it possible to meet some conventionally infeasible clinical treatment planning demands.

The modulation of carbon ion physical dose by the joint optimization also implies a modulation of the LET. The LET is a fundamental concept in LEM based RBE estimation and is implicitly included in the depth dependant α^C, β^C predictions. Conventional effect based carbon ion optimization prioritizes target coverage over the conformity of LET distributions to target structures. This is visible in figure IV.11 where a high LET weighted dose region is situated at the distal edge of the carbon ion beam at the interface with the brainstem. Jointly optimized plans, on the other hand, limit the LET weighted dose to the center of the GTV where it is a desirable trait. The LET distributions presented in this thesis result from a dose weighted average of precomputed beam specific LET look up tables and provide a good basis for a first analysis. Future studies in jointly optimized treatments would benefit from a more accurate Monte Carlo based investigation of the LET distribution.

In this study the benefit of jointly optimized plans are presented as a reduction in cumulative biological effect to OARs. However the translation of such biological effects to normal tissue complications in patients is unclear. Thus a realistic evaluation of the benefits of

combined treatment in patients is challenging. Furthermore, the underlying concept of spatio-temporal optimization also demands a re-evaluation of healthy tissue tolerances with respect to fractionation. The current knowledge on the relationship between dose per fraction and biological effect is based on data from standard fractionation schemes and sparse data from radiosurgery/dose escalation studies. It does not span the entire dose-effect curve and the effects and mechanisms are not fully understood for very small doses (<1 Gy) or very large doses (>16 Gy) and must be investigated further (Grellier and Belkacemi, 2020; Kirkpatrick et al., 2011, 2008).
In the spatio-temporal optimization of photon–carbon ion treatments large variations in temporal biological effect distributions are seen (hyperfractionation versus hypofractionation). Also in the combination of photons and carbon ions the spatial distribution of fraction biological effects are heterogeneous as carbon ions may deliver larger effective doses to smaller regions of critical structures as compared to photons. Therefore conventional mean dose normal tissue tolerances used for photon treatments may not be directly transferable to carbon ion treatments. Hoffmann and Nahum (2013) propose an approach to include the fractionation sensitivity of normal tissues into dose tolerances for varying fractionation schedules and Perkó et al. (2018) propose an approach for the inclusion of spatial dose distributions to normal tissue mean dose tolerances.

V.6 Fractionation objective for infiltrative diseases

In radiotherapy treatment planning, the fractionation scheme is conventionally decided by the radiation oncologist based on empirical knowledge of specific fractionation schedules. For unimodal treatments this decision is based on the relative difference of radiosensitivity parameters between tumour tissue and healthy tissue. The fractionation schedule is thus an inherent part of treatment plan design. Joint optimization allows for a spatio-temporal redistribution of biological effect, i.e., central subvolumes of the target volume are hypofractionated, whereas subvolumes with adjacent healthy tissue are hyperfractionated. However, for target volumes infiltrated by tumour tissue, the ideal treatment would require a maximally fractionated delivery of the prescribed biological effect. As presented in section III.4.4, this challenge was solved through explicit definition of conflicting treatment objectives that independently consider the biological effect delivered to tumour tissue and healthy tissue, located at the same voxel location. For a photon–carbon ion treatment in such a voxel, the individual contribution of each modality to the required uniform fractionation schedule now depends on the location of the voxel within the carbon ion beam as seen in section III.1. Considering the LEM IV model for carbon ions, for a voxel located at the Bragg peak the ideal fractionated treatment consists of an only photon treatment due to a complete lack of fractionation capacity of carbon ions here. For voxels located at the entrance channel and at the fragmentation tail, the ideal combination utilizes both photons and carbon ions. Naturally the ideal combination of photons and carbon ions also depends on the RBE prediction

model used. Such considerations greatly complicate the interpretability of jointly optimized photon–carbon ion treatments.
The proton–carbon ion treatment plan presented in section IV.6, illustrates the importance of such a fractionation objective against the motivation of spatial conformity. In terms of physical dose deposition characteristics protons are similar to carbon ions, in that they are similar in reducing the integral dose to healthy tissue. However, radiobiologically protons are assumed to be comparable to photons and have a uniform RBE over the entire beam path. Therefore such a proton–carbon ion jointly optimized plan would be driven primarily by the biological objectives of fractionation for the CTV and adjacent critical structures rather than the physical conformity objectives. As observed in the results, the proton–carbon ion plan is qualitatively similar to the photon–carbon ion plan. Both plans utilize lower RBE radiation, that have a fractionation potential, within the CTV and at interface of the target volume and healthy tissue.
This study assumes a uniform distribution of healthy tissue and tumour tissue within the CTV. The ratio between the cell density of tumour and healthy tissue is codified by the penalties of the underdosage objective and overdosage objective within the CTV. However, tumour cells can be found several centimetres away from the palpable tumour and is characterised by a continuous gradient in tumour cell density (Kelly et al., 1987; Matsukado et al., 1961; Watanabe et al., 1992). There have been various publications in literature that model tumour progression for glioblastoma (Menze et al., 2021; Unkelbach et al., 2014a,b; Wurzel et al., 2005). Such predictions could be potentially used to define an objective weight map that reflects the real tumour cell density distribution and hence motivate a larger contribution of carbon ions at the GTV–CTV interface.

V.7 Impact of Local Effect Model version selection

Another fundamental issue when considering carbon ion radiotherapy is the choice of RBE estimation model. The two primary models used in carbon ion therapy clinics are the LEM I and MKM. This study employs an updated version, LEM IV version, of the clinically used LEM I model. LEM IV allows for better modelling of invitro cell survival data (Friedrich et al., 2012; Scholz and Kraft, 1996) and, compared to LEM I, predicts a lower RBE in the build-up and tail region of the beam (Gillmann et al., 2014; Grün et al., 2012). This does not argue against the clinical use of LEM I as a conservative RBE model for planning single-modality carbon treatments. However these differences have a much more substantial effect in individual contributions of each modality in a jointly optimized treatment. Paradigmatically, the difference in the predicted α^C, β^C parameters of carbon ions implies a difference in fractionation effect observed for the build-up and tail region of the carbon ion beam. This difference can be seen in the result presented in section IV.7, which compares two photon–carbon ion jointly optimized plans, considering the two LEM versions. The LEM IV plan is identical to that presented in section IV.5.1. LEM I predicts a lower fractionation effect

with carbon ions, hence it disadvantages carbon ions and consequently increases the photon component. For this result, the reader must bear in mind that the glioblastoma patient case was optimized with different machine datasets, which are reflected in differences in spot placement grid and physical beam characteristics.
In summary, although the concept of fractionation with carbon ions is not as great a concern in clinical practice, the underlying models for carbon ion RBE estimation play a big role in the actual physical dose distributions of each modality in a optimal combined treatment. This implementation of joint optimization depends on the LQ model parameters estimated by the carbon ion RBE model.
Recent exploration of the various RBE models suggest that LEM I and LEM IV preformed best at high LET conditions but yielded an overestimation and underestimation at low–midrange LET conditions. A modified MKM, on the other hand, exhibited superior agreement with *in vitro* and *in vivo* measurements. However the presented results suggest a large variability in RBE (±20%-30%) (Mein et al., 2020). Future trials and studies must focus on updation and verification of RBE models for carbon ions with larger patient cohorts. Meanwhile, joint optimization research should investigate the possible implications of models such as the modified MKM on combined treatments.

V.8 Physical uncertainty

Combined photon–carbon ion treatments face similar concerns as particle therapy modalities regarding uncertainties. Highly modulated carbon ion beams are susceptible to the effect of range and setup errors in the treatment workflow. The increased heterogeneity of dose/effect distributions from carbon ion beams achieved with joint optimization may raise greater concerns with regard to treatment plan robustness. In principle, Fabiano et al. (2020b) have demonstrated that this issue can be addressed with stochastic joint optimization for photon-proton treatments. Technically, this approach can be easily translated to photon–carbon ion treatments. For carbon ions, however, modifications of the LET distributions and effect of uncertainty should also be taken into account. LET distributions for Patient I are presented in figure IV.11. Joint optimization modulates carbon ion beams to place high LET regions away from OARs and towards the centre of the GTV, which reduces the maximum variance of biological effect in adjacent critical structures. This, however, does not discount the need for robust optimization to maintain uniform biological effect in the target volumes over the course of treatment.

V.9 Outlook

To the authors knowledge, this is the first systematic study into jointly optimized photon–carbon ion treatments. The previous section presented a discussion of the methodology and results of this study which suggest a potential benefit to future patients. This study was limited to intracranial indications where the issues of inter-fraction and intra-fraction motion are minimal. With a robust solution other challenging indications, particularly with a fractionation gain, such saccral chordomas with OARs overlapping with the target volume (Unkelbach et al., 2018), non-small cell lung cancer (Klement et al., 2020) and malignant gliomas (Laperriere et al., 2002). Such a planning strategy would also benefit particle boost treatments such as those for adenoid cystic carcinomas (Akbaba et al., 2019a; Jensen et al., 2015; Lang et al., 2018; Schulz-Ertner et al., 2003) and perineal particle boost treatments for localized prostatic carcinoma (Johansson et al., 2012; Shipley et al., 1979). Translating such treatments into clinical practice, however, requires more rigorous methods to reduce the currently observed biological and physical uncertainty.

The robust optimization of jointly optimized treatments is challenging due the effects and interplay of random and systematic uncertainties in treatment. A stochastic optimization based robust solution would involve the simultaneous optimization of multiple uncertainty scenarios for the two modalities. Such an approach is computationally intensive and would involve the generation of multiple dose influence matrices for each modality and scenario. One approach to efficiently optimize such a treatment would be to consider a PTV margin for photons and a scenario based optimization approach for carbon ions.

V.9.1 Biological models

The clinical application of a jointly optimized treatment requires dose–response models with greater resolution within the back drop of different fractionation schedules and mixed radiation treatment fields. Most "high" resolution dose-effect models are based on *in vitro* data, whereas, most *in vivo* dose-effect models are only explored for standard fractionation schemes and sparse data in animal models for photons (Joiner and van der Kogel, 2009). Future studies should endeavour to (1) establish a dose–biological effect relation with respect to clinical endpoints for a range of α/β parameters (2) establish a dose–effect model that verifies the cumulation of biological effects over different homogeneous and heterogeneous fractionation schedules and (3) to model the cumulative effects of mixed radiation fields.

This implementation of biological optimization of combined treatments only considers the cell kill component of the LQ model for biological effect accumulation. As presented in section II.2.1.3, there are several possible extensions to the LQ model that include tumour repopulation and oxygen enhancement ratio.

In the context of photon treatments, the oxygenation of the tumour plays an important role in treatment outcome. Carbon ion treatments, on the other hand, are considered to be

more insensitive to oxygenation of the tumour and hence are ideal for treating large hypoxic tumours (Harting et al., 2007; Joiner and van der Kogel, 2009). Therefore, a more accurate model of biological effects of the photon fractions include the OER as

$$\varepsilon^{\gamma} = n^{\gamma}(\alpha^{\gamma}\ OER \times d + \beta^{\gamma}(OER \times d)^2) \tag{V.1}$$

Such an implementation would potentially disadvantage photons and provide a motivation to utilize a greater proportion of carbon ions within the GTV of hypoxic tumours.
The model of cumulative biological effects have no time-dependent component, i.e. the cumulative biological effect does not depend on the order of photon and particle fractions. A practical approach to the ordering of fractions may be to evenly distribute carbon fractions throughout the treatment. In the glioblastoma example, this would amount to delivering one carbon and four proton fractions per week. Thereby, a fixed percentage of the total effect is delivered over the course of each week. In the next step of theoretical investigation, modelling of tumour repopulation would allow for optimization of the sequence of radiation fraction administration. Tumour repopulation with a constant exponential growth rate can be expressed within the LQ model as

$$\varepsilon = n^{\gamma}\varepsilon^{\gamma} + n^{C}\varepsilon^{C} - log_e 2(T - T_k)/T_p \tag{V.2}$$

where n fractions of d Gy are delivered over a time of T days and repopulation with a cell doubling time of T_p is not initiated until day T_k (Fowler, 2010; Joiner and van der Kogel, 2009). Bortfeld et al. (2015) present an approach to optimize fractionation schedules in the presence of tumour repopulation. Key findings of this paper suggest that faster tumour growth motivates a shorter overall treatment duration. Furthermore accelerated repopulation suggests larger fraction doses later in the treatment to account for tumour proliferation and increased radioresistance. In the context of combined treatments, this would imply a theoretical benefit in delivering carbon ion fractions after photons fractions.
Such extensions of the LQ model are not commonly used in radiotherapy as the availability of data on the input parameters are either insufficient or show a large variability.
A theoretical alternative to the use of the LQ model to estimate a cumulative treatment efficacy would be the use of TCP and NTCP models (Nahum and Uzan, 2012; Nuraini and Widita, 2019). TCP and NTCP are statistical dose–response models that are defined for specific clinical endpoints ideally collated from large patient cohorts. However, particle therapy is a relatively young field, the use of such models would be premature due to insufficient survival and treatment follow up studies.

V.9.2 Extension to other particle therapy modalities

Among the particle therapy modalities investigated in the past, protons and carbon ions have obtained wider acceptance in the radiotherapy field. There has been a recent resurgence in interest in Helium ions as its physical and radiobiological characteristics placing it between protons and carbon ions. In terms of a differential biological effect in tumour tissue and healthy tissue, helium ions are predicted to be more desirable than carbon ions and less than protons (Grün et al., 2015). This implies a potential benefit from fractionation with Helium ions, more than that for carbon ions, and an improvement in conformity over protons. Therefore helium ions would also be a suitable candidate for photon–particle combined therapies. Helium ion radiation treatments are purely experimental and there are no studies that present wider *in vivo* biological effect estimates. Given the similarity in joint optimization results between protons and carbon ions, helium ions would probably not exhibit greater gains in combined treatments.
The modularity of the joint optimization implementation in matRad allows for the future inclusion and investigation of any combination of radiation modalities within the context of LQ model. The inclusion of new modalities can be simply done with the compilation of a base data set which would contain beam geometry and quality information and energy specific effective α, β curves based on an RBE estimation model (LEM or MKM).

V.9.3 Cost effectiveness of mixed modality treatments

The joint optimization strategy facilitates the determination of optimal treatment plans given any, and primarily reduced, number of carbon fractions. As the combined treatment plans are at least as good as conventional treatment strategies, jointly optimized treatments make best use of the available treatment resources, thereby improving the cost effectiveness and accessibility of limited particle therapy resources to a larger population of patients. The joint optimization strategy also provides a framework to investigate gains achieved with a given fraction allocation. This would support fraction allocation decisions based on a cost–benefit trade-off. One step further would involve the inclusion of real world variables, for example cost or slot availability, into the optimization objective function to improve and extend patient care.

VI
Conclusion

The main objective of this thesis was the development, implementation and evaluation of a treatment planning framework that synergistically optimizes photon–carbon ion combined treatments. A simultaneous optimization of the two modalities based on the accumulated biological effect would optimally exploit the strengths of each modality. The clinical approach to combined treatments consists of a naive combination of independently optimized photon and carbon ion plans based on the RBE weighted dose. Previous work on joint optimization addresses photon–proton treatments based on a cumulative BED but does not take into consideration the variable RBE associated with particle therapy modalities.

This thesis presents the first investigation into the joint optimization of combined photon–carbon ion treatments. The joint optimization workflow was independently implemented within the open source dose calculation and treatment planning framework matRad. As such, the implementation may be released as open source code to act as the ideal starting point for future internal and external research. Apart from the software implementation and resulting treatment plans, this thesis also investigated the influence of underlying treatment parameters. Namely: (1) the impact of predetermined fractionation schedules on the joint optimized plans, (2) the influence of choice of LQ model parameters on the fractionation considerations within the target volume and (3) the implications of the choice of LEM model, for carbon ion RBE estimation, on the overall treatment. These concepts were then applied in a more clinical treatment planning study for infiltrative tumours, focussing on glioblastoma patient cases.

The joint optimization strategy for combined treatments stands at the intersection of radiation physics, radiobiology and optimization techniques, the fundamentals for which are laid out in chapter II. The optimization, presented in section III.1, is carried out on the total cumulative biological effect contributions of all photon and carbon ion fractions. Where biological effect contributions of each modality is computed using the LQ model assuming a predetermined $\alpha^{\gamma}/\beta^{\gamma}$ ratio for each volume of interest. In this estimation of biological effect, the variable

RBE of carbon ions are incorporated using effective α^C, β^C estimates obtained from LEM IV. The joint optimization framework utilizes the existing basic dose calculation, biological effect calculation for carbon ions and optimization capabilities of matRad for photons, protons and carbon ions.

The validation of the joint optimization framework was done with a qualitative comparison of a photon–proton combined treatment with results previously published in literature. The fundamentals of a joint optimized photon–carbon ion treatment are presented with a biological effect based comparison of joint optimized treatments with independently optimized simply combined treatments and unimodal photon and carbon ion treatment for a spinal metastasis patient case. It reveals that joint optimized plans cumulatively present an improved high biological effect conformity and reduction in integral dose to healthy tissue. This gain is achieved through two competing means: (1) spatial redistribution of fluence between photons and carbon ions and (2) temporal administration of biological effects between the two modalities. These methods utilized by the joint optimization strategy are driven by two competing objectives: Firstly, reduction of mean dose to healthy tissue which motivates the optimizer to, generally, use carbon ions to deliver a larger percentage of the prescribed biological effect, as compared to photons. Secondly, the sparing of healthy tissue through fractionation. As carbon ions have a higher RBE and reduced fractionation capacity, they deliver a larger effect to OARs and healthy tissue. At regions of the target volume with healthy tissue involvement the optimizer utilizes photon fractions, with a lower RBE and larger fractionation potential, in addition to the carbon ion fraction, to distribute the biological effect uniformly over all available fractions. Such a solution is characterized by inhomogeneous photon and carbon ions dose distributions that selectively hypofractionate deep regions of the target and hyperfractionate target subregions adjacent to critical structures. Additionally a theoretical concurrent irradiation strategy, was evaluated where both photons and carbon ions were assumed to be delivered in all fractions. One would expect that carbon ions, now with more fractions available to fractionate dose, would be solely used. However, here photons were utilized in areas surrounding OARs in order to deliver a lower RBE weighted collateral dose. In summary, the joint optimization strategy takes into account the physical and radiobiological characteristics of photons and carbon ions and delivers a plan that, for comparable target coverage, exhibits a benefit in healthy tissue considering biological effects. Naturally, such model-based approaches critically depend on the underlying models. In the case of joint optimized treatments, it pertains to the RBE estimation model for carbon ions and the LQ models used to accumulate biological effects over multiple fractions. Uncertainty in these models not only affects the overall treatment plan but also the individual contributions of each modality. Also, the highly modulated fields used here are subject to physical range and setup uncertainties which would quickly degrade treatment plan quality. Such uncertainties have not been addressed in this study and should be the subject of future research.

To study the impact of fraction allocation on treatment plan quality, photon–carbon ion treatments were optimized for a range of fraction distributions and compared against photon–proton plans. This result suggests that the ideal fraction distribution may call for a reduction in the carbon ion fractions owing to their reduced fractionation capacity. Furthermore, it can be observed that the joint optimized treatment also depends on other treatment decisions such as beam angle selection. The effects of suboptimal beam angle selection can be, to an extent, mitigated by the fluence redistribution between photons and carbon ions seen in joint optimized plans.

This study also investigates the implications of an assumed fractionation gain from a differential α/β ratio between tumour tissue and healthy tissue. Without the fractionation gain, the objective to fractionate dose in healthy tissue is voided. Therefore the driving factor in such an optimization is the spatial conformity of dose which is generally best achieved by the use of carbon ions. This result demonstrates that, without a fractionation gain, the joint optimized treatment is almost identical to a unimodal carbon ion treatment. Here again, the presented results show that suboptimal carbon ion beam angle selection can be mitigated with a joint optimized solution.

The choice of LEM model for carbon ions also plays an important role in the joint optimized outcome. This influence was investigated with a comparison of joint optimized plans considering LEM I and LEM IV. Compared to LEM IV, LEM I predicts a higher RBE in the beam entrance channel, before the Bragg peak, and in the fragmentation tail, whereas LEM IV models *in vitro* cell survival data better. This increased effectiveness and reduced fractionation benefit in healthy tissue predicted by LEM I results in considerable reduction of carbon ion contributions in a joint optimized plan as compared to LEM IV.

Finally, combined photon–carbon ion plans were optimized for six glioblastoma patient cases. In order to model the mixed tissue composition of the CTV in treatment objectives, a composite of an underdosage objective considering tumour LQ parameters and overdosage objective considering healthy tissue parameters was formulated. In this joint optimized plan, photons were preferentially used to fractionate dose to healthy tissue within the CTV whereas carbon ions are used to deliver dose to the center of the GTV to reduce integral dose to the external healthy brain. The joint optimized plans overall present a benefit from reduction in cumulative near maximum biological effects in adjacent critical structures and superior conformality. With joint optimized treatments it is also possible to produce a spectrum of plans that could more closely mimic clinical priorities in sparing of OARs as illustrated with an external brain sparing prioritized plan.

In summary, this thesis presents a novel joint optimization approach to combined photon–carbon ion treatments that accounts for both fractionation and variable RBE of carbon ions within the LQ framework. This synergistic optimization exploits the complementary physical and radiobiological advantages of both modalities and allows for a spatial and temporal redistribution of biological effects between modalities.

Future research in joint optimization should focus on the mitigation of physical and biological uncertainties in order to provide a robust solution that would improve patient care. Particularly with respect to the biological uncertainties associated with LQ model parameter estimation and *in vivo* RBE estimation for carbon ions. Furthermore, it is worth investigating other more comprehensive biological models at the core of joint optimization strategy in order to take a step towards personalized radiotherapy treatments.

VII
Summary

Carbon ion therapy is a promising treatment modality that is not widely accessible to patients due to limited resources and a high cost of treatment. Therefore, it is necessary to consider mixed modality treatments where carbon ions are utilized in combination with the more widely available and accessible, photon therapy. In contemporary clinical combined treatments, photon fractions and carbon ion fractions are separately optimized and simply accumulated based on the RBE weighted dose. Such a "naive" combination does not fully exploit physical and radiobiological advantages emerging from the interplay of both modalities. Carbon ions excel at delivering high RBE conformal dose to the target volume and avoid delivering dose to distal healthy tissue. Photons, besides generally larger integral dose, have a lower RBE and are desirable to irradiate target subvolumes that are adjacent to healthy tissue or have healthy tissue infiltrated by tumour tissue, due to the greater fractionation potential. This thesis presents a novel method to exploit these differences by simultaneously optimizing photon and carbon ion fluence contributions in order to answer the question: what is the ideal combined photon-carbon ion fluence distribution given a specific fraction allocation between photons and carbon ions?

The joint optimization framework allows for the synergistic optimization of photon–carbon ion treatments based on the cumulative biological effect, incorporating both the variable RBE of carbon ions and the fractionation effect within the linear quadratic (LQ) model. As a part of this study, the joint optimization workflow was implemented within the open source treatment planning toolkit matRad.

Joint optimization strategies yield individually non-conformal photon and carbon ion dose distributions that cumulatively deliver a homogeneous conformal biological effect distribution in the target volume. Compared to conventional combined treatments, joint optimized treatments exhibit better conformity and better sparing of critical structures through a spatial redistribution of dose between modalities and a non-uniform fractionation schedule within the target volume. Depending on the fraction allocation between modalities, there exists

an optimized temporal distribution of biological effect where parts of the target volume are hypofractionated while areas around dose limiting critical structures are spared through fractionation. The additional degrees of freedom from the spatial and temporal redistribution of fluence enables the exploration of a new spectrum of plans that can better address physical and radiobiological treatment planning challenges.

Apart from a proof of concept, the impact of key underlying treatment parameters were also investigated. With regards to fraction allocation for photon–carbon ion treatments, the joint optimized treatments were shown to benefit from a reduction in carbon ion fractions due to their limited fractionation capacity. The choice of LQ model parameters and an assumed fractionation benefit drives the biological motivation to fractionate dose, without it the joint optimization was purely driven by the physical characteristics and beam angles selected for treatment. Furthermore, the choice of LEM version for carbon ion RBE estimation predicts the fractionation capacity of carbon ions. The clinically used LEM I predicts a higher effectiveness of carbon ions in the entrance region and fragmentation tail as compared to LEM IV. Therefore the use of LEM I in joint optimization results in a lowering of carbon ion contributions in order to spare healthy tissue located at the entrance channel and fragmentation tail.

Finally, the method was demonstrated for six glioblastoma patients, where the CTV contains tumour infiltrated healthy tissue that would benefit from a fractionated treatment. In comparison to the current clinical standard of independently optimized photon–carbon ion plans, the optimal plan dose to CTV was primarily delivered by photons while carbon ions are restricted to the GTV with variations depending on tumour size and location. The joint optimization approach results in a targeted application of carbon ions that (1) reduces dose in normal tissues within the target volume which can only be protected through fractionation and (2) boosts central target volume regions in order to reduce integral dose.

In conclusion, this thesis presents the first joint optimization framework that allows for an evidence based and mathematically optimal allocation of photons and carbon ions in mixed modality treatments.

VIII
Zusammenfassung

Kombinierte Photonen-Kohlenstoffionen-Bestrahlungsplanung

Die Bestrahlung mit Kohlenstoff-Ionen ist eine vielversprechende Therapiemodalität, die aufgrund begrenzter Ressourcen und hoher Kosten für Patienten nicht allgemein zugänglich ist. Daher ist es notwendig, gemischte Strahlentherapien in Betracht zu ziehen, bei denen Kohlenstoffionen in Kombination mit der weithin verfügbaren und zugänglichen Photonentherapie eingesetzt werden. Bei den gegenwärtigen klinischen Kombinationsbehandlungen werden die Photonen- und Kohlenstoffionenfraktionen separat optimiert und direkt deren RBW-gewichtete Dosen akkumuliert. Diese "naive" Kombination schöpft die physikalischen und strahlenbiologischen Vorteile der beiden Modalitäten nicht vollständig aus. Kohlenstoffionen zeichnen sich durch hohe RBW und Komformalität im Zielvolumen aus, während die Dosierung von distalem, gesunden Gewebe vermieden wird. Neben der generell größeren integralen Dosis sind Photonen hingegen, aufgrund des niedrigeren RBW sowie größeren Fraktionierungspotenzials wünschenswert, um Zielsubvolumina zu bestrahlen, die an gesundes Gewebe angrenzen oder bei denen gesundes Gewebe von Tumorgewebe infiltriert ist. In dieser Arbeit wird eine neuartige Methode zur gleichzeitigen Optimierung von Photonen- und Kohlenstoffionen-Fluenzbeiträgen unter Ausnutzung der Unterschiede beider Modalitäten vorgestellt und so die Frage beantwortet: Was ist die ideale kombinierte Photonen-Kohlenstoffionen-Fluenzverteilung zwischen Photonen und Kohlenstoffionen bei gegebenem Fraktionierungsschema?

Das entwickelte Framework ermöglicht die synergistische Optimierung von Photonen-Kohlenstoffionen-Behandlungen basierend auf dem kumulativen biologischen Effekt, wobei sowohl die variable RBW von Kohlenstoffionen als auch der Fraktionierungseffekt innerhalb des linear-quadratischen (LQ) Modells berücksichtigt werden. Als Teil dieser Studie wurde das gemeinsame Optimierungsframework im Open-Source toolkit matRad implementiert.

Gemeinsame Optimierungsstrategien führen zu jeweils inhomogenen, nicht konformalen Dosisverteilungen der Photonen- und Kohlenstoffionenbeiträge, die kumulativ jedoch eine

homogene biologische Effektverteilung im Zielvolumen liefern. Im Vergleich zu konventionell kombinierten Bestrahlungsplänen weisen gemeinsam optimierte Pläne eine bessere Konformität und eine bessere Schonung kritischer Organe durch eine räumliche Umverteilung der Dosis zwischen den Modalitäten und einen ungleichmäßigen Fraktionierungsplan innerhalb des Zielvolumens auf. Abhängig von der Fraktionsverteilung zwischen den Modalitäten gibt es eine optimierte zeitliche Verteilung des biologischen Effekts, bei der Teile des Zielvolumens hypofraktioniert werden, während Bereiche um dosislimitierende kritische Organe durch Fraktionierung geschont werden. Die zusätzlichen Freiheitsgrade der räumlichen und zeitlichen Umverteilung der Fluenz ermöglichen die Erforschung eines neuen Spektrums von Plänen, die den Herausforderungen der physikalischen und strahlenbiologischen Bestrahlungsplanung besser gerecht werden können.
Neben einem Proof-of-Concept wurden auch die Auswirkungen der wichtigsten zugrunde liegenden Behandlungsparameter untersucht. Im Hinblick auf die Ausgestaltung des Fraktionsschemas von Photonen-Kohlenstoffionen-Behandlungen wurde gezeigt, dass die gemeinsam optimierten Behandlungen von einer Reduzierung der Kohlenstoffionen-Fraktionen aufgrund ihrer begrenzten Fraktionierungskapazität profitieren. Die Wahl der LQ-Modellparameter und ein angenommener Fraktionierungsvorteil treiben die biologische Motivation zur Dosisfraktionierung an. Ohne sie wurde die gemeinsame Optimierung rein von den physikalischen Eigenschaften und den für die Behandlung gewählten Strahlwinkeln getrieben. Darüber hinaus sagt die Wahl des biologischen Modells zur Abschätzung der RBW der Kohlenstoff-Ionen die Fraktionierungskapazität von Kohlenstoff-Ionen voraus. Das klinisch verwendete LEM I schätzt eine höhere Effektivität der Kohlenstoff-Ionen im Eingangsbereich und Fragmentierungsschweif im Vergleich zu LEM IV. Daher führt die Verwendung von LEM I in der Optimierung zu einer Verringerung des Kohlenstoffionen-Beitrags, um gesundes Gewebe zu schonen, welches sich im Eingangskanal und Fragmentierungsschwanz befindet.
Die Methode für sechs Glioblastom-Patienten demonstriert, bei denen das CTV tumorinfiltriertes gesundes Gewebe enthält, das von einer fraktionierten Behandlung profitieren würde. Im Vergleich zum derzeitigen klinischen Standard von unabhängig optimierten Photonen-Kohlenstoffionen-Plänen wurde die optimale Plandosis für das CTV primär durch Photonen geliefert, während der Beitrag der Kohlenstoff-Ionen auf das GTV beschränkt wird; in Abhängigkeit von Tumorgröße und -lage. Der gemeinsame Optimierungsansatz führt zu einer gezielten Anwendung von Kohlenstoff-Ionen, die (1) die Dosis in normalen Geweben innerhalb des Zielvolumens, die nur durch Fraktionierung geschützt werden können, reduziert und (2) die Dosis in zentralen Zielvolumenregionen erhöht, um die integrale Dosis zu reduzieren.
Zusammenfassend stellt diese Arbeit den ersten gemeinsamen Optimierungsansatz vor, der eine evidenzbasierte und mathematisch optimale Allokation von Photonen und Kohlenstoff-Ionen in gemischtmodalen Behandlungen ermöglicht.

Bibliography

Adeberg, S., Bernhardt, D., Harrabi, S. B., Uhl, M., Paul, A., Bougatf, N., Verma, V., Unterberg, A., Wick, W., Haberer, T., Combs, S. E., Herfarth, K., Debus, J., and Rieken, S. (2017). Sequential proton boost after standard chemoradiation for high-grade glioma. *Radiotherapy and Oncology*, 125(2):266–272. 34

Adibi, A. and Salari, E. (2018). Spatiotemporal radiotherapy planning using a global optimization approach. *Physics in Medicine and Biology*, 63(3):035040. 31

Ahnesjö, A. and Aspradakis, M. M. (1999). Dose calculations for external photon beams in radiotherapy. 27

Akbaba, S., Ahmed, D., Lang, K., Held, T., Mattke, M., Hoerner-Rieber, J., Herfarth, K., Rieken, S., Plinkert, P., Debus, J., and Adeberg, S. (2019a). Results of a combination treatment with intensity modulated radiotherapy and active raster-scanning carbon ion boost for adenoid cystic carcinoma of the minor salivary glands of the nasopharynx. *Oral Oncology*, 91:39–46. 34, 99

Akbaba, S., Ahmed, D., Mock, A., Held, T., Bahadir, S., Lang, K., Syed, M., Hoerner-Rieber, J., Forster, T., Federspil, P., Herfarth, K., Plinkert, P., Debus, J., and Adeberg, S. (2019b). Treatment Outcome of 227 Patients with Sinonasal Adenoid Cystic Carcinoma (ACC) after Intensity Modulated Radiotherapy and Active Raster-Scanning Carbon Ion Boost: A 10-Year Single-Center Experience. *Cancers*, 11(11):1705. 34

Alber, M., Meedt, G., Nüsslin, F., and Reemtsen, R. (2002). On the degeneracy of the IMRT optimization problem. *Medical Physics*, 29(11):2584–2589. 45

Alexander, A., Soisson, E., Renaud, M.-A., and Seuntjens, J. (2012). Direct aperture optimization for FLEC-based MERT and its application in mixed beam radiotherapy. *Medical Physics*, 39(8):4820–4831. 34, 38

American Cancer Society (2018). Global Cancer Facts & Figures 4th Edition. 1

Astrahan, M. (2008). Some implications of linear-quadratic-linear radiation dose-response with regard to hypofractionation. *Medical Physics*, 35(9):4161–4172. 16, 90

Atun, R., Jaffray, D. A., Barton, M. B., Bray, F., Baumann, M., Vikram, B., Hanna, T. P., Knaul, F. M., Lievens, Y., Lui, T. Y., Milosevic, M., O'Sullivan, B., Rodin, D. L., Rosenblatt, E., Van Dyk, J., Yap, M. L., Zubizarreta, E., and Gospodarowicz, M. (2015). Expanding global access to radiotherapy. 1

Barendsen, G. (1968). Response of cultured cells, tumours and normal tissues to radiations of different linear energy transfer. *Current topics in radiation research quarterly*, 4. 19

Barendsen, G. W. (1982). Dose fractionation, dose rate and iso-effect relationships for normal tissue responses. *International Journal of Radiation Oncology, Biology, Physics*, 8(11):1981–1997. 17

Bedford, J. S. (1991). Sublethal damage, potentially lethal damage, and chromosomal aberrations in mammalian cells exposed to ionizing radiations. *International Journal of Radiation Oncology, Biology, Physics*, 21(6):1457–1469. 13

Bennan, A. B. A., Unkelbach, J., Wahl, N., Salome, P., and Bangert, M. (2021). Joint optimization of photon – carbon ion treatments for Glioblastoma. *International Journal of Radiation Oncology*Biology*Physics*. 117

Bethe, H. (1930). Zur Theorie des Durchgangs schneller Korpuskularstrahlen durch Materie. *Annalen der Physik*, 397(3):325–400. 9

Bloch, F. (1933). Zur Bremsung rasch bewegter Teilchen beim Durchgang durch Materie. *Annalen der Physik*, 408(3):285–320. 9

Böhlen, T. T., Brons, S., Dosanjh, M., Ferrari, A., Fossati, P., Haberer, T., Patera, V., and Mairani, A. (2012). Investigating the robustness of ion beam therapy treatment plans to uncertainties in biological treatment parameters. *Physics in Medicine and Biology*, 57(23):7983–8004. 91

Bortfeld, T. (2006). IMRT: A review and preview. *Physics in Medicine and Biology*, 51(13):R363–R379. 12

Bortfeld, T., Ramakrishnan, J., Tsitsiklis, J. N., and Unkelbach, J. (2015). Optimization of radiation therapy fractionation schedules in the presence of tumor repopulation. *INFORMS Journal on Computing*, 27(4):788–803. 100

Bortfeld, T., Schlegel, W., and Rhein, B. (1993). Decomposition of pencil beam kernels for fast dose calculations in three-dimensional treatment planning. *Medical Physics*, 20(2):311–318. 28, 44

Boskos, C., Feuvret, L., Noel, G., Habrand, J.-L., Pommier, P., Alapetite, C., Mammar, H., Ferrand, R., Boisserie, G., and Mazeron, J.-J. (2009). Combined Proton and Photon Conformal Radiotherapy for Intracranial Atypical and Malignant Meningioma. *International Journal of Radiation Oncology*Biology*Physics*, 75(2):399–406. 34

Burnet, N. G., Thomas, S. J., Burton, K. E., and Jefferies, S. J. (2004). Defining the tumour and target volumes for radiotherapy. *Cancer Imaging*, 4(2):153–161. 25

Charlie Ma, C. and Lomax, T. (2012). *Proton and Carbon Ion Therapy*. CRC Press. 12

Cisternas, E., Mairani, A., Ziegenhein, P., Jäkel, O., and Bangert, M. (2015). matRad – a multi-modality open source 3D treatment planning toolkit. In *IFMBE Proceedings*, volume 51, pages 1608–1611. 44

Combs, S. E., Bohl, J., Elsässer, T., Weber, K. J., Schulz-Ertner, D., Debus, J., and Weyrather, W. K. (2009). Radiobiological evaluation and correlation with the local effect model (LEM) of carbon ion radiation therapy and temozolomide in glioblastoma cell lines. *International Journal of Radiation Biology*, 85(2):126–137. 52

Combs, S. E., Kieser, M., Rieken, S., Habermehl, D., Jäkel, O., Haberer, T., Nikoghosyan, A., Haselmann, R., Unterberg, A., Wick, W., and Debus, J. (2010). Randomized phase II study evaluating a carbon ion boost applied

after combined radiochemotherapy with temozolomide versus a proton boost after radiochemotherapy with temozolomide in patients with primary glioblastoma: The CLEOPATRA Trial. *BMC Cancer*, 10(1):478. 34, 52, 54, 94

Combs, S. E., Wagner, J., Bischof, M., Welzel, T., Wagner, F., Debus, J., and Schulz-Ertner, D. (2008). Postoperative Treatment of Primary Glioblastoma Multiforme With Radiation and Concomitant Temozolomide in Elderly Patients. *International Journal of Radiation Oncology Biology Physics*, 70(4):987–992. 52

Cosset, J. M. (2016). L'aube de la radiothérapie, entre coups de génie, drames et controverses. 1

Curtis, S. B. (1986). Lethal and potentially lethal lesions induced by radiation–a unified repair model. *Radiation research*, 106(2):252–270. 13

Debus, J., Schulz-Ertner, D., Schad, L., Essig, M., Rhein, B., Thillmann, C. O., and Wannenmacher, M. (2000). Stereotactic fractionated radiotherapy for chordomas and chondrosarcomas of the skull base. *International Journal of Radiation Oncology Biology Physics*, 47(3):591–596. 51

Delgado-López, P. D. and Corrales-García, E. M. (2016). Survival in glioblastoma: a review on the impact of treatment modalities. 52

Douglas, B. G. and Fowler, J. F. (1976). The effect of multiple small doses of X rays on skin reactions in the mouse and a basic interpretation. *Radiation Research*, 66(2):401–426. 16

Elsässer, T., Krämer, M., and Scholz, M. (2008). Accuracy of the Local Effect Model for the Prediction of Biologic Effects of Carbon Ion Beams In Vitro and In Vivo. *International Journal of Radiation Oncology Biology Physics*, 71(3):866–872. 22

Elsässer, T. and Scholz, M. (2007). Cluster effects within the local effect model. *Radiation Research*, 167(3):319–329. 22

Fabiano, S., Balermpas, P., Guckenberger, M., and Unkelbach, J. (2020a). Combined proton–photon treatments – A new approach to proton therapy without a gantry. *Radiotherapy and Oncology*, 145:81–87. 35, 39

Fabiano, S., Bangert, M., Guckenberger, M., and Unkelbach, J. (2020b). Accounting for range uncertainties in the optimization of combined proton-photon treatments via stochastic optimization. *International Journal of Radiation Oncology*Biology*Physics*. 35, 37, 39, 93, 98

Fernandes, C., Costa, A., Osório, L., Lago, R. C., Linhares, P., Carvalho, B., and Caeiro, C. (2017). Current Standards of Care in Glioblastoma Therapy. In *Glioblastoma*, pages 197–241. Codon Publications. 52

Feuvret, L., Noel, G., Weber, D. C., Pommier, P., Ferrand, R., De Marzi, L., Dhermain, F., Alapetite, C., Mammar, H., Boisserie, G., Habrand, J. L., and Mazeron, J. J. (2007). A Treatment Planning Comparison of Combined Photon-Proton Beams Versus Proton Beams-Only for the Treatment of Skull Base Tumors. *International Journal of Radiation Oncology Biology Physics*, 69(3):944–954. 34, 51

Fitzek, M. M., Thornton, A. F., Varvares, M., Ancukiewicz, M., Mcintyre, J., Adams, J., Rosenthal, S., Joseph, M., and Amrein, P. (2002). Neuroendocrine tumors of the sinonasal tract: Results of a prospective study incorporating chemotherapy, surgery, and combined proton-photon radiotherapy. *Cancer*, 94(10):2623–2634. 34

Fossati, P., Vavassori, A., Deantonio, L., Ferrara, E., Krengli, M., and Orecchia, R. (2016). Review of photon and proton radiotherapy for skull base tumours. *Reports of Practical Oncology and Radiotherapy*, 21(4):336–355. 51

Fowler, J. F. (1989). The linear-quadratic formula and progress in fractionated radiotherapy. *British Journal of Radiology*, 62(740):679–694. 17

Fowler, J. F. (2010). 21 Years of biologically effective dose. *British Journal of Radiology*, 83(991):554–568. 17, 100

Frese, M. C. (2011). *Potentials and risks of advanced radiobiological treatment planning for proton and carbon ion therapy*. PhD thesis. 31, 33, 40

Friedrich, T., Durante, M., and Scholz, M. (2011). The Local Effect Model (LEM): Basics and applications. 20, 24

Friedrich, T., Scholz, U., Elssser, T., Durante, M., and Scholz, M. (2012). Calculation of the biological effects of ion beams based on the microscopic spatial damage distribution pattern. In *International Journal of Radiation Biology*, volume 88, pages 103–107. Int J Radiat Biol. 22, 97

Furusawa, Y., Fukutsu, K., Aoki, M., Itsukaichi, H., Eguchi-Kasai, K., Ohara, H., Yatagai, F., Kanai, T., and Ando, K. (2000). Inactivation of aerobic and hypoxic cells from three different cell lines by accelerated 3He-, 12C- and 20Ne-Ion beams. *Radiation Research*, 154(5):485–496. 22, 24

Gaddy, M. R., Yildiz, S., Unkelbach, J., and Papp, D. (2018). Optimization of spatiotemporally fractionated radiotherapy treatments with bounds on the achievable benefit. *Physics in Medicine and Biology*, 63(1):015036. 31, 33

Gao, H. (2019). Hybrid proton-photon inverse optimization with uniformity-regularized proton and photon target dose. *Physics in Medicine and Biology*, 64(10):105003. 34, 39

Gill, B., Oermann, E., Ju, A., Suy, S., Yu, X., Rabin, J., Kalhorn, C., Nair, M. N., Voyadzis, J.-M., Unger, K., Collins, S. P., Harter, K. W., and Collins, B. T. (2012). Fiducial-free CyberKnife stereotactic body radiation therapy (SBRT) for single vertebral body metastases: acceptable local control and normal tissue tolerance with 5 fraction approach. *Frontiers in Oncology*, 2(APR):39. 49

Gillmann, C., Jäkel, O., Schlampp, I., and Karger, C. P. (2014). Temporal lobe reactions after carbon ion radiation therapy: Comparison of relative biological effectiveness-weighted tolerance doses predicted by local effect models i and IV. *International Journal of Radiation Oncology Biology Physics*, 88(5):1136–1141. 97

Grellier, N. and Belkacemi, Y. (2020). Biologic effects of high doses per fraction. *Cancer/Radiotherapie*, 24(2):153–158. 96

Grün, R., Friedrich, T., Elsässer, T., Krämer, M., Zink, K., Karger, C. P., Durante, M., Engenhart-Cabillic, R., and Scholz, M. (2012). Impact of enhancements in the local effect model (LEM) on the predicted RBE-weighted target dose distribution in carbon ion therapy. *Physics in Medicine and Biology*, 57(22):7261–7274. 22, 97

Grün, R., Friedrich, T., Krämer, M., Zink, K., Durante, M., Engenhart-Cabillic, R., and Scholz, M. (2015). Assessment of potential advantages of relevant ions for particle therapy: A model based study. *Medical Physics*, 42(2):1037–1047. 101

Guan, F., Peeler, C., Bronk, L., Geng, C., Taleei, R., Randeniya, S., Ge, S., Mirkovic, D., Grosshans, D., Mohan, R., and Titt, U. (2015). Analysis of the track- and dose-averaged LET and LET spectra in proton therapy using the geant 4 Monte Carlo code. *Medical Physics*, 42(11):6234–6247. 12

Gupta, V., Krug, L. M., Laser, B., Hudka, K., Flores, R., Rusch, V. W., and Rosenzweig, K. E. (2009). Patterns of local and nodal failure in malignant pleural mesothelioma after extrapleural pneumonectomy and photon-electron radiotherapy. *Journal of Thoracic Oncology*, 4(6):746–750. 33

Hall, E. J. and Giaccia, A. J. (2006). *Radiobiology for the Radiologist*, volume 6. Lippincott Williams & Wilkins. 13, 15, 17

Harting, C., Peschke, P., Borkenstein, K., and Karger, C. P. (2007). Single-cell-based computer simulation of the oxygen-dependent tumour response to irradiation. *Physics in Medicine and Biology*, 52(16):4775–4789. 100

Hawkins, R. B. (2017). Effect of heterogeneous radio sensitivity on the survival, alpha beta ratio and biologic effective dose calculation of irradiated mammalian cell populations. *Clinical and Translational Radiation Oncology*, 4:32–38. 93

Henderson, F. C., McCool, K., Seigle, J., Jean, W., Harter, W., and Gagnon, G. J. (2009). Treatment of chordomas with CyberKnife: Georgetown university experience and treatment recommendations. *Neurosurgery*, 64(2 SUPPL.):A44–A53. 51, 54

Hochberg, F. H. and Pruitt, A. (1980). Assumptions in the radiotherapy of glioblastoma. *Neurology*, 30(9):907–911. 52

Hoffmann, A. L. and Nahum, A. E. (2013). Fractionation in normal tissues: The $(\alpha;/\beta)$eff concept can account for dose heterogeneity and volume effects. *Physics in Medicine and Biology*, 58(19):6897–6914. 96

Husain, Z. A., Sahgal, A., De Salles, A., Funaro, M., Glover, J., Hayashi, M., Hiraoka, M., Levivier, M., Ma, L., Martínez-Alvarez, R., Paddick, J. I., Régis, J., Slotman, B. J., and Ryu, S. (2017). Stereotactic body radiotherapy for de novo spinal metastases: Systematic review International Stereotactic Radiosurgery Society practice guidelines. 48

ICRU (2010). Prescribing, Recording, and Reporting Photon-Beam Intensity-Modulated Radiation Therapy (IMRT):. *Journal of the ICRU*, 10(1):NP.3–NP. 25

ICRU (2014). Report 90. *Journal of the ICRU*, 14(1):NP.2–NP. 10

Inaniwa, T., Furukawa, T., Kase, Y., Matsufuji, N., Toshito, T., Matsumoto, Y., Furusawa, Y., and Noda, K. (2010). Treatment planning for a scanned carbon beam with a modified microdosimetric kinetic model. *Physics in Medicine and Biology*, 55(22):6721–6737. 20

Jensen, A. D., Nikoghosyan, A. V., Poulakis, M., Höss, A., Haberer, T., Jäkel, O., Münter, M. W., Schulz-Ertner, D., Huber, P. E., and Debus, J. (2015). Combined intensity-modulated radiotherapy plus raster-scanned carbon ion boost for advanced adenoid cystic carcinoma of the head and neck results in superior locoregional control and overall survival. *Cancer*, 121(17):3001–3009. 34, 99

Johansson, S., Åström, L., Sandin, F., Isacsson, U., Montelius, A., and Turesson, I. (2012). Hypofractionated Proton Boost Combined with External Beam Radiotherapy for Treatment of Localized Prostate Cancer. *Prostate Cancer*, 2012:1–14. 99

Joiner, M. and van der Kogel, A. (2009). *Basic Clinical Radiobiology Fourth Edition*. CRC press. 2, 13, 15, 17, 18, 19, 94, 99, 100

Joiner, M. C., Marples, B., Lambin, P., Short, S. C., and Turesson, I. (2001). Low-dose hypersensitivity: Current status and possible mechanisms. In *International Journal of Radiation Oncology Biology Physics*, volume 49, pages 379–389. Int J Radiat Oncol Biol Phys. 16, 90

Jones, B., Dale, R. G., Deehan, C., Hopkins, K. I., and Morgan, D. A. (2001). The role of biologically effective dose (BED) in clinical oncology. *Clinical Oncology*, 13(2):71–81. 17

Karger, C. P. and Peschke, P. (2018). RBE and related modeling in carbon-ion therapy. *Physics in Medicine and Biology*, 63(1):1–2. 18, 20, 21

Kelly, P. J., Daumas-Duport, C., Kispert, D. B., Kall, B. A., Scheithauer, B. W., and Illig, J. J. (1987). Imaging-based stereotaxic serial biopsies in untreated intracranial glial neoplasms. *Journal of Neurosurgery*, 66(6):865–874. 97

Khan, F. M. and Gibbons, J. P. (2019). *Khan's the physics of radiation therapy*, volume 45. Wolters Kluwer Health. 7, 8, 12

Kirkpatrick, J. P., Marks, L. B., Mayo, C. S., Lawrence, Y. R., Bhandare, N., and Ryu, S. (2011). Estimating normal tissue toxicity in radiosurgery of the CNS: application and limitations of QUANTEC. *Journal of radiosurgery and SBRT*, 1(2):95–107. 96

Kirkpatrick, J. P., Meyer, J. J., and Marks, L. B. (2008). The Linear-Quadratic Model Is Inappropriate to Model High Dose per Fraction Effects in Radiosurgery. *Seminars in Radiation Oncology*, 18(4):240–243. 16, 96

Klement, R. J., Sonke, J. J., Allgäuer, M., Andratschke, N., Appold, S., Belderbos, J., Belka, C., Dieckmann, K., Eich, H. T., Flentje, M., Grills, I., Eble, M., Hope, A., Grosu, A. L., Semrau, S., Sweeney, R. A., Hörner-Rieber, J., Werner-Wasik, M., Engenhart-Cabillic, R., Ye, H., and Guckenberger, M. (2020). Estimation of the α/β

ratio of non-small cell lung cancer treated with stereotactic body radiotherapy. *Radiotherapy and Oncology*, 142:210–216. 99

Kopp, B., Mein, S., Dokic, I., Harrabi, S., Böhlen, T. T., Haberer, T., Debus, J., Abdollahi, A., and Mairani, A. (2020). Development and Validation of Single Field Multi-Ion Particle Therapy Treatments. *International Journal of Radiation Oncology Biology Physics*, 106(1):194–205. 36, 37

Kraft, G. (2000). Tumor therapy with heavy charged particles. *Progress in Particle and Nuclear Physics*, 45(SUPPL.2):S473–S544. 18, 20

Krämer, M. and Scholz, M. (2006). Rapid calculation of biological effects in ion radiotherapy. *Physics in Medicine and Biology*, 51(8):1959–1970. 22

Krämer, M., Scifoni, E., Schmitz, F., Sokol, O., and Durante, M. (2014). Overview of recent advances in treatment planning for ion beam radiotherapy. *European Physical Journal D*, 68(10):306. 34, 36

Krayenbuehl, J., Oertel, S., Davis, J. B., and Ciernik, I. F. (2007). Combined Photon and Electron Three-Dimensional Conformal Versus Intensity-Modulated Radiotherapy With Integrated Boost for Adjuvant Treatment of Malignant Pleural Mesothelioma After Pleuropneumonectomy. *International Journal of Radiation Oncology*Biology*Physics*, 69(5):1593–1599. 33

Kueng, R., Mueller, S., Loebner, H. A., Frei, D., Volken, W., Aebersold, D. M., Stampanoni, M. F. M., Fix, M. K., and Manser, P. (2020). TriB-RT: simultaneous optimization of photon, electron and proton beams. *Physics in Medicine & Biology*. 35, 39

Lang, K., Baur, M., Akbaba, S., Held, T., Kargus, S., Bougatf, N., Bernhardt, D., Freier, K., Plinkert, P. K., Rieken, S., Debus, J., and Adeberg, S. (2018). Intensity modulated radiotherapy (IMRT) + carbon ion boost for adenoid cystic carcinoma of the minor salivary glands in the oral cavity. *Cancers*, 10(12). 99

Laperriere, N., Zuraw, L., and Cairncross, G. (2002). Radiotherapy for newly diagnosed malignant glioma in adults: A systematic review. 99

Llacer, J., Deasy, J. O., Bortfeld, T. R., Solberg, T. D., and Promberger, C. (2003). Absence of multiple local minima effects in intensity modulated optimization with dose volume constraints. *Physics in Medicine and Biology*, 48(2):183–210. 29

Lomax, A. J., Boehringer, T., Coray, A., Egger, E., Goitein, G., Grossmann, M., Juelke, P., Lin, S., Pedroni, E., Rohrer, B., Roser, W., Rossi, B., Siegenthaler, B., Stadelmann, O., Stauble, H., Vetter, C., and Wisser, L. (2001). Intensity modulated proton therapy: A clinical example. *Medical Physics*, 28(3):317–324. 12

Lomax, A. J., Pedroni, E., Rutz, H., and Goitein, G. (2004). The clinical potential of intensity modulated proton therapy. *Zeitschrift fur Medizinische Physik*, 14(3):147–152. 12

López Alfonso, J. C., Parsai, S., Joshi, N., Godley, A., Shah, C., Koyfman, S., Caudell, J., Fuller, C., Enderling, H., and Scott, J. (2017). Temporally feathered intensity modulated radiation therapy: a planning technique to reduce normal tissue toxicity. *Temporally feathered intensity-modulated radiation therapy: A planning technique to reduce normal tissue toxicity*, page 184044. 31

Ma, C. and Wang, L. (2013). *Equivalent Path Length*, page 224. Springer Berlin Heidelberg, Berlin, Heidelberg. 26

MacKie, T. R., Bielajew, A. F., Rogers, D. W., and Battista, J. J. (1988). Generation of photon energy deposition kernels using the EGS Monte Carlo code. *Physics in Medicine and Biology*, 33(1):1–20. 27

Malouff, T. D., Peterson, J. L., Mahajan, A., and Trifiletti, D. M. (2019). Carbon ion radiotherapy in the treatment of gliomas: a review. 52

Matsukado, Y., MacCarty, C. S., and Kernohan, J. W. (1961). The growth of glioblastoma multiforme (astrocytomas, grades 3 and 4) in neurosurgical practice. *Journal of neurosurgery*, 18(5):636–644. 97

McMahon, S. J. (2019). The linear quadratic model: Usage, interpretation and challenges. *Physics in Medicine and Biology*, 64(1). 15

McNamara, A., Willers, H., and Paganetti, H. (2020). Modelling variable proton relative biological effectiveness for treatment planning. 19

Mein, S., Klein, C., Kopp, B., Magro, G., Harrabi, S., Karger, C. P., Haberer, T., Debus, J., Abdollahi, A., Dokic, I., and Mairani, A. (2020). Assessment of RBE-Weighted Dose Models for Carbon Ion Therapy Toward Modernization of Clinical Practice at HIT: In Vitro, in Vivo, and in Patients. *International Journal of Radiation Oncology Biology Physics*, 108(3):779–791. 98

Menze, B., Isensee, F., Wiest, R., Wiestler, B., Maier-Hein, K., Reyes, M., and Bakas, S. (2021). Analyzing magnetic resonance imaging data from glioma patients using deep learning. *Computerized Medical Imaging and Graphics*, 88:101828. 97

Míguez, C., Jiménez-Ortega, E., Palma, B. A., Miras, H., Ureba, A., Arráns, R., Carrasco-Peña, F., Illescas-Vacas, A., and Leal, A. (2017). Clinical implementation of combined modulated electron and photon beams with conventional MLC for accelerated partial breast irradiation. *Radiotherapy and Oncology*, 124(1):124–129. 34, 38

Mizuta, M., Date, H., Takao, S., Kishimoto, N., Sutherland, K. L., Onimaru, R., and Shirato, H. (2012a). Graphical representation of the effects on tumor and OAR for determining the appropriate fractionation regimen in radiation therapy planning. *Medical Physics*, 39(11):6791–6795. 36

Mizuta, M., Takao, S., Date, H., Kishimoto, N., Sutherland, K. L., Onimaru, R., and Shirato, H. (2012b). A Mathematical Study to Select Fractionation Regimen Based on Physical Dose Distribution and the Linear–Quadratic Model. *International Journal of Radiation Oncology*Biology*Physics*, 84(3):829–833. 36

Moyers, M. F., Sardesai, M., Sun, S., and Miller, D. W. (2010). Ion Stopping Powers and CT Numbers. *Medical Dosimetry*, 35(3):179–194. 26

Mueller, S., Fix, M. K., Joosten, A., Henzen, D., Frei, D., Volken, W., Kueng, R., Aebersold, D. M., Stampanoni, M. F., and Manser, P. (2017). Simultaneous optimization of photons and electrons for mixed beam radiotherapy. *Physics in Medicine and Biology*, 62(14):5840–5860. 34, 38

Mueller, S., Manser, P., Volken, W., Frei, D., Kueng, R., Herrmann, E., Elicin, O., Aebersold, D. M., Stampanoni, M. F., and Fix, M. K. (2018). Part 2: Dynamic mixed beam radiotherapy (DYMBER): Photon dynamic trajectories combined with modulated electron beams. *Medical Physics*, 45(9):4213–4226. 34, 38

Nahum, A. E. and Uzan, J. (2012). (Radio)biological optimization of external-beam radiotherapy. *Computational and Mathematical Methods in Medicine*, 2012:13. 100

Newhauser, W. D. and Zhang, R. (2015). The physics of proton therapy. *Physics in Medicine and Biology*, 60(8):R155–R209. 9, 10, 26

Nikoghosyan, A. V., Karapanagiotou-Schenkel, I., Münter, M. W., Jensen, A. D., Combs, S. E., and Debus, J. (2010). Randomised trial of proton vs. carbon ion radiation therapy in patients with chordoma of the skull base, clinical phase III study HIT-1-Study. *BMC Cancer*, 10. 51

Nikoghosyan, A. V., Schulz-Ertner, D., Herfarth, K., Didinger, B., Münter, M. W., Jensen, A. D., Jäkel, O., Hoess, A., Haberer, T., and Debus, J. (2011). Acute toxicity of combined photon IMRT and carbon ion boost for intermediate-risk prostate cancer – Acute toxicity of 12C for PC. *Acta Oncologica*, 50(6):784–790. 34

Noël, G., Habrand, J. L., Mammar, H., Pontvert, D., Haie-Méder, C., Hasboun, D., Moisson, P., Ferrand, R., Beaudré, A., Boisserie, G., Gaboriaud, G., Mazal, A., Kérody, K., Schlienger, M., and Mazeron, J. J. (2001). Combination of photon and proton radiation therapy for chordomas and chondrosarcomas of the skull base: The Centre de Protonthérapie D'Orsay experience. *International Journal of Radiation Oncology Biology Physics*, 51(2):392–398. 34, 51

Nuraini, R. and Widita, R. (2019). Tumor Control Probability (TCP) and Normal Tissue Complication Probability (NTCP) with Consideration of Cell Biological Effect. In *Journal of Physics: Conference Series*, volume 1245, page 12092. Institute of Physics Publishing. 100

Oelfke, U. and Bortfeld, T. (2001). Inverse planning for photon and proton beams. *Medical Dosimetry*, 26(2):113–124. 29, 30, 31, 40

Paganetti, H., Niemierko, A., Ancukiewicz, M., Gerweck, L. E., Goitein, M., Loeffler, J. S., and Suit, H. D. (2002). Relative biological effectiveness (RBE) values for proton beam therapy. *International Journal of Radiation Oncology Biology Physics*, 53(2):407–421. 19

Palma, B. A., Sánchez, A. U., Salguero, F. J., Arráns, R., Sánchez, C. M., Zurita, A. W., Hermida, M. I. R., and Leal, A. (2012). Combined modulated electron and photon beams planned by a Monte-Carlo-based optimization procedure for accelerated partial breast irradiation. *Physics in Medicine & Biology*, 57(5):1191. 34, 38

Parodi, K., Mairani, A., and Sommerer, F. (2013). Monte Carlo-based parametrization of the lateral dose spread for clinical treatment planning of scanned proton and carbon ion beams. *Journal of Radiation Research*, 54(SUPPL.1):i91. 28

Peeters, A., Grutters, J. P., Pijls-Johannesma, M., Reimoser, S., De Ruysscher, D., Severens, J. L., Joore, M. A., and Lambin, P. (2010). How costly is particle therapy? Cost analysis of external beam radiotherapy with carbon-ions, protons and photons. *Radiotherapy and Oncology*, 95(1):45–53. 3

Perkó, Z., Bortfeld, T., Hong, T., Wolfgang, J., and Unkelbach, J. (2018). Derivation of mean dose tolerances for new fractionation schemes and treatment modalities. *Physics in Medicine and Biology*, 63(3):035038. 96

Podgorsak, E. B. (2016). *Radiation Physics for Medical Physicists*. Graduate Texts in Physics. Springer International Publishing, Cham. 8

PTCOG (2020). PTCOG - Facilities in Operation. URL: `https://www.ptcog.ch/index.php/facilities-in-operation` [Accessed: 06-01-2021]. 3

Renaud, M., Serban, M., and Seuntjens, J. (2017). On mixed electron–photon radiation therapy optimization using the column generation approach. *Medical Physics*, 44(8):4287–4298. 34, 38

Renaud, M. A., Serban, M., and Seuntjens, J. (2019). Robust mixed electron–photon radiation therapy optimization. *Medical Physics*, 46(3):1384–1396. 34, 38

Saberian, F., Ghate, A., and Kim, M. (2016). Optimal fractionation in radiotherapy with multiple normal tissues. *Mathematical Medicine and Biology*, 33(2):211–252. 36

Salvat, F. and Fernández-Varea, J. M. (2009). Overview of physical interaction models for photon and electron transport used in Monte Carlo codes. *Metrologia*, 46(2). 7

Sánchez-Parcerisa, D., Gemmel, A., Jäkel, O., Parodi, K., and Rietzel, E. (2012). Experimental study of the water-to-air stopping power ratio of monoenergetic carbon ion beams for particle therapy. *Physics in Medicine and Biology*, 57(11):3629–3641. 11

Schaffner, B., Pedroni, E., and Lomax, A. (1999). Dose calculation models for proton treatment planning using a dynamic beam delivery system: An attempt to include density heterogeneity effects in the analytical dose calculation. *Physics in Medicine and Biology*, 44(1):27–41. 28

Schlegel, W., Bortfeld, T., Grosu, A.-L., Pan, T., and Luo, D. (2008). *New Technologies in Radiation Oncology*, volume 49. Soc Nuclear Med. 18

Scholz, M., Kellerer, A. M., Kraft-Weyrather, W., and Kraft, G. (1997). Computation of cell survival in heavy ion beams for therapy: The model and its approximation. *Radiation and Environmental Biophysics*, 36(1):59–66. 22

Scholz, M. and Kraft, G. (1996). Track structure and the calculation of biological effects of heavy charged particles. *Advances in Space Research*, 18(1-2):5–14. 20, 21, 97

Schulz-Ertner, D., Haberer, T., Jäkel, O., Thilmann, C., Krämer, M., Enghardt, W., Kraft, G., Wannenmacher, M., and Debus, J. (2002). Radiotherapy for chordomas and low-grade chondrosarcomas of the skull base with carbon ions. *International Journal of Radiation Oncology Biology Physics*, 53(1):36–42. 51

Schulz-Ertner, D., Karger, C. P., Feuerhake, A., Nikoghosyan, A., Combs, S. E., Jäkel, O., Edler, L., Scholz, M., and Debus, J. (2007). Effectiveness of Carbon Ion Radiotherapy in the Treatment of Skull-Base Chordomas. *International Journal of Radiation Oncology Biology Physics*, 68(2):449–457. 51

Schulz-Ertner, D., Nikoghosyan, A., Didinger, B., Münter, M., Jäkel, O., Karger, C. P., and Debus, J. (2005). Therapy strategies for locally advanced adenoid cystic carcinomas using modern radiation therapy techniques. *Cancer*, 104(2):338–344. 34

Schulz-Ertner, D., Nikoghosyan, A., Jäkel, O., Haberer, T., Kraft, G., Scholz, M., Wannenmacher, M., and Debus, J. (2003). Feasibility and toxicity of combined photon and carbon ion radiotherapy for locally advanced adenoid cystic carcinomas. *International Journal of Radiation Oncology Biology Physics*, 56(2):391–398. 34, 51, 99

Schulz-Ertner, D., Nikoghosyan, A., Thilmann, C., Haberer, T., Jäkel, O., Karger, C., Kraft, G., Wannenmacher, M., and Debus, J. (2004). Results of carbon ion radiotherapy in 152 patients. In *International Journal of Radiation Oncology Biology Physics*, volume 58, pages 631–640. Elsevier Inc. 51

Schuppert, C., Paul, A., Nill, S., Schwahofer, A., Debus, J., and Sterzing, F. (2020). A treatment planning study of combined carbon ion-beam plus photon intensity-modulated radiotherapy. *Physics and Imaging in Radiation Oncology*, 15:16–22. 34, 37

Seltzer, S. M., Bartlett, D. T., Burns, D. T., Dietze, G., Menzel, H. G., Paretzke, H. G., and Wambersie, A. (2011). Fundamental quantities and units for ionizing radiation. *Journal of the ICRU*, 11(1):1–41. 9, 11

Shewchuk, J. R. (1994). *An Introduction to the Conjugate Gradient Method Without the Agonizing Pain*. Carnegie Mellon University, USA. 46

Shipley, W. U., Tepper, J. E., Verhey, L. J., Mendiondo, O. A., Goitein, M., Suit, H. D., Prout, G. R., and Koehler, A. M. (1979). Proton Radiation as Boost Therapy for Localized Prostatic Carcinoma. *JAMA: The Journal of the American Medical Association*, 241(18):1912–1915. 99

Sinclair, W. K. (1966). *The shape of radiation survival curves of mammalian cells cultured in vitro*. International Atomic Energy Agency (IAEA). 14

Stupp, R., Mason, W. P., Van Den Bent, M. J., Weller, M., Fisher, B., Taphoorn, M. J., Belanger, K., Brandes, A. A., Marosi, C., Bogdahn, U., Curschmann, J., Janzer, R. C., Ludwin, S. K., Gorlia, T., Allgeier, A., Lacombe, D., Cairncross, J. G., Eisenhauer, E., and Mirimanoff, R. O. (2005). Radiotherapy plus concomitant and adjuvant temozolomide for glioblastoma. *New England Journal of Medicine*, 352(10):987–996. 52

Takagi, M., Demizu, Y., Nagano, F., Terashima, K., Fujii, O., Jin, D., Mima, M., Niwa, Y., Katsui, K., Suga, M., Yamashita, T., Akagi, T., ichi Sakata, K., Fuwa, N., and Okimoto, T. (2018). Treatment outcomes of proton or carbon ion therapy for skull base chordoma: a retrospective study. *Radiation Oncology*, 13(1):232. 51

Ten Eikelder, S. C., Den Hertog, D., Bortfeld, T., and Perkó, Z. (2019). Optimal combined proton-photon therapy schemes based on the standard BED model. *Physics in Medicine and Biology*, 64(6). 36, 92

Uhl, M., Mattke, M., Welzel, T., Roeder, F., Oelmann, J., Habl, G., Jensen, A., Ellerbrock, M., Jäkel, O., Haberer, T., Herfarth, K., and Debus, J. (2014). Highly effective treatment of skull base chordoma with carbon ion irradiation using a raster scan technique in 155 patients: First long-term results. *Cancer*, 120(21):3410–3417. 51

Unkelbach, J., Bangert, M., De Amorim Bernstein, K., Andratschke, N., and Guckenberger, M. (2018). Optimization of combined proton–photon treatments. *Radiotherapy and Oncology*, 128(1):133–138. 35, 37, 39, 48, 49, 58, 88, 99

Unkelbach, J., Chapman, P. H., Bussière, M. R., Loeffler, J. S., and Shih, H. A. (2016). Spatiotemporal Fractionation Schemes for Irradiating Large Cerebral Arteriovenous Malformations. *International Journal of Radiation Oncology Biology Physics*, 95(3):1067–1074. 31

Unkelbach, J., Menze, B. H., Konukoglu, E., Dittmann, F., Ayache, N., and Shih, H. A. (2014a). Radiotherapy planning for glioblastoma based on a tumor growth model: Implications for spatial dose redistribution. *Physics in Medicine and Biology*, 59(3):771–789. 97

Unkelbach, J., Menze, B. H., Konukoglu, E., Dittmann, F., Le, M., Ayache, N., and Shih, H. A. (2014b). Radiotherapy planning for glioblastoma based on a tumor growth model: Improving target volume delineation. *Physics in Medicine and Biology*, 59(3):747–770. 97

Unkelbach, J. and Papp, D. (2015). The emergence of nonuniform spatiotemporal fractionation schemes within the standard BED model. *Medical Physics*, 42(5):2234–2241. 31, 33

Unkelbach, J., Zeng, C., and Engelsman, M. (2013). Simultaneous optimization of dose distributions and fractionation schemes in particle radiotherapy. *Medical Physics*, 40(9):091702. 31

van Leeuwen, C. M., Oei, A. L., Crezee, J., Bel, A., Franken, N. A., Stalpers, L. J., and Kok, H. P. (2018). The alfa and beta of tumours: A review of parameters of the linear-quadratic model, derived from clinical radiotherapy studies. *Radiation Oncology*, 13(1). 15, 51, 94

Vassiliev, O. N., Wareing, T. A., McGhee, J., Failla, G., Salehpour, M. R., and Mourtada, F. (2010). Validation of a new grid-based Boltzmann equation solver for dose calculation in radiotherapy with photon beams. *Physics in Medicine and Biology*, 55(3):581–598. 27

Wächter, A. and Biegler, L. T. (2006). On the implementation of an interior-point filter line-search algorithm for large-scale nonlinear programming. *Mathematical programming*, 106(1):25–57. 44

Watanabe, M., Tanaka, R., and Takeda, N. (1992). Magnetic resonance imaging and histopathology of cerebral gliomas. *Neuroradiology*, 34(6):463–469. 97

Wathen, A. J. (2015). Preconditioning. *Acta Numerica*, 24:329–376. 46

Wenkel, E., Thornton, A. F., Finkelstein, D., Adams, J., Lyons, S., De La Monte, S., Ojeman, R. G., and Munzenrider, J. E. (2000). Benign meningioma: Partially resected, biopsied, and recurrent intracranial tumors treated with combined proton and photon radiotherapy. *International Journal of Radiation Oncology Biology Physics*, 48(5):1363–1370. 34

Wieser, H. P. (2020). *Probabilistic Treatment Planning for Carbon Ion Therapy - heiDOK*. PhD thesis, Heidelberg University, Heidelberg. 22

Wieser, H. P., Cisternas, E., Wahl, N., Ulrich, S., Stadler, A., Mescher, H., Muller, L. R., Klinge, T., Gabrys, H., Burigo, L., Mairani, A., Ecker, S., Ackermann, B., Ellerbrock, M., Parodi, K., Jakel, O., and Bangert, M. (2017). Development of the open-source dose calculation and optimization toolkit matRad. *Medical Physics*, 44(6):2556–2568. 29, 30, 44

Wieser, H. P., Wahl, N., Gabryś, H. S., Müller, L. R., Pezzano, G., Winter, J., Ulrich, S., Burigo, L., Jäkel, O., and Bangert, M. (2018). Matrad-an Open-Source Treatment Planning Toolkit for Educational Purposes. *Medical Physics International Journal*, 6(1). 44

Wilkens, J. J. and Oelfke, U. (2005). Optimization of radiobiological effects in intensity modulated proton therapy. *Medical Physics*, 32(2):455–465. 30, 31

Wilkens, J. J. and Oelfke, U. (2006). Fast multifield optimization of the biological effect in ion therapy. *Physics in Medicine and Biology*, 51(12):3127–3140. 30

Wu, Q. and Mohan, R. (2000). Algorithms and functionality of an intensity modulated radiotherapy optimization system. *Medical Physics*, 27(4):701–711. 29, 30, 34

Wurzel, M., Schaller, C., Simon, M., and Deutsch, A. (2005). Cancer cell invasion of brain tissue: Guided by a prepattern? *Journal of Theoretical Medicine*, 6(1):21–31. 97

Xiong, W., Li, J., Chen, L., Price, R. A., Freedman, G., Ding, M., Qin, L., Yang, J., and Ma, C. M. (2004). Optimization of combined electron and photon beams for breast cancer. *Physics in Medicine and Biology*, 49(10):1973–1989. 34, 38

Yáñez, M. L., Miller, J. J., and Batchelor, T. T. (2017). Diagnosis and treatment of epidural metastases. *Cancer*, 123(7):1106–1114. 48

Zaider, M. and Rossi, H. H. (1980). The synergistic effects of different radiations. *Radiation research*, 83(3):732–739. 30

Disclosure

This work was funded by the German Cancer Research Center (DKFZ). Glioblastoma patient data originated from patients treated at the Heidelberg Ion-Beam Therapy Center (HIT) and was used with consent. The proposed methodology for the joint optimization of photons and carbon ions presented in chapter III was developed by myself. The generation of results presented in chapter IV was fully carried out on my own and represents the core results of this dissertation.

Parts of the results presented in this thesis were published in advance in peer reviewed journals:
Publication 1: Bennan, A.B.A., Unkelbach, J., Wahl, N., Salome, P. and Bangert, M.
Joint optimization of photon – carbon ion treatments for Glioblastoma (International Journal of Radiation Oncology, Biology, Physics)(Bennan et al., 2021)

Publication 1 presents an application of the joint optimized photon–carbon ion combined treatment strategy to infiltrative diseases focussing on glioblastoma. I solely developed the joint optimization frame work, implemented the treatment planning strategy and conducted the treatment planning study with guidance from Bangert, M., Unkelbach, J. and Wahl, N. The acquisition of data was aided by Salome, P. The methodology for this published result is presented in section III.4.4 and the corresponding results are presented in section IV.5

Besides the lead author papers above I contributed to the following publication which is not part of this manuscript but partly related to this topic :

Unkelbach, J., Fabiano, S., Bennan, A.B.A., Mueller, S., Bangert, M.
Joint optimization of radiotherapy treatments involving multiple radiation modalities.
(*accepted for publication* IEEE Transactions on Radiation and Plasma Medical Sciences)

The following list contains my scientific contributions grouped together in workshop talks, conference talks and posters from 2017–2020:
(1) Bennan, A.B.A., Bangert, M., Unkelbach, J. Joint optimization of combined photon–carbon ion treatments for infiltrative tumors. ESTRO 39, 2020
(2) Bennan, A.B.A., Unkelbach, J., Hauswald, H., Ellerbrock, M., Bangert, M. Fractionation considerations in jointly optimized photon–carbon ion treatment plans. ICCR, Montreal, 2019.

Curriculum Vitae

DATE OF BIRTH: 21/08/1992 PLACE OF BIRTH: Mumbai, India

NOVEMBER 2017 PRESENT DAY	PhD Student, **German Cancer Research Center** *Heidelberg, Germany* - Radiotherapy Optimization, Development of mixed modality treatment planning strategies focussing on photon-carbon ion treatments
JULY 2019 SEPTEMBER 2019	Research stay, **University Hospital Zurich (USZ)** *Zurich, Switzerland* - Department of Radiation Oncology, Purpose: research exchange to develop mixed modality radiotherapy treatment planning strategies
NOVEMBER 2016 SEPTEMBER 2017	Master Thesis project, **Erasmus MC Cancer Institute** *Rotterdam, The Netherlands* - Department of radiation oncology, Purpose: Implimenting TG43 dose engine and development of Brachytherapy TPS module within in-house Erasmus-iCycle TPS
SEPTEMBER 2016 NOVEMBER 2016	Internship, **Erasmus MC Cancer Institute** *Rotterdam, The Netherlands* - Department of radiation oncology, Purpose: evaulation and comparison of treatment planning optimizers in clinical TPS for Brachytherapy
AUGUST 2015 SEPTEMBER 2017	Master of Science, **Delft University of Technology** *Delft, The Netherlands* - Biomedical Engineering Focussing on medical physics for medical imaging and radiotherapy
AUGUST 2011 AUGUST 2015	Bachelor of Technology, **Manipal Institute of Technology** *Manipal, Karnataka, India* - Biomedical Engineering Emphasis on electronics and image processing

Acknowledgments

"If I have seen further, it is by standing on the shoulders of giants." - Isaac Newton.

First and foremost, I would like to express my deepest gratitude to Dr. Mark Bangert for giving me the opportunity to work on this exciting project at the Radiotherapy Optimization group. Our conversations have always given me comfort in difficult stretches, applause at the smallest successes and more questions than I had started out with. He was officially my supervisor for nearly two years but unofficially has always made time to guide me all along this doctoral journey. Secondly, I would like to thank Dr. Niklas Wahl, who taking over as group leader has jumped onto the metaphorical speeding train with ease and understanding. Niklas' enthusiasm and diligence has inspired me through the final lap of this marathon. Both Mark and Niklas, have shown me the forest when I glared at trees and I am truly grateful for the perspectives that I now see.

I would also like to thank my doctoral father Prof. Dr. Oliver Jäkel for his support and guidance in navigating this PhD project. The thesis advisory committee comprised of Prof. Jäkel, PD Dr. Henrik Hauswald, and Prof. Dr. Jan Unkelbach deserve a special mention for their encouragement and constructive input over the course of 3.5 years. They have been the rudder by which this ship has stayed its course. I would like to especially thank Prof. Unkelbach and the team at the University Hospital of Zurich for hosting me for three, very fruitful and enjoyable, months of the research stay. Discussions with Prof. Unkelbach have always challenged me to go further and ask new questions regarding my work.

I am very grateful to all the colleagues at the medical physics in radiation oncology department, German Cancer Research Center, Heidelberg who have made this a very memorable part of my life. I would like to especially thank my friends Dr. Hans-Peter Wieser, Dr. Hubert Gabrys, Ahmad Neishabouri, Noa Homolka, Martina Palkowitsch and Isabela Paredes Cisneros for their camaraderie and invaluable support through thick and thin.

I am deeply grateful to Sarah, my constant. I thank you for the joy, the sacrifice and the constant sound of laughter in my life. I would also like to thank the Hauber family for giving me a home away from home. I am grateful to my friends whose words of cheer have lifted many a dark cloud.

Last but not the least, I extend an ineffable gratitude to my family. Rhea, my younger sister, chief partner in mischief and role model in courage. Achcha, for your toil and many sacrifices that have given me the opportunity to be the person I am today. Amma, the stoic and the curious child who is my rock, my lullaby and my friend. Thank you.

AMDG

Eidesstattliche Versicherung

1. Bei der eingereichten Dissertation zu dem Thema
   Combined photon - carbon ion radiotherapy treatment planning
   handelt es sich um meine eigenständig erbrachte Leistung.

2. Ich habe nur die angegebenen Quellen und Hilfsmittel benutzt und mich keiner unzulässigen Hilfe Dritter bedient. Insbesondere habe ich wörtlich oder sinngemäß aus anderen Werken übernommene Inhalte als solche kenntlich gemacht.

3. Die Arbeit oder Teile davon habe ich bislang nicht an einer Hochschule des In- oder Auslands als Bestandteil einer Prüfungs- oder Qualifikationsleistung vorgelegt.

4. Die Richtigkeit der vorstehenden Erklärungen bestätige ich.

5. Die Bedeutung der eidesstattlichen Versicherung und die strafrechtlichen Folgen einer unrichtigen oder unvollständigen eidesstattlichen Versicherung sind mir bekannt. Ich versichere an Eides statt, dass ich nach bestem Wissen die reine Wahrheit erklärt und nichts verschwiegen habe.

Heidelberg, 02 June, 2021

Ort, Datum	Unterschrift